The University of Adelaide
Department of Geology and Geophysics

LONGITUDINAL DUNES:
THEIR GENESIS AND ORDERING

by

George Kuang Yee Tseo

Volume One

January, 1986

A thesis submitted to the University of Adelaide
in fulfilment of the requirements for the
degree of
Doctor of Philosophy

Frontispiece 1. Linear dunes of the southwestern Rub 'al Khali, Saudi Arabia. (HANNA, 1969, courtesy of Arabian American Oil company).

This thesis contains no material that has been accepted for the award of any other degree or diploma in any University and, to the best of my knowledge and belief, it contains no material previously written or published by another person except where due reference is made in the text. I consent to this thesis being made available for photocopying and loan if applicable if accepted for the award of the degree.

Abstract

Longitudinal dune ordering and longitudinal dune genesis are two separate phenomena. Moreover, longitudinal dune fields in which dune separation is nearly uniform may be controlled by genesis and ordering mechanisms different from those for longitudinal dune fields in which dune separation is variable.

Longitudinal dune fields with nearly uniform dune spacing or wavelength are characterized by mean dune width to mean wavelength ratios of 0.4 or greater and by an average mean wavelength of $\sim$ 2.4 km or approximately twice the thickness of the planetary boundary layer. The extreme organization of these dune fields and their wavelengths can be explained in terms of the ordering being due to planetary boundary layer scale secondary flow in the form of paired vortices known as roll vortices.

Longitudinal dune fields with variable mean dune spacing are characterized by mean dune width to mean dune spacing ratios of 0.3 or less with mean dune spacings less than $\sim$ 1 km. These types of longitudinal dune fields also show high density of dune coalescences and their controlling mechanism may result in the situation where adjacent dunes within a certain critical separation converge and coalesce whereas those farther apart remain discrete. A characteristic dune separation is thereby established although a high degree of variability remains. An aerodynamic coalescence mechanism in part dependent upon local topography and wind conditions helps explain the wide range of mean dune spacings for global linear dune fields.

Earlier empirical work on roll vortices suggests that they occur in desert regions, especially those containing unvegetated longitudinal dunes of uniform spacing. It is shown qualitatively that the stable orientation for roll vortices amongst established longitudinal dunes is precisely that orientation that would promote dune growth. Of various techniques by which roll vortices may be observed and measured, the one most applicable to desert work for both practicability and the quality of the data obtained involves the airplane measurement of horizontal temperature variation. Australian desert dune fields are unsuitable for roll vortices observation because of their variable dune spacing, which would disrupt organised secondary circulation. Moreover, the vegetation present throughout most of the Australian deserts makes it difficult to find dunes over and around which general studies of wind over bare obstacles can be conducted.

One possible mechanism for dune coalescence is horizontal pressure gradients within longitudinal dune fields due to flow constriction between closely

spaced adjacent dunes. Arguments against this possibility outweigh arguments for it; although, the Reynolds number analysis is favorable.

Wind/sand-transport/sand-form systems may be inherently unstable longitudinally, and this instability may manifest itself in the form of ordered longitudinal deposition ridges. An inviscid, incompressible quantitative model of instability in linear sand banks in shallow tidal seas is modified and applied to desert dunes, but the results obtained are poor. Viscid, compressible flow models result in the formation of roll vortices, and given that these roll vortices do not shift laterally, loose sediment would be transported and deposited in an ordered array of ridges. Steady roll vortices over relatively featureless terrain are, however, considered unlikely, but roll vortices confined by established longitudinal dunes would foster both dune growth and dune ordering.

The propagation of linear dunes to leeward of ridges of alluvial debris on fringes of exposed lake and river beds indirectly results from three aerodynamic instabilities, of which the primary one is the stagnation pressure instability established over the windward faces of debris mounds during oblique winds. Centrifugal instability of the flow over the leeward concave slope and momentum deprivation instability due to bottom saltation are of subsidiary importance. Roll vortices generated to the lee of debris mounds as a result of the instabilities causes the longitudinal sand deposition which ultimately produces series of linear dunes. Many of the linear dunes emerging from debris mounds subsequently coalesce within tens of kilometers thereby increasing the apparent order of the system. This mode of dune genesis is observable in the Australian linear dune fields, which have variable spacing. It is also a conceivable formative mechanism for longitudinal dune fields with uniform spacing.

Field techniques were devised for (i) monitoring deposition/erosion over any sandy area using a grid of implanted stakes (ii) ascertaining of sand firmness patterns over any sandy area using a pole penetrometer and (iii) observing various forms of primary and secondary flow over and around a linear dune, including leeward rotors, windward rotors, quasi-laminar flow and roll vortices, using tethered kites. Wind vector monitoring over a linear dune revealed that during oblique winds, maximum wind speed and maximum vertical wind component were attained just to windward of the crest, and the horizontal wind component experienced a deflection towards the normal over the crest with respect to the dune's longitudinal axis. The study dune's periodic summits were observed to migrate leeward along the dune's longitudinal axis while maintaining their spacing, and its main body was observed to migrate laterally.

Frontispiece 2. Linear dunes of the northwest Simpson Desert, Australia. (E. Tad Nichols).

Acknowledgements

Table of Contents

Chapter Seven: Complex flow model

Chapter Eight: Dune genesis

Glossary of Quantitative Symbols

Note: Most of the symbols used in the appendices and a few of the symbols in the text that are used only very locally are not included in this glossary.

Chapter One

$\overline{W} \equiv$ mean dune width of a specific dune field

$\overline{\lambda} \equiv$ mean wavelength (dune spacing) for a specific dune field

Chapter Three

$\text{Ra} \equiv \frac{\beta g \psi h^4}{\kappa \nu} \equiv$ Rayleigh number (dimensionless)

$\quad \beta \equiv$ initial vertical density gradient of a fluid layer [kg m^{-4}]

$\quad \psi \equiv$ fluid expansion coefficient [m^2 l kg^{-1} s^{-1} °C^{-1}]

$\quad g \equiv$ gravitational acceleration = 9.8 m/s^2

$\quad \kappa \equiv$ thermometric conductivity [m l s^{-3} °C^{-1}]

$\quad \nu \equiv$ kinematic viscosity [m^2 s^{-1}]

$T_N \equiv$ wavenumber of transverse roll vortices

$L_N \equiv$ wavenumber of longitudinal roll vortices

$T_W \equiv$ wavelength of transverse roll vortices

$L_W \equiv$ wavelength of longitudinal roll vortices

$\varepsilon \equiv$ angle between the two sets of roll vortices

Chapter Four

$u \equiv$ flow velocity vector component in the x-direction

$v \equiv$ flow velocity vector component in the y-direction

$w \equiv$ flow velocity vector component in the z-direction

$T \equiv$ temperature

$\rho_v \equiv$ humidity

$f \equiv$ secondary flow frequency

$\lambda \equiv$ secondary flow wavelength

$\varsigma \equiv$ lateral velocity of secondary flow relative to a moving observer

Chapter Six

Note: For this chapter, the x-direction axis is aligned with the longitudinal axis of the regular topographic corrugations of the bottom boundary within the systems considered. The y-direction axis is aligned with the transverse axis of the corrugations.

$t \equiv$ time

$\vec{U} \equiv$ flow velocity vector

$U \equiv |\vec{U}| \equiv$ magnitude of $\vec{U}$

$U_{max} \equiv$ maximum U

$I(t) \equiv$ time dependence of U

$\qquad 0 \leq I(t) \leq 1$

$\qquad U = U_{\max} I(t)$

$U \equiv U_{\max}$ beginning at (2) in the derivation.

$I \equiv I(t)$ beginning at (2) in the derivation.

$h \equiv$ fluid layer depth

$H \equiv$ far fluid depth – the fluid layer thickness at a far
$\qquad$ distance from the topographic corrugations

$H \equiv$ characteristic depth scale

$\alpha \equiv$ angle between the flow and the corrugations

$P \equiv$ pressure

$\mu \equiv$ viscosity

$\rho \equiv$ density

$\nu \equiv \mu/\rho \equiv$ kinematic viscosity

$\nabla^2 \equiv \frac{\partial^2}{\partial x^2} + \frac{\partial^2}{\partial y^2} + \frac{\partial^2}{\partial z^2}$

$\omega_i \equiv i -$ direction component of the angular velocity of the earth's
$\qquad$ rotation at any given point on the earth's surface

X, Y and Z $\equiv$ extraneous forces in the x-, y- and z-directions

$C \equiv$ drag coefficient in drag law for turbulant flow (see below)

$\qquad \vec{\tau} \equiv \rho C |\vec{U}| \vec{U}$

$\qquad \vec{\tau} \equiv$ shear vector

$C_m \equiv C/U^{m-2}$

$\qquad m \equiv$ constant coefficient, usually 2

$f \equiv$ Coriolis coefficient

$\vec{Q} \equiv$ sediment transport vector

$Q \equiv$ rate of sediment transport

$\Gamma \equiv$ "function of"

$\vec{U}_{cr} \equiv$ threshold flow velocity vector for sand transport

$\gamma \equiv$ non-dimensional scaling factor

$n \simeq 2$

$\Lambda \equiv$ downslope transport enchancement factor

$\vec{v} \equiv y$-direction component of the flow velocity vector

$\gamma' \equiv$ some constant coefficient

$p \equiv$ sand bed porosity

$\gamma'' \equiv \frac{\gamma'}{1-p}$

$\gamma''' \equiv \gamma/\gamma''$

$L \equiv$ characteristic length scale = corrugation wavelength

$\delta \equiv$ magnitude of the perturbation of u

$a(t)$ and $b(t) \equiv$ time dependence of δ

$a = a(t)$ and $b = b(t)$ after (5) in the derivation

$\varpi(t) \equiv a(t) + b(t)i$

$k = \frac{2\pi H}{CL}$

$S \equiv$ scaling coefficient for the sediment transport equation

$q \equiv m\cos^2\alpha + \sin^2\alpha$

$\ell \equiv k\sin\alpha$

$r \equiv m\sin^2\alpha + \cos^2\alpha$

$\sigma(k,\alpha) \equiv \delta^{-1}\frac{d\delta}{dt} =$ deposition rate

$\hat{\Lambda} = C/\tan(\text{friction angle})$

$\alpha_{\text{opm}} \equiv$ optimum α

$k_{\text{opm}} \equiv$ optimum k

$L_{\text{opm}} \equiv$ optimum $L =$ optimum corrugation wavelength

Chapter Seven

Note: For this chapter, the x-direction axis is aligned with the mean flow, and the y-direction axis is transverse to the mean flow. Also, barred quantities indicate mean values, and primed quantities indicate perturbation values.

$\vartheta \equiv$ some constant coefficient

$c_H \equiv$ specific heat

$c_p \equiv$ specific heat at constant pressure

$K_h \equiv$ coefficient of heat diffusion

$R \equiv$ gas constant

$\nabla q \equiv i\frac{\partial q}{\partial x} + j\frac{\partial q}{\partial y} + k\frac{\partial q}{\partial z}$

$\quad q \equiv$ some scalar

$\text{div}\vec{G} \equiv \nabla \cdot \vec{G} = \frac{\partial G_x}{\partial x} + \frac{\partial G_y}{\partial y} + \frac{\partial G_z}{\partial z}$

$\quad \vec{G} \equiv$ some vector

$\vec{G} \cdot \nabla q = iG_x\frac{\partial q}{\partial x} + jG_y\frac{\partial q}{\partial y} + kG_z\frac{\partial q}{\partial z}$

$K_m \equiv$ Austausch coefficient of turbulant diffusivity

$\quad K_m$ is assumed constant

$\eta \equiv$ instability wavenumber

$\chi \equiv \chi_r + i\chi_i$

$\quad \chi_r \equiv$ real wave speed

$\quad \chi_i \equiv$ instability growth factor

$\quad\quad \chi_i \geq 0 \leftrightarrow$ instability growth

$\quad\quad \chi_i = 0 \leftrightarrow$ static instability

$\quad\quad \chi_i \leq 0 \leftrightarrow$ instability decay

$\Psi = \Phi(z)\exp\left[i\eta(y - \chi t)\right]$

$\equiv$ stream function

where $v' \equiv \frac{\partial \Psi}{\partial z}$ and $w' \equiv \frac{\partial \Psi}{\partial y}$

$u' = u(z)\exp\left[i\eta(y - \chi t)\right]$

$T = T(z)\exp\left[i\eta(y - \chi t)\right]$

$\lambda \equiv 2\pi/\eta \equiv$ secondary flow wavelength

$\varrho \equiv$ perturbation phase angle

Chapter Eight

$P_o \equiv$ stagnation pressure

Chapter One

1.1　　　　　　　　　　　**Introduction**

The "problem of longitudinal dunes" is one of the oldest in desert geomorphology. Sandridges frequently of considerable size, roughly aligned with the dominant winds and organized into ordered systems occupy large areas of many modern deserts and were, moreover, typical of dune fields that extended over the Sahel and much of Australia during the late Pleistocene. Many longitudinal dune fields exhibit a nearly uniform interdune spacing; the distilled impression is of extreme orderliness. It becomes a point of conviction that a causal mechanism exists. Yet after more than a century of investigation, none of the several proposed mechanisms for longitudinal dune genesis and evolution has attained general acceptance.

The original purpose of this study was to derive a viable physical model for longitudinal dune field genesis, but as the investigation proceeded, it gradually became apparent that the problem was more complicated than had initially been realized or than is at present commonly recognized. First, longitudinal dune genesis and longitudinal dune ordering are separate phenomena, each with its own set of possible mechanisms. Moreover, there are the two major types of longitudinal dune fields – those with a characteristic but still variable dune spacing and those with nearly uniform dune spacing – and the ordering mechanisms for these two types of longitudinal dune fields may be different.

This dissertation deals mainly with longitudinal dune genesis and the ordering of longitudinal dunes into fields with uniform dune separation. In the broader context, this work on longitudinal dune ordering is an initial, simplest-case analysis of longitudinal dune ordering in general. This work may serve as point of departure for investigations into evolution of longitudinal dune fields with variable dune spacing and even for investigation into evolution of the few very complicated variant types of longitudinal dune fields.

1.2　　　　　　　　　　**Dissertation synopsis**

In the remainder of this chapter, longitudinal dunes and longitudinal dune fields are first defined according to their dynamic characteristics. Then their general geomorphic features are described. Extreme variations of both longitudinal dunes and longitudinal dune fields are also noted. The global distribution of longitudinal dune fields is then discussed.

Chapter Two is divided into two parts. The first is a review of literature concerning Australian relic longitudinal dunes and their implications for paleoclimate. The second is a review of geomorphological literature on topics intergrally related to the problem of longitudinal dunes such as wind regimes in longitudinal dune fields, theories of dune formation and stratigraphy.

Longitudinal dune coalescence as a possible control on longitudinal dune ordering is briefly discussed in **Chapter Three**, which otherwise deals with the review and assessment of past fluid dynamical research relevant to the problem of longitudinal dune ordering.

Chapter Four is a discussion and assessment of various available empirical techniques for the detection and observation of secondary circulation. **Chapter Five** is predominantly concerned with field observations of primary and secondary flow around a longitudinal dune, deposition/erosion patterns over it and its topographic change and migration.

Longitudinal dune ordering may result from a predominant longitudinal instability within wind/sand-transport/sand-form systems during simple – irrotational and incompressible – flows, and this mechanism is examined in **Chapter Six**.

Longitudinal dune genesis and ordering as a result of planetary boundary layer scale longitudinal secondary flow in complex – rotational and incompressible* – flows is considered piecemeal. The empirical evidence of longitudinal secondary flow and its influence upon sediment transport is discussed in detail in **Chapter Three**, but the quantitative discussion of secondary flow and its implications for dune development and ordering are not considered until **Chapter Seven**, after the quantitative treatment of simple flow.

Longitudinal dune genesis to the lee of obstacles, especially elongate alluvial debris mounds, is discussed in **Chapter Eight,** and **Chapter Nine** is a synopsis of conclusions.

---

* Compressibility or the local variability of fluid density is a significant factor only for situations in which flow velocity approaches the ambient speed of sound [SCHLICHTING, 1960].

1.3   **Nomenclature**

The term "longitudinal dune" has a specific morphodynamic implication. The natural inference is that dunes so labelled are in the form of ridges oriented parallel or nearly so to the dominant winds.

This sort of morphodynamic distinction is not suggested in the terms "linear dune," "sief dune," "sand ridge," and "linear sand hill." These terms merely connote a predominance of one horizontal dimension over the other. There is no implied orientation with respect to the strong winds. Nevertheless, these purely morphologic terms are used interchangeably in the extant literature.

Terminological problems arising from investigations of linear dunes have been summarized by MAINGUET (1984a) and RUBIN and HUNTER (1985). One suggested set of solutions is to use terms such as "linear dune", "elongate dune" and "narrow sand edifices", to refer to linear sand ridges oblique to the dominant winds and to restrict "sandridge" to refer to linear sand ridges of considerable length and nearly parallel to the dominant winds [MAINGUET, 1984a].

Alternatively, it has been suggested that "linear dune," "elongate dune," "sief dune," "linear sand hill" and all other inherently descriptive terms to be used only as morphologic terms in reference to any linear sand ridges regardless of their orientation with respect to the mean strong winds [RUBIN and HUNTER, 1985]. This complements an earlier arbitrary definition of "longitudinal dune" as any linear sand ridge whose longitudinal axis is within 15° of the direction of the mean strong winds [HUNTER et al., 1983]. Finally, HUNTER and RUBIN (1985) assign the term "transverse dune" to linear sand ridges whose longitudinal axis is within 15° to the normal of the direction of the mean strong winds and the term "oblique dune" to all remaining instances of linear sand ridges. This latter set of recommended usages is adopted for the remainder of this thesis.

Despite the paucity of good wind data in and in the vicinity of linear dune fields, the distinction between longitudinal, transverse and oblique dunes is legitimate if to a degree arbitrary. This is particularly true within the context of this thesis, which deals with the almost conceptual investigation of the possible mechanisms for the genesis and ordering of true longitudinal dunes.

1.4 General longitudinal dune characteristics

1.4.1 Dune asymmetry

In general, linear dunes are asymmetric in transverse section with a fairly straight or slightly convex windward flank and a slightly concave leeward flank (Fig. 1A). The sense of asymmetry of the linear dunes in some areas reverses periodically, presumably because of oblique storm winds from different quarters [BAGNOLD, 1941; WOPFNER and TWIDALE, 1967]. General mechanisms for longitudinal dune asymmetry are discussed briefly in the later part of Section 3.2.6.

The linear dunes on the northern side of Qarhan Lake (a dried salt lake) in the Qaidam Basin, Qinghai Province, People's Republic of China are exceptional in that the slopes of both flanks are nearly straight or slightly concave and converge at about 70° to form relatively sharp and symmetric crests (Fig. 1B) [BOWLER, pers. comm., 1983]. The surfaces of these dunes are loosely cemented by halite and have been described as "spongy." This cementation constrains sediment movement over parts of the dunes in such a way that over these parts, sediment is being removed faster than it is being replaced. For this reason, these dune flank slopes are nearly straight or slightly concave.

1.4.2 Linearity

In Landsat imagery, the individual dunes of certain Arabian and North African linear dune fields, many of which extend unbroken for more than a hundred kilometers, appear amazingly straight in plan. Plates 1D and 2 show portions of Rub' al khali, Saudi Arabia, and Plate 3 shows a portion of Erg Bilma, Niger.

At the other end of the spectrum, the longitudinal dunes of the Strzelecki Desert, south central Australia, hint at sinuosity, and those of the Negev Desert, southern Israel and the Sinai, are very obviously sinusoidal (Pl. 4) and are aptly referred to as snaking dunes.

1.4.3 The application of the definition
of longitudinal dunes

From the annual wind rose of Erg Bilma (Pl. 3), it appears that the dunes of Erg Bilma may be truly longitudinal. This can be said with certainty only if the annual wind rose derives from a long term statistical survey, one that accounts for say thirty or forty years. Therefore, to determine whether any linear dune is longitudinal as well is not trivial. For this reason, a general study of longitudinal dunes, such as this, is in respects simpler than a study of the longitudinal dunes in a specific region. In each instance, the direction of the predominant winds must be determined, taking care not to mistake this with the direction of mean sand transport (App. 1). Throughout this thesis, particular linear dune fields are not referred to as longitudinal dune fields unless some observational evidence exists to justify the more precise classification.

1.4.4 Secondary features and morphologic complexities

Linear dunes lacking secondary features are rare; in fact, all linear dunes that have been seen during this study have had surface ripples, the longitudinal axes of which are normal to the direction of their formative winds. More significantly, large scale secondary features often occur on linear dunes [McKEE, 1979]. For example, in the Namib Desert, Southwest Africa, star dunes and crescentic dunes occupy the crests of linear dunes [LANCASTER, 1983].

The main body of a linear dune may itself be complex in form [McKEE, 1979]. In the Rub' al Khali, as in other places, linear dunes occur as compound structures, each dune having a pair of crests in juxtaposition (Pls 1C and 1D) (App. 2).

1.4.5 Dune fields

From inspection of aerial images, it seems that highly ordered linear dune fields occur in nature. In Plate 2, for example, apparently simple, mutually-parallel and evenly-spaced linear dunes occur in a great system.

Linear dune fields of low organization and variable dune spacing are also prevalent. These are characterized by a significant percentage of dunes that are forked due to either bifurcation or coalescence (Pl. 5 and Frontispiece 2). These

forks almost invariably open upwind and are in appearance the opposite to being streamlined. Their shape has prompted the names "tuning fork junction" and "Y junction", the latter of which is adopted for use here.

Y junctions in linear dunes are probably usually the result of coalescence. The single ridge extending downwind from the junction is due to the growth of the dune along its longitudinal axis after coalescence.

Dramatic departures from the two major types of linear and longitudinal dune fields are found in central and western China (Pls 6, 7 and 8). These sand ridges are possibly longitudinal in that they may, in the axis of their general trend, be aligned with the predominant winds. The suggestive labels used to refer to them – "honeycomb," "dendritic" and "fishinghook" type linear dunes – seem apt [*China tames her deserts: A photographic record*, 1977].

1.5   Geographical prevalence

Linear dunes cover fifty percent of the world's large sandy deserts [TSOAR, 1978; McKEE, 1979]. They have been cited to i) occupy more than seventy percent of northern African dune deserts, ii) dominate Arabian sand seas, Soviet arid zones and Australian arid zones and iii) occupy significant portions of the deserts of southern Africa and the American Southwest [McKEE, 1979; TWIDALE, 1981]. Large linear dune fields also occur in central and western China.

Evidence of ancient linear dunes exists in the stratigraphic record [TANNER, 1965; GLENNIE, 1972; STEELE, 1982], and a recent paper revises the interpretation of preserved crossbedding and specifically notes that linear dunes may have been much more prevalent than has been appreciated [RUBIN and HUNTER, 1985].

1.5.1   Two morphodynamic categories
of linear dune fields

Let $\frac{\overline{W}}{\overline{\lambda}}$ be defined as the ratio between the mean dune width and the mean dune spacing for any given linear dune field, where $\overline{W}$ is the mean dune width and $\overline{\lambda}$ is the mean dune spacing. For the 12 linear dune fields included in the survey summarized in Table 1, all, with one exception, are characterized by either $\frac{\overline{W}}{\overline{\lambda}} \leq 0.30$ or $\frac{\overline{W}}{\overline{\lambda}} \geq 0.40$. The exception is the field of complex linear dunes in the northern Sahara, Algeria, for which $\frac{\overline{W}}{\overline{\lambda}} \simeq 0.34$.

The four linear dune fields of the first category $\left(\frac{\overline{W}}{\overline{\lambda}} \leq 0.30\right)$ are located in northern Arizona, U.S. (Pl. 9), the Simpson Desert, central Australia (Pl. 5 and Frontispiece 2), the Great Sandy Desert, northwestern Australia (Pl. 1B) and the northeastern Rub' al Khali, Saudi Arabia. The aerial imagery of each of these displays variable mean dune spacing and a relatively large number of Y junctions. Moreover, mean dune spacing varies considerably and is in all instances less than 1 km. The linear dune field on the Navajo Indian Reservation bears striking resemblance to those of the Simpson Desert and the Great Sandy Desert in spite of $\overline{W}$ and $\overline{\lambda}$ values respectively ~ 5 and ~ 8 times less than those for its Australian counterparts.

Linear dune fields of the second category $\left(\frac{\overline{W}}{\overline{\lambda}} \geq 0.40\right)$ display lower densities of Y junctions. These dune fields are located in the northeastern Rub' al Khali, Saudi Arabia, the Kalahari Desert, southern Africa, the southwestern Sahara, Mauritania, the southern Sahara, Niger, the southwestern Rub' al Khali, Saudi Arabia, the Namib Desert, Southwest Africa (Namibia), the northern Sahara, Algeria, the southern Sahara, Niger and the western Rub' al Khali, Saudi Arabia. Mean dune spacing for the dune fields of this category are on average ~ 2.4 km or approximately twice the thickness of the planetary boundary layer.

The two major types of linear dune fields, as qualitatively distinguished by the criteria of dune spacing uniformity and Y junctions density, seem to correspond well to the two categories of linear dune fields as defined by $\frac{\overline{W}}{\overline{\lambda}}$. The latter may indeed be morphodynamic categories. The high density of Y junctions of the first category and the organization and wavelengths of the second may be of great importance in understanding their respective ordering mechanisms. For the first category, that mechanism which controls dune coalescence may determine their low organization (Abs. and Sec. 3.1.1.). For the second category, the extreme ordering and wide spacing may be due to planetary boundary layer scale secondary flow in the form of paired vortices (Chs 3 and 7).

Chapter Two

2.1 **Australian relic linear dune fields and
their implications for paleoclimate**

The world's second most extensive system of linear dune fields exists in
Australia. These dune fields, for reasons reviewed below, are believed to be
relic longitudinal dune fields; consequently, their overall pattern holds certain
implications for the paleoclimate. It is the connection between longitudinal
dune fields and the climate that provides the broader context for this study
and motivates the following discussion of past research in this area.

It has been suggested that the Australian linear dunes may have been
true longitudinal dunes at the time of their formation during the last glacial
period [SPRIGG, 1979, BOWLER, 1982]. Some of the sand of linear dunes
in the Strzelecki and Simpson Deserts, central Australia, originated tens of
thousands of years ago thereby possibly placing the genesis of the dunes before
the end of the Pleistocene [WASSON, 1983b and 1984]. Using the ^{14}C data
of WASSON [1983a and b], Holocene lateral migration rates of the dunes have
been estimated as being on the order of 1 cm a year [RUBIN, 1985]; therefore, it
was concluded that the general pattern of the central Australian dunefields have
changed insignificantly since their establishment in the late Pleistocene [RUBIN,
1985].

In some places in South Australia and southwest Queensland, linear
dunes rest on late Pleistocene alluvial and lacustrine sediments [TWIDALE,
1972a]. These dunes may have been true longitudinal dunes more recently during
Holocene times [WOPFNER and TWIDALE, 1967; TWIDALE, 1972a and 1981].
The possibility of Holocene formation of the Australian dunes is not refuted by
dimensional analysis of the evolutionary timescale for longitudinal dune ordering
(Sec. 6.3.13). Presently, many of the Australian linear dunes display active crests,
and at least one linear dune in northeast South Australia is known to migrate
laterally (Sec. 5.14). It is possible that spasmodic episodes of subtantial regional
lateral migration and longitudinal extension have been occurring throughout
Australian linear deserts since the early Holocene [TWIDALE, 1981; TWIDALE
and WOPFNER, 1981]. The extension of ancient linear dunes into present
temperate regions seems to support this idea.

Presently, most Australian linear dunes are partially stabilized by sparse
and low level vegetation [MADIGAN, 1936; BUCKLEY, 1981a-c], by wet cores
[TWIDALE, 1981] (Sec.s 5.1 and 5.20) and in some cases possibly by some

carbonate cement [KING, 1956 and 1960]. The generally dense vegetation between dunes throughout Australian linear dune deserts strongly suggests that the large scale pattern of the dunes is stable. Though a few constituent dunes remain partially active, the Australian linear dune fields as systems are relic. The Australian linear dunes occur mainly in lowlands, within ancient drainage basins, the deposits of which are the source of dune sediment. In central Australia, some of the linear dunes are presently longitudinal [BROOKFIELD, 1970]. In the central region, modern winds are presumably closest in orientation to that of the ancient winds of the period(s) of dune formation. Most of the linear dunes of central Australia are presently oblique [BROOKFIELD, 1970; RUBIN, 1985].

The linear dunes of Australia form a great, elongated horseshoe arc that covers a substantial portion of the continent (Fig. 2) [JENNINGS, 1968]. In the Great Victoria Desert, South Australia and Western Australia, they run west-east, which is to say that if they were active they would build out along their longitudinal axes from west to east. In the Tanami Desert, Northern Territory, the linear dunes run southeast-northwest, and in the Simpson Desert, South Australia and Northern Territory, they run south southeast-north northwest. The linear dunes of the Great Sandy Desert, South Australia and Western Australia, run east-west. The active linear dune systems of northern Africa form a similar arc [BAGNOLD, 1941] though here the pattern is not so distinct [MAINGUET, 1980 and 1984b] (Fig. 3). The Australian continental arc of dunes is speculated to be a trace of the late Pleistocene summer anticyclone (surface high pressure system) [SPRIGG, 1980] (Fig. 4).

Some privately-collected continuous wind measurements from five sites around Australia have been analyzed to show that during the observation periods, which totalled about two years and included at least one continuous year for each site, the strong winds occurred mainly during summer anticyclones [SPRIGG, 1980]. A similar conclusion was drawn from an analysis of Australian Bureau of Meteorology long range wind statistics for Oodnadatta. "[The analysis suggests] that the strongest winds occur immediately behind a cold front which is being pushed rapidly to the northeast by a high pressure system moving east across southern South Australia" [BURROWS, pers. comm., 1984]. Hence, there exists some empirical data to support the conjecture that in Australia, the strong winds are associated with the summer surface high pressure systems. It is interesting to note that two of SPRIGG's data collection points were within linear dune fields of the Simpson and Strzelecki Deserts, South Australia. Such long term wind records for loci within linear dune fields are rare and potentially valuable for investigations of genesis and ordering mechanisms.

A mean trace of modern southern summer anticyclones does not coincide with the Australian continental dune arc (Fig. 5), but has a substantially greater radius of curvature. Interestingly, in northern Africa the present mean wind pattern seems to coincide well with the linear dune pattern [MAINGUET, 1984b; MAINGUET, pers. comm., 1985] (Fig. 3); however, it is not known whether the African mean wind pattern corresponds to the northern summer anticyclone.

In Australia, the area of greatest divergence between the continental dune arc and the summer anticyclone is the area of the southeastern bend of the arc. Here, true longitudinal dunes being freshly initiated are oblique with respect to the relict linear dunes in the same area. A case in point would be the area of the northeastern rim of Lake Frome where the most recent dunes run almost due south-north and the ancient dunes run east northeast- west southwest (Fig. 6). Such instances lend credence to the possibility that the Australian continental arc of relic linear dunes was once a continental system of longitudinal dunes and therefore still reflects in its pattern the mean trace of the ancient summer anticylcone. By implication, the ancient summer anticyclone may have been more compact than its successor system and presumably more intense as well (App. 3).

2.2   **Review of geomorphological literature**

This section serves to review significant literature on the study of longitudinal dunes from a geomorphological point of view. Topics covered include wind regimes associated with longitudinal dune fields, theories of longitudinal dune genesis, stratigraphy and dune coalescence junctions.

2.2.1   Wind regimes associated with longitudinal dunes

Parallelism between prevalent winds and active longitudinal dunes was first observed in the Indian desert [BLANFORD, 1876]. Similar conclusions were later made regarding dune fields in the northern Sahara [BEADNELL, 1910 and 1934; KING, 1918; HUME, 1925; BALL, 1927; BAGNOLD, 1931 and 1933; KÁDÁR, 1934; MAINGUET and CALLOT, 1978; WARREN, 1970], Australia [MADIGAN, 1936] and southwestern Africa [GEVERS, 1936]. For the most part, the prevalent winds were taken to be unidirectional. A wind regime in which strong winds occur at more or less equal frequency and intensity from two different but not necessarily widely divergent directions has also been associated with longitudinal dunes in northern Africa, central

Australia, Israel and southwestern Africa [BAGNOLD, 1941; COOPER, 1958; McKEE and TIBBITTS, 1964; WOPFNER and TWIDALE, 1967; TSOAR, 1978; LANCASTER, 1980]. Finally, grossly disproportionate strong winds from nearly opposite directions have been observed aligned with certain Libyan linear dunes [BEADNELL, 1934]. Morphodynamically, this mode of bidirectionality is identical to unidirectionality, for the effect on linear dune development and linear dune field development of two sets of mutually opposite winds parallel to linear dunes would be the same as that of a single set of parallel winds.

The asymmetry of longitudinal dunes in many deserts has been attributed to short term strong winds that blow from directions substantially different from the mean direction of the prevailing winds and oblique to the dunes [WOPFNER and TWIDALE, 1967; CLARKE and PRIESTLEY, 1970] (Sec. 3.2.6). Under the assumption that linear dunes are not formed by parallel winds but by nearly parallel but distinctly oblique winds, dune asymmetry is taken as evidence of leeward lateral migration of the linear dunes [RUBIN, 1985], which has been observed [BESSLER, 1975] (Sec. 5.14).

Linear dunes in some places, such as Libya, are nearly symmetric but for their crests, whose sense of asymmetry at any given time depends upon the direction of storm winds [BAGNOLD, 1941; WOPFNER and TWIDALE, 1967]. Such dunes develop a series of barchan-like slip faces (Fig. 7 and Pl. 10).

Wind data and analyses for many of the world's major dune fields have been compiled by McKEE [1979], who concluded that the wind regimes associated with longitudinal dune fields displayed strong winds over greater spectra of directions than did wind regimes associated with barchan dune fields. It should be noted that general conclusions of surveys may be open to question unless the component studies are all reliable and conducted using a similar procedure. Incidentally, barchan dunes are commonly considered to be associated with unidirectional winds [VERLAQUE, 1958; FINKEL, 1959; HASTENRATH, 1967; CLOS-ARCEDUC, 1967].

2.2.2   The possible slight divergence between
                 longitudinal dunes and predominant winds

Some researchers believe that longitudinal dunes are oriented ~ 15° off alignment to the direction of the mean strong winds. In some longitudinal dune fields, the individual dunes run a little to right of windward, and in others the dunes run a little to left. One explanation of this is that although mean wind

determination often takes into account the entire planetary boundary layer, in which the wind turns considerably with height, only wind close to the surface directly affects dune development [MABBUTT et al., 1969; WARREN, 1976b]. Unfortunately,   the paucity of reliable wind records for desert regions prevents testing of this idea. Theoretically, an angle of $\sim 13°$ between longitudinal dunes and predominant winds would be   expected if ordering is induced by organized planetary boundary layer scale secondary flow (Secs 3.2.16, 3.2.10 and 3.2.12).

2.2.3   Linear dune formation

Several mechanisms have been advanced in explanation of linear dunes. First, it has been argued that linear dunes are formed by the linear erosion of unconsolidated sediment [FRERE, 1870; ENQUIST, 1932]. Linear dunes formed by this excavation mechanism have been termed "windrift" dunes [MELTON, 1940]. Some linear dunes on the eastern margin of Lake Eyre, south central Australia, have been attributed to the windrift mechanism because of their non-eolian substrate cores [KING, 1956 and 1960]. Non-eolian sediment mixed with eolian sediment within linear dunes may be explained by the erosion of bed material and its incorporation into linear dunes during their lateral migration and extension [RUBIN, 1985].

Certain dunes in the Simpson Desert have alluvial cores or some alluvial material in them [FOLK, 1971]; although, in other Simpson Desert dunes no traces of alluvial core material have been found [MABBUTT and SULLIVAN, 1968]. Linear dunes completely constructed of eolian sand have been found in the Strzelecki and Simpson Deserts [WOPFNER and TWIDALE, 1967]. Augering on a dune may not necessarily produce evidence of an alluvial core even if the dune under examination does indeed have an alluvial history [FOLK, 1971]. For larger dunes, the top cover of eolian material may be so thick as to render auger results inconclusive.

Algerian linear dunes thought to have hard cores of non-eolian material [CHUDEAU, 1920; AUFRÈRE, 1931, pg. 373] have been compared to yardangs [AUFRÈRE, 1930]. Yardangs, which are linear and possibly longitudinal erosional forms, occur in central Asia [HEDIN, 1904; STEIN, 1909], Egypt [WALTHER, 1924], Peru [BOSWORTH, 1922] and western United States [BLACKWELDER, 1934].

Whether linear dunes are erosional or depositional features has long been a source of controversy. RUBIN [1985] sites evidence of linear dunes formed

both by erosion into non-eolian material [KING, 1960; FOLK, 1971; BREED and BREED, 1979] and deposition of wind blown sediment [WOPFNER and TWIDALE, 1967; MABBUTT and SULLIVAN, 1968; FOLK, 1971; BREED and BREED, 1979; TWIDALE, 1981; WASSON, 1983b]. Sand ridge linearity may be independent of the mode of formation.

In places where sediment is relatively scarce and linear dunes exist on floors of firm material, it is possible that the dunes form behind obstacles and grow as fresh sediment is introduced from sources external to that area [BEADNELL, 1910; MELTON, 1940; MADIGAN, 1936; TWIDALE, 1972a; WASSON and HYDE, 1983a and 1984; RUBIN, 1984]. For example in the Simpson Desert, linear dunes form to the lee of transverse debris ridges [TWIDALE, 1972a and 1981] (Ch. 8).

It has been proposed that true longitudinal dunes only occur in areas where sediment is not only scarce but actually in the process of depleting [MAINGUET and CHEMIN, 1983]. In a simple longitudinal dune field model, the introduction of nonconstant sediment reserves affects rate of deposition and not ordering (Sec. 6.3.15). Within the Strzelecki and Simpson Deserts, central Australia, linear dunes occur on beds of eolian sand as well as on substrate of predominantly solid material [RUBIN, 1985].

It has been proposed that in older deserts, linear dunes are produced when barchan dunes link together in the process of migration [SOKOLOW, 1984]. It was earlier suggested that from a single barchan dune a chain of barchan dunes may develop under the influence of bidirectional winds [BAGNOLD, 1941] (Fig. 8). This chain eventually becomes a linear dune. The specific scenario is as follows: 1. A barchan dune migrates under the influence of the mean winds. 2. Storm winds oblique to the direction of the mean strong winds extend the windward wing of the crescent-shaped barchan dune. 3. The barchan dune continues to migrate, and its wing windward of the oblique strong winds continues periodically to lengthen. This elongated wing forms nearly parallel to the mean oblique strong winds so that it eventually cuts across the path of the main barchan dune. 4. With time, the elongated wing extends beyond the other wing of the barchan and out of the other wing's wind shadow. 5. Drifting sand accumulates at the end of the far extended wing, and a secondary barchan dune forms. 6. The process of wing extension repeats itself for the secondary barchan. 7. The chain of barchans that is eventually produced becomes a single linear dune. LANCASTER [1980] pointed out that relatively gentle winds are responsible for barchan formation and migration, and once barchans entered

areas prone to divergent storm winds, extension into linear chains of barchans is possible.

This process is interesting and appealing because of the resemblance of many linear dunes to a series of linked barchans (Pl. 10). A strong argument for this mechanism has been made for some linear dunes in the northern Namib Desert using field wind evidence [LANCASTER, 1980]. Interestingly, snow barchans have been observed in the process of linkage [HANNES and HANNES, 1982] (Pl. 11).

Near-surface pairs of longitudinal air currents with mutually opposed transverse components have been offered as a possible mechanism for the formation of shallow, linear sand deposits [BAGNOLD, 1941] (Fig. 9). These air currents supposedly occur during wind storms.

A theory similar to the above attributes longitudinal dune genesis and ordering to pairs of steady or quasi-steady helical air currents with mutually opposed senses of rotation sometimes known as roll vortices [BAGNOLD, 1952] (Fig. 10). Roll vortices, when they occur close to the ground, are limited in their vertical extent by the top of the planetary boundary layer and therefore have a maximum depth of about 1 km. The wavelength or spacing of longitudinal dunes that form in the zones of surface flow divergence of these helical currents will be in the area of 2 to 4 km. This idea has gained favor among some workers in the field, including several meteorologists and fluid dynamicists [WILSON, 1972; HOUBOLT, 1968; HANNA, 1969; WIPPERMAN, 1969; HORST, 1970a and b; BROWN, 1980]. Other researchers seriously doubt it [BOWLER, pers. comm., 1982; BENNETT, pers. comm., 1982]. To date, no other mechanism for the ordering of longitudinal dunes has been formally put forward, and roll vortices and their possible roles in both the genesis and ordering of longitudinal dunes are a major concern of this dissertation.

2.2.4 Dune structure

The internal structure of linear dunes depends upon their mode of formation and migration. According to RUBIN [1985] both stationary windrift linear dunes and windrift linear dunes migrating laterally while eroding the bed material, whether loose or solid, will display no internal stratification (Fig. 11a and b). Linear dunes neither eroding or depositing material while migrating laterally will have uniformly inclined internal strata regardless of the mode of formation (Fig. 11c). Linear dunes depositing material while migrating laterally

will have thick primary stata comprised of fine substrata, and the thick strata
will be oppositely inclined to the substrata (Fig. 11d and 11e). Linear dunes
built vertically upwards while remaining horizontally fixed, such as linear dunes
created by equal oblique winds from either side [BAGNOLD, 1941 and others],
would display symmetrically stacked crossbeds [BAGNOLD, 1941] (Fig. 11f).
Given a great rate of deposition during migration, whole dune forms will be
preserved in the stratigraphy. In section, these dune forms would be manifested
in asymmetrically stacked layers of crossbeds (Fig. 11g).

Crossbeds of the form associated with modern active linear dunes are
relatively rare in the stratigraphic record of ancient sedimentary rocks. As
implied above, under most circumstances crossbeds in linear dunes are either not
deposited or erased during lateral migration. Therefore, the scarcity of crossbeds
in the stratigraphic record is not necessarily indication of the scarcity of linear
dunes during ancient times [RUBIN and HUNTER, 1985].

Crossbeds in some modern active linear dunes (e.g. the spectacular
crossbeds in the longitudinal dunes studied by TSOAR, 1978) have been taken
as evidence against dune growth due to roll vortices. Roll vortice pairs in the
planetary boundary layer are asymmetric (Fig. 17), and it can be shown through
qualitative argument that the stability of roll vortice pairs among established
longitudinal dunes requires that their surface flow convergence or air uplift zones
be positioned over the dunes (Sec. 3.2.11). Therefore, uneven deposition due to
the unequal vortices could result in crossbeds. The effect of infrequent oblique
storm winds would then deepen these crossbeds.

2.2.5   Y junctions

Y junctions usually open into the direction of the predominant winds. For
the section of the Simpson Desert shown in Figure 12, more than 96% of the Y
junctions open to windward with respect to the present mean strong winds.

In aerial imagery of Simpson Desert dunes, Y junctions appear quite
distinct (Pl. 5 and Frontispiece 2), but on the ground, they are much less obvious.
In the Simpson, they can be so subtle that positive identification can be obtained
only after careful inspection. There, and perhaps elsewhere, the plateaus within
the forks are nearly at a level with the crests of the constituent linear dunes
close to the junctions. Away from the junctions, the elevated ground within the
forks slope down gently, eventually becoming level with the interdune corridors
(Fig. 13).

It has been suggested that the structure of Simpson Desert Y junctions is the result of wind excavation [KING, 1960]. However, this windrift type mechanism has been criticized on the basis of several physical arguments [MABBUTT and SULLIVAN, 1968], the most convincing of which is the one that makes use of the principle of mass conservation. If an erosional mechanism were responsible for the formation of Y junctions, then the cross-sectional area of the single dune section downwind from the junction should be greater than the sum of the cross-sectional areas of the two dune sections windward of the junction. This is because the two windward sections are presumably simply the remnants of a single dune section that had formerly been very similar to the single dune section downwind from the junction. In more precise terms, the mass of material of a unit length of the unexcavated portion of a linear dune, as gauged by the cross-sectional area, should be greater than the mass of material of a unit length of the excavated portion of a linear dune. From field measurements, it is known that there is little difference between the cross-sectional area of the dune section to leeward of a junction and the sum of the cross-sectional areas of the two dune sections to windward.It is more plausible that Y junctions are the result of the coalescence of two linear dunes rather than the partial excavation of one dune.

Y junctions of aqueous longitudinal sediment ridge systems open to flowward in some natural and laboratory instances [DZULYNSKI and WALTON, 1965; ALLEN, 1967]. These sediment ridge systems consisted of shallow sediment bed form features (of order of magnitude 10^2 or less in height) in relatively shallow water (about 0.05 m in mean depth) and are believed to have been created by roll vortices. This laboratory trial has been sited as possible empirical evidence for the formation of Y junctions in eolian linear dune fields by roll vortices [FOLK, 1971]. For several reasons the analogy is unlikely to be valid. First, the differences in fluid layer depth, flow speed, fluid density and viscosity between the eolian and aqueous cases is such that their comparative Reynolds number analysis indicates dynamical dissimilarity (App. 4). The Reynolds number for desert longitudinal dunes is of the order of 10^8 and that for shallow aqueous bedform is of the order of 10^4. Second, it has not been firmly established that the shallow aqueous longitudinal bed form ridges were produced by roll vortices.

The Reynolds number for any given setting gauges the relative significance of viscous force against inertial force only. Therefore, the Reynolds number cannot provide a comprehensive dynamical description for settings in which other forces are not well balanced. In a desert, for example, thermal buoyancy force

is unlikely to be exactly offset by gravity. More importantly for this study, the degree of dynamical similarity between a natural setting and a laboratory setting or between two different natural settings may not necessarily be accurately reflected by their comparative Reynolds number analyses. This cautionary note should be borne in mind during the reading of the next chapter where several comparative Reynolds number analyses are made.

Chapter Three

Introduction to the dune coalescence mechanism
for longitudinal dune ordering

Qualitative consideration of roll vortices

3.1 **Longitudinal dune coalescence
as a possible mechanism for
longitudinal dune ordering**

Longitudinal dune coalescence may underlie ordering for longitudinal dune
fields of variable dune spacing. By induction, if all adjacent longitudinal dunes
within a certain critical distance of one another coalesce while those separated
by more than the critical distance remain discrete, then a certain minimum
dune spacing is established throughout the dune field and a low degree of
order is attained. This ordering mechanism is attractive because it readily
explains the downwind transformation of originally non-uniform, randomly-
spaced longitudinal dunes to subsequently better ordered longitudinal dunes
(Pl. 12).

At this stage, it is reasonable to assume an aerodynamic dune coalescence
mechanism controlled to some extent by local topography and wind conditions
(App. 5). Therefore, dune fields ordered by such a mechanism would probably
vary in the values of their characteristic parameters such as mean dune spacing.
Recall that for linear dune fields with variable dune spacing and high Y junction
density, mean dune spacing varies over a wide range (Sec. 1.5.1).

3.1.1 **The analogy of converging ships
and coalescing longitudinal dunes**

It has been suggested that longitudinal dunes coalesce for similar reasons
that ships travelling through the water in parallel converge if they are initially
within a certain distance of one another [SPRIGG, pers. comm., 1983]. This
interesting speculation takes into consideration the fluid dynamical communica-
tion between adjacent longitudinal dunes through their interaction with the air
flow.

A naive understanding of the mechanism at work in the case of converging
ships may be obtained by an application of Bernoulli's theorem, from which it

follows that, where gravity and frictional effects may be disregarded, an increase in the velocity of a fluid is accompanied by a decrease in its pressure. Like water flow from a channel of larger width to one of smaller width, water flow between the hulls of two parallel-travelling ships that are within a certain distance of one another is constricted. The constricted flow increases in velocity and decreases in pressure. Consequently, each ship experiences a pressure gradient force directed towards the other ship (Fig. 14). The increase in flow speed due to flow constriction has to do with momentum conservation (Sec. 6.3).

The rigorous analysis of converging ships takes into consideration cross currents, surface drag, form drag and the possible interactions of these different hydrodynamical factors [TUCK and NEWMAN, 1974]. Any similar analysis of coalescing longitudinal dunes would almost certainly be more complex. Even as two ships travelling in parallel begin to converge, they remain in parallel. As two longitudinal dunes approach coalescence, they become curved, significantly complicating the aerodynamics of the situation.

The analysis for converging ships assumes an inviscid fluid which is tantamount to assuming irrotationality. Intermolecular attraction is so weak in an inviscid fluid that internal friction is negligible; hence, such a fluid cannot turn or rotate. The inviscid fluid assumption is, strictly speaking, never valid, for all fluids have some internal friction. However, for laminar flows under certain conditions, viscosity can be safely ignored. This is the case for water flow around the slender bodies of ships' hulls at relatively low speeds. For dunes in the desert, the inviscid flow assumption would probably be less accurate; flow around dunes is seldom laminar. Various forms of secondary flow have been observed around a linear dune (Ch. 5). That the flow is characteristically turbulent does not necessarily preclude the possibility of accurate inviscid models for longitudinal dune genesis and ordering. Viscid models would be required only if secondary flow plays a significant role in genesis and ordering (Chs 6 and 7).

In the aqueous case of ships in the water, the forcing agent is water, and it experiences significant drag only over the relatively small surface of the ships' hulls. For the vast area over which the water is in contact with the atmosphere, the water experiences negligible drag. In the eolian case of desert dunes, the forcing agent is air, and it experiences comparable drag both over the surfaces of the longitudinal dunes and over the vast interdune corridors. The uniform surface drag upon the air over dunes and interdune corridors probably diminishes the potential constriction of flow, and this adds greater weight to doubts that horizontal pressure gradients arising from flow constriction could cause dune coalescence. It is interesting to note that a Reynolds number analysis

of converging ships and coalescing dunes is favourable (App. 6). In both cases, the Reynolds number is of order 10^9. This does not, however, indicate dynamical similarity, for the two instances are only superficially similar.

3.2   **Qualitative consideration of roll vortices**

Roll vortices as an ordering mechanism for longitudinal dune fields with uniform dune spacing is a highly contested theory. Presumably, planetary boundary layer scale roll vortices cannot exist close to the ground because of surface drag. In fact, large roll vortices do occur near the surface, and when winds are aligned with active sand ridges, both surface and form drag are negligible*. It is entirely feasible for roll vortices to order longitudinal dunes. What follows is a detailed though largely qualitative discussion of roll vortices as described theoretically, produced in the laboratory and observed in the field. The possibility of longitudinal dune ordering by roll vortices is then considered in light of empirical evidence and theoretical understanding.

3.2.1   Roll vortices

When in a flowing fluid an instability develops that is too great for frictional forces to damp, that instability may manifest itself in the form of vortices or vortex sheets, depending upon the flow conditions. Longitudinal roll vortices, which may be thought of as organized convection cells, were first observed inadvertently and in such unlikely experimental media as soapy water in a tub and alcohol and water upon a microscopic slide [THOMSON, 1882; WEBER, 1855]. In these instances, instability was thermally induced.

Cooling from above creates a vertical temperature gradient within the fluid layer such that cooler, denser fluid is underlain by hotter, less dense and therefore more buoyant fluid. The ordered rising of the buoyant fluid and sinking of the displaced top fluid results in the formation of clearly discernible convection patterns. Heating from below similarly produces convection cells. Highly structured polygonal convection cells were produced in laboratory experiments using various stationary fluids including air, water, carbon dioxide and paint with gold flake [BÉNARD, 1900 and 1928; TERADA, 1928; GRAHAM, 1933;

---

* Surface drag is negligible due to lack of vegetation, and form drag is minimized because linear dunes do not present themselves as obstacles during parallel winds.

BRUNT, 1937, 1939 and 1951; CHANDRA, 1938]. These convection cells are called Bénard cells, and their ideal internal structure appears in Figure 15.

When horizontal shear was applied to fluid layers heated from below, the polygonal cells gave way first to uniform roll vortices transverse to the direction of shear and then, as the shear increased, to roll vortices longitudinal to the direction of shear. Photographs of the longitudinal roll vortices, referred to elsewhere in the text simply as roll vortices, show their slight divergence from the direction of shear, which happens to coincide with the direction of flow. Facing the same direction towards which shear is directed, the longitudinal axis of the roll vortices would be oriented within fifteen degrees to the right. In laboratory generation of roll vortices, shear is administered to thin layers of gas and smoke by moving the glass ceilings of the fluid chambers (Pl. 13 and Fig 16).

The set of Navier-Stokes equations of fluid motion, which fully account for all the various forces and factors governing every type of flow, are highly complex, and their exact solution is known only for a few cases. For this reason, early theoretical work on organized convection cells was confined to very restricted cases and performed using the simplest forms of the Navier-Stokes equations. This limited theoretical work focused on thermally induced convection [RAYLEIGH, 1916; JEFFREYS, 1928; PELLEW and SOUTHWELL, 1940; SUTTON, 1950; KUETTNER, 1965]. This form of instability is associated with the name of Rayleigh, and the dimensionless parameter used to determine the likelihood of thermal convective instability is known as the Rayleigh number. It is expressible by the quantitative statement

$$\text{Ra} = \frac{\beta g \psi h^4}{\kappa \nu}$$

where Ra$\equiv$Rayleigh number (dimensionless), β $\equiv$initial vertical density gradient within the fluid layer [kg m^{-4}], g $\equiv$gravitational acceleration, ψ $\equiv$fluid expansion coefficient [m^2 l kg^{-1} s^2 °C^{-1}], h $\equiv$fluid layer thickness, κ $\equiv$thermometric conductivity of the fluid [m l s^{-3} °C^{-1}] and ν $\equiv$kinematic viscosity of the fluid [m^2 s^{-1}].

The Rayleigh number is a ratio that compares the buoyancy forces of a fluid as induced by a vertical density gradient, which is in turn due to a vertical temperature gradient, with the fluid's intermolecular viscous forces. Critical values for the Rayleigh number above which a fluid is thermally unstable have been calculated for various sets of boundary conditions (Tab. 2).

Subsequent to their initial discovery, production in the laboratory and mathematical analysis, roll vortices have continued to be studied both empirically

and theoretically [GORTLER, 1940 and 1959; FALLER, 1963; FALLER and KAYLOR, 1965 and 1966; GREGORY, STUART and WALKER, 1955; STERN, 1960; BARCILON, 1965; LILLY, 1966; HORST, 1970a and b; WIPPERMAN, 1969; BROWN, 1970, 1972 and 1974; LEMONE, 1973 and 1976], and the history of this research has been recorded [BROWN, 1980].

3.2.2   Secondary flow model

A quantitative model of compressible, viscous, rotational boundary layer flow with laminar mean components and lateral and vertical perturbation components develops boundary layer scale roll vortices over land and water [BROWN, 1970]. Using flow shear as the sole instability agent results in a slight imbalance in the energy budget equation, which is resolved by taking into account the effect of thermally-induced buoyancy force [LEMONE, 1973 and 1976]. Coriolis force and the remaining contributing forces are largely insignificant [LEMONE, 1973 and 1976]. A revised quantitative model agrees well with empirical results [LEMONE, 1973].

Flow shear may be a necessary condition for boundary layer roll vortice production [BROWN, 1980]. It is actually the lateral component of flow shear, due to the deflective effect of Coriolis force upon the mean flow shear, that instigates roll vortices. Therefore, Coriolis force assumes an important indirect role in boundary layer roll vortice production. The interaction between roll vortices and other kilometer-scale eddies may also be important in roll vortice development [LEMONE, 1973]; however, neither the extent or nature of this effect are yet known.

Radar imagery of roll vortices (Fig. 17) do not show the distortion of the lower left-hand side of each roll developed in the model due to surface friction [BROWN, 1970] (Figs 18 and 19). More importantly, model imagery does not display roll assymetry as clearly seen in radar imagery.

3.2.3   Indirect empirical evidence
                                  of roll vortices in the desert

Roll vortices have been detected and measured over the Great Lakes and fairly flat to rolling terrain in Oklahoma [LEMONE, 1976]. The Oklahoma observations were made in June; therefore, thermal conditions during the experiment are probably similar to those in deserts during their hot windy

seasons. Because longitudinal dunes offer negligible surface and form drag, they may be dynamically similar to featureless midwestern plains. In conclusion, the Oklahoma experiment may be valid indirect evidence of roll vortices in deserts.

3.2.4   The secondary importance
of thermal buoyancy force
in roll vortice production

In Australia, the mean strong winds occur during summer anticyclones, which correspond to surface high pressure systems. Summer surface high pressure systems are characterized by clear skies and therefore high insolation (*incoming solar radiation*). Consequently, the heating of the air just above the surface through conduction must be relatively intense. The same would likely be true for most deserts in the world though there is no comprehensive study to confirm this.

Consider the instance of a desert with intense bottom heating during strong winds. Assume further that the buoyancy force induced by this bottom heating is the primary source of energy for roll vortices. During the occurrence of roll vortices, the warmer bottom air exchanges with the cooler top air. As this exchange progresses, the original vertical temperature and density gradients are diminished in strength. At some point, these vertical gradients are so weak that convection is no longer possible. The roll vortices dissipate and are reformed only after bottom heating manages to recharge the vertical thermal gradients. This, of course, will be more difficult the second time, for the top air has probably not cooled down to its original low temperature. Bottom heating may have to continue for a longer period before the minimum vertical thermal gradients are reached and roll vortices can again occur. After several generations of roll vortices, the system of the boundary layer, the surface, the insolation and the conductive heating from the surface may no longer be able to sustain convection. Clearly, thermal buoyancy force as a primary energy source for roll vortice production would allow for only periodic and possibly temporary roll vortice generation. Investigations to date offer nothing to indicate that roll vortice production under any set of circumstances during high winds is periodic or temporary. It is unlikely that thermal buoyancy force is a primary energy source for the production of roll vortices in the boundary layer.

The secondary nature of thermal buoyancy force is supported by observation of roll vortices in the northern hemisphere mid-latitudes, notably Colorado, during the northern winter [FRISCH, MILLER and STRAUCH, 1974; KELLY,

1982]. It is interesting to note that these empirical studies were single and double Doppler radar trials during snow fall (Sec. 4.4).

Once roll vortices are formed, thermal buoyancy force as well as flow shear are important sources of energy for roll vortices growth.

3.2.5   Coriolis force as a factor in roll vortice production and longitudinal dune ordering

Coriolis force as a direct factor in roll vortice production is tertiary and far less important than the secondary factor of thermal buoyancy force. Table 3 is a comparison of Coriolis force to thermal buoyancy force for four trial periods during the Oklahoma experiments.

As mentioned earlier, flow shear is indirectly dependent upon Coriolis force, and flow shear is the primary mechanism for roll vortice production. Because of this, approaching the equator, where Coriolis force vanishes, roll vortice generation diminishes*. Therefore, the occurrence of ordered, equatorial longitudinal dune fields would be strong evidence against roll vortices as an ordering mechanism.

Longitudinal dune fields do not exist on the equator, and this is due not to any direct morphodynamical causes but to the general absence of deserts at low latitudes. Global climatic controls confine arid zones to the latitudes between 15° and 45° in both hemispheres. Great equatorial systems of unordered longitudinal yardangs [FAROUK EL-BAZ, BREED and GROLIER, 1979] and polar systems of transverse dunes [TSOAR, GREELEY and PETERFREUND, 1979] may have been identified on imagery of the Martian surface. To date, no longitudinal dune fields have been found on Martian surface imagery [BREED, GROLIER and McCAULEY, 1979].

Finally, Coriolis force is thought to have the important effect upon roll vortices of distorting them laterally, and giving rise to roll vortices asymmetry.

---

* Roll vortices generation will not stop entirely at the equator, for other factors such as flow curvature will continue to create shear.

3.2.6   Roll vortices asymmetry

In the northern hemisphere, Coriolis force is directed toward the right, and it induces a widening of the right-hand side rolls of atmospheric roll vortice pairs (Fig. 17). The opposite occurs in the southern hemisphere. Roll vortices asymmetry has been used to account for the asymmetry of the north-south oriented central Australian longitudinal dunes, whose avalanche slopes are usually on the right-hand side [MABBUTT, WOODING and JENNINGS, 1969]. The predominant winds in central Australia are directed from south to north; therefore the left-hand side flanks of sand ridges would be built up with more sand by the larger and more energetic left-hand side rolls of roll vortice pairs. The smaller right-hand side flanks would bear the steeper slopes. Alternatively, it has been suggested that storm winds significantly divergent from the direction of mean strong winds create asymmetry in central Australian dunes [CLARKE and PRIESTLEY, 1970].

3.2.7   Centrifugal force as a factor
                              in roll vortice production and
                              longitudinal dune ordering

There is no significant centrifugal force contribution to boundary layer scale roll vortices production over the land or water except possibly over the vast concave slopes of large mountain ranges. It is doubtful that centrifugal force plays a significant role in longitudinal dune ordering; although, it may be more important in longitudinal dune genesis through its influence on smaller scale (wavelength of order 10^2 m) roll vortices production (Sec. 8.2.2).

3.2.8   Laboratory production of roll vortices

Roll vortices nearly aligned with the direction of shear have been produced in trials where the fluid is contained in a cylindrical tank and shear is provided by tank rotation [FALLER, 1963; FALLER and KAYLOR, 1966; GREGORY, STUART and WALKER, 1955; STERN, 1960; HORST, 1970a and b] (Figs 20 and 21, Pl. 14)*. Shear in a rotation tank is directed spirally away from the center of the basin (Fig. 22).

---

* A photograph of a large rotation tank is available in FALLER and KAYLOR, 1966.

The axes of shear are spiral rather than circular because of the radial component of the shear vector due to centrifugal force. The axes of shear approach being circular, however, because the tangential component of the shear vector due to tangential friction as the basin rotates predominates. Additional shear can be generated by moving fluid radially across the floor of the tank during rotation [FALLER and KAYLOR, 1966]; this is done by withdrawing fluid at the center and introducing it at the rim (Fig. 20). When this is done, the axes of shear become substantially less circular and more radial because of the additional radial component of the shear vector due to radial friction as fluid is moved across the floor of the tank.

During trials in which a circular basin lined on the bottom with soft China clay was rotated without additional radial flow, parallel, evenly-spaced grooves aligned nearly parallel to the direction of the shear developed [GREGORY, STUART and WALKER, 1955]. These longitudinal grooves are believed to have been created by stationary roll vortices in the fluid flow (Pl. 15). During trials in which a deep basin was rotated and then decelerated, a bottom bed of loose sand also developed longitudinal, parallel, evenly-spaced features [HORST, 1960a and b] (Pl. 16). Note that here "longitudinal" connotes alignment with the shear axes (Fig. 23).

In these trials, deceleration was the main factor contributing to flow instability. The ordered longitudinal features that formed in the sand were taken to be valid indirect evidence of roll vortices formation of longitudinal dunes in the desert. This possibility will be examined more closely in the section that follows.

During trials in which fluid was moved radially across the bottom of a rotating basin, stationary vortices were produced [FALLER and KAYLOR, 1966]. In Plates 17 and 18, the longitudinal axes of the roll vortices are substantially less circular than those implied in Plates 15 and 16. Also, these roll vortices, which display a common direction of rotation, are not paired but separated by some distance from one another. Were two of them to come together, shear too great for the rolls to withstand would be produced in the interface region. This, incidentally, argues against the theory that longitudinal dunes are ordered by series of adjacent roll vortices of the same sense of rotation [MAINGUET, pers. comm., 1985]. Interface shear is minimized for turbulence manifested in the form of roll vortices.

3.2.9   A rotation tank experiment as a viable
model for longitudinal dune field evolution

The rotation tank trials utilizing deceleration to promote instability and
a bed of loose sand to record the impressions left by roll vortices produced has
been sited as a viable model for longitudinal dune field evolution [HORST, 1970a
and b] (Figs 21 and 23, Pl. 16). These trials must be examined closely to assess
the validity of the claim.

The depth of the fluid contained in the deep basin or canister used in
the experiment is perhaps one order of magnitude greater than the depth of the
roll vortices formed at the bottom. The relevant instability layer is therefore
shallow in comparison to the fluid depth. For roll vortices in the desert, it is
unclear whether the relevant fluid layer is the planetary boundary layer only
or the PBL plus some other portion of the atmosphere. Consequently, nothing
certain can be said about the comparative depths of the roll vortices and the
relevant fluid layer. However, because wind conditions change abruptly at the
top of the planetary boundary layer, it probably is the relevant fluid layer, in
which case, the depths of the roll vortices and the relevant fluid layer are nearly
equal. In this respect then, the canister experiment probably does not provide
an adequate analogy.

It should be noted that throughout the trials fluid depth was not constant
but varied from 1 to 4 canister radii. Also, during each trial, fluid depth varied
radially due to the effect of centrifugal force. That is, fluid depth was greater close
to the canister wall. The significance of this radial depth variation upon the
outcome of the experiment is unknown.

Before assessing the validity of the analogy between i) the fluid used
in the experiment and air and ii) deceleration and flow shear, a brief review
of experimental procedure is in order. Metal canisters of radii varying from
7.0×10^{-2} m to 22.0×10^{-2} m were used. These were partially filled with a mixture
of water and glycerine at 23°C to varying depths. At the greatest glycerine
concentrations, the fluid mixture viscosity was 8 times that of pure water. A thin
layer of sand was allowed to settle in the fluid-filled canister, and the canister
was attached to a turntable with a braking mechanism. During rotation, the
canister could be decelerated from a rate of 200 rotations per minute to standstill
in half a second. During the experimental trials, the turntable was accelerated
to various specific rotational rates, and once uniform motion was established for

the entire system of canister, fluid and sediment layer, the brakes were applied, stopping the canister quickly. The fluid stopped more gradually, probably over an interval of time between two and three orders of magnitude greater than the half second required for the brakes to stop the canister. It was during these periods of gradual deceleration that ordered, longitudinal sand streaks formed, presumably by action of stationary longitudinal roll vortices. No interpretable results were obtained for trials in which initial turntable rates were under 12 rotations a minute or over 96 rotations a minute.

To calculate an underestimate of mean deceleration for the trials, a turntable rate of 50 rotations per minute or, in frequency units, 0.83 s^{-1} is assumed. Fluid within a 0.10 m radius canister is taken to go to rest within 10 seconds after braking.

An acceleration expression is derived by dividing the total change in fluid velocity by the time elapsed for this change to take place. Fluid velocity at any point is the product of angular velocity and its distance from the center of curvature. Since the locus of interest is taken to be stationary, the radius of curvature at that point is constant. Acceleration becomes the product of the radius of curvature at the point in question and the ratio between the total change in fluid angular velocity and the total change in time (App. 7). Note that if the canister radius is taken to be the radius of curvature, then the acceleration calculated using the derived expression is actually for a point in the fluid next to the canister wall. The calculated acceleration at the canister wall is -0.0083 m/s^2.

The absolute value of this acceleration is of the same order of magnitude as 0.00111 m/s^2, which is the Coriolis acceleration for a sand-moving wind of magnitude 11.1 m/s or approximately 40 km/hr. As discussed earlier, Coriolis force is purely tertiary for roll vortice instigation in the planetary boundary layer. In fact, Coriolis force is characteristically one to two orders of magnitude less than thermal buoyancy force in roll vortice instigation (Tab. 3), and in this function, thermal buoyancy force is itself secondary to flow shear. Therefore, it would seem that much less force is required to produce roll vortices in the rotation canister than in the planetary boundary layer. This is somewhat surprising, for the much higher viscosity of the gel and water mixture in comparison to air would suggest a correspondingly far greater minimal force to produce roll vortices. Since it takes comparatively so little force to produce what is supposedly roll vortices-formed longitudinal sand streaks in gel and water solution, it is well within dynamic feasibility for the relatively much stronger agents of flow shear and thermal

buoyancy force to instigate roll vortices in the atmosphere and, moreover, for these roll vortices to produce longitudinal dunes.

The Reynolds number analysis of spiral longitudinal sand streaks in rotation canisters and longitudinal dunes in deserts is unfavorable (App. 8). The difference between the Reynolds numbers of the two cases is of order of magnitude 10^4. Vastly different viscosity effects are suggested. The Froude number analysis of the two instances is favourable (App. 9). Froude number compares inertial forces to gravitational forces, and the Froude numbers for rotation canister longitudinal sand streaks and longitudinal dunes in the desert are of the same order of magnitude. In this instance, however, the Froude number analysis is of minor significance. For both longitudinal dune fields in the desert and longitudinal sand streaks in rotation canisters, gravitational force does not significantly contribute to instability. What the favorable Froude number analysis does show is that gravity is of comparable dynamical importance in the two situations.

Neither was the canister bottom heated or the top of the fluid cooled; therefore, it is reasonable to assume that thermal buoyancy forces were insignificant if they existed at all in the gel and water. Thermal buoyancy forces are certainly present and probably significant in deserts during the summer months of high winds. Hence, it is unlikely that the two instances are comparable or similar so far as buoyancy forces are concerned.

In conclusion, though only partial dynamical similarity between rotation canister longitudinal sand streaks and desert longitudinal dunes can be demonstrated, the rotation canister experiment may still be a viable model for longitudinal dune genesis and ordering. An additional image of a sand streak pattern obtained during the rotation canister trials is provided in Plate 19.

3.2.10   Transverse roll vortices

Under certain conditions, a secondary set of roll vortices will superpose upon the primary roll vortices aligned with the flow [KUO, 1963; FALLER and KAYLOR, 1966; HORST, 1970a and b; STERN, 1960; WIPPERMAN, 1969]. Over fairly featureless terrain, the longitudinal roll vortices will occur at a mean angle of between 13° and 16° to the left of the mean flow [GREGORY, STUART and WALKER, 1955; FALLER, 1963; FALLER and KAYLOR, 1965; PLANCK, 1966; ANGELL, PACK and DICKSON, 1968; HORST, 1970a and b] and transverse roll vortices, if they are generated, will occur at 90° to the

longitudinal roll vortices. In the southern hemisphere where Coriolis force is directed to the left, longitudinal roll vortices will be ~ 15° to the right of the mean flow. It is the effect of Coriolis force upon the mean flow that creates the angular difference between the mean flow and longitudinal roll vortices. "Mean flow" is here defined as geostrophic flow, which is the air flow as determined solely by Coriolis force and pressure gradient force. The geostrophic flow approximates the mainstream above the planetary boundary layer.

Interestingly, the calculated angular divergence of longitudinal roll vortices from the mean flow is a function of the ratio between the wavelengths of longitudinal and transverse roll vortices [WIPPERMAN, 1969]. As can be seen from Figure 24, on which is plotted the ratio between the measured and calculated angular divergences against the wavelengths ratio, at low values of the wavelengths ratio, the measured angular divergence is greater than the calculated angular divergence. At wavelengths ratio of ~ 0.7, the measured and calculated values of the angular divergence are virtually identical. At higher wavelengths ratios, calculated angular divergences are greater than measured angular divergences.

In a linear dune field, stability criteria of longitudinal roll vortices require that longitudinal roll vortices orient themselves such that zones of surface divergence coincide with dune crests (Sec. 3.2.11). This may occur even when the wind is as much as 45° oblique to the dunes. Hence, both orientation and wavelength of longitudinal roll vortices within a linear dune field is fixed by the orientation and wavelength of the dune field. Transverse roll vortices must remain approximately orthogonal to the mean flow; therefore, their orientation with respect to longitudinal roll vortices will vary with the circumstances. In any given situation, the wavelength of transverse roll vortices depends upon the angle between them and coexisting longitudinal roll vortices and can be calculated using the following wavenumber equation derived by WIPPERMAN (1969):

$$T_N = L_N \exp\left(\frac{2\pi \tan \varepsilon}{2\pi}\right),$$

where $\varepsilon > 0$ and $\varepsilon \equiv$ angle between the two sets of roll vortices, $T_N \equiv$ wavenumber of the transverse roll vortices and $L_N \equiv$ wavenumber of the longitudinal roll vortices. For example, in the instance where $\varepsilon = 15°$, $T_N/L_N = 0.850$. The ratio of the wavelengths is 1.18, or slightly more formally $T_W/L_W = L_N/T_N = 1.18$, where $T_W \equiv$ wavelength of the transverse roll vortices and $L_W \equiv$ wavelength of the longitudinal roll vortices. Therefore, if, for instance, $L_W = 2$ km, then $T_W = 2.36$ km.

The above corresponds to the case where mean winds are only a few degrees off alignment with the dunes. For cases where mean winds are at a greater angle to the mean winds, transverse roll vortices are significantly smaller than the primary longitudinal roll vortices. For a wind at about 24° to 27° oblique to linear dunes ($\varepsilon = 40°$) $L_W = 2$ km and $T_W = 0.0616$ km. Table 4 shows different ε and their corresponding T_N/L_N and T_W/L_W ratios.

Certain linear dune fields in northern Africa and Australia have dunes with periodic notches cut transversely across them (Pls 20 and 21). To the lee of these notches are deposition tails approximately normal to the longitudinal axes of the dunes. The wavelengths of the notches are considerably less than the wavelengths of the dunes, and the mechanism responsible for these notches has been hypothesized to be transverse roll vortices [WIPPERMAN, 1969]. Note that in the northern African linear dunes, the transverse deposition tails propagate to the left of the main dunes and in the Australian linear dunes, they propagate to the right of the main dunes. This agrees with theory, which stipulates that because of the opposite effect of Coriolis force in the two hemispheres, transverse roll vortices in the northern African linear dune field will be incident upon right-hand side dune flanks, and transverse roll vortices in the Australian linear dune field will be incident upon left-hand side dune flanks.

3.2.11 Roll vortices stability

Only when roll vortices surface divergence or air uplift zones coincide with linear dunes are they unconditionally stable. In such a configuration, were roll vortices to be shifted laterally in either direction, the natural tendency of the system would be to regain equilibrium by a shift of the roll vortices back to their original positions.

In Figure 25, a situation of initial unconditional stability (A) is offset when the roll vortices shift laterally towards the right (B). Consequently, a force towards the right is exerted on the left-hand side flank of the dune, and the roll vortices move back towards the left under the compulsion of this force (C). A situation of unconditional stability is regained (D).

Only one other quasi-steady roll vortices orientation is possible other than that associated with unconditional stability. That is when the roll vortices are positioned so that their zones of surface convergence or air downdraft coincide with the linear dunes. This situation is conditionally stable, for the disturbance of equilibrium through a lateral shift of the roll vortices results in a permanant readjustment of the system towards a situation of unconditional stability.

In Figure 26, an initial situation of conditional stability exists (A); the forces of the wind to either side of the linear dune are balanced. A lateral shift of the roll vortices to the right is accompanied by a force directed towards the left (B). This force compels the roll vortices farther to the right (C). At some point, a single vortice is situated over a dune such that it and its adjacent pair are disrupted (D). When the roll vortices reform, the surface divergence zones coincide with the dunes and a situation of unconditional stability is attained (E).

3.2.12   Natural occurrence of roll vortices

Empirical evidence of roll vortices in the planetary boundary layer was first obtained through the monitoring of neutral buoyancy balloons using tracking theodolites [GIFFORD, 1953; ANGELL, PACK, HOLZWORTH and DICKSON, 1966; ANGELL, PACK and DICKSON, 1968]. Subsequently, roll vortices in the boundary layer have been detected using acoustic radar [BROWN and HALL, 1978] and measured through electrical detection using an instrumented plane [MARKSON, 1975]. They have been detected using towers mounted with temperature and humidity sensors and anemometers for all three wind components [LEMONE, 1972]. They have been measured using airplanes instrumented with temperature and humidity sensors and anemometers for all three wind components [LEMONE, 1973 and 1976; LENSCHOW, 1970; LILLY and LENSCHOW, 1974].

Single and double Doppler radar will yield actual visual images of secondary circulation [KELLY, 1982 and 1984; BERGER and DOVIAK, 1979; HILDERBRAND, 1980; KROPFLI and KOHN, 1978]. Normally, Doppler radar effectiveness depends upon the moisture content of the air. The resolution of a radar image is a function of the particulate density of the body of air surveyed and water droplets (or snow flakes) are usually the primary component of air particulates. In light of this, it would seem that Doppler radar would not be a suitable choice for desert research, especially for phenomena that supposedly occurs during hot and dry windy seasons. However, chaff dispensed into the air by aircraft has been used to excellent effect in conjunction with double Doppler radar [KROPFLI and KOHN, 1978] (Fig. 17). Generally, observations show that roll vortices near the ground are oriented at less than 20° to the geostrophic wind.

It has been observed that winds generally need to be moderate to strong and atmospheric conditions slightly unstable for roll vortices production [KUETTNER, 1959; LEMONE, 1973]. Conditions of slight instability conducive

for roll vortices production have been related to cold, surface high pressure systems for the northern hemisphere mid-latitudes [KUETTNER, 1959].

3.2.13   High inversions

Roll vortices have been associated with inversion layers [BROWN, 1970]. Surface layer heating and subsequent mixing can cause the secondary flow layer to become adiabatic and the layer directly above it to develop an inversion [BROWN, 1970]. There is some evidence linking planetary boundary layer scale roll vortices and capping inversions [KUETTNER, 1959].

3.2.14   Low inversions

During the occurrence of summer surface high pressure systems, when the sky is clear and solar radiation near maximum, surface heating should be intense. Surface cooling after sunset should similarly be relatively very great, and the low level inversions induced by surface cooling will be of peak potential strength. With the resumption of intense surface heating in the mornings, the air close to the ground quickly warms up and becomes less dense. The low level jet formed in the vicinity of the low level inversion layer descends due to its greater density. Consequently, strong winds occur at surface level during the late morning. Flow shear, thermal buoyancy force and Coriolis force may then act upon the surface flow to induce roll vortices. This hypothetical sequence of events arose out of analyses of untethered neutral buoyancy balloon and surface anemometer data collected in the vicinity of In Salah, Algeria [WARREN and KNOTT, 1983].

At Oodnadatta, a settlement on the southwestern fringe of the Simpson Desert, Australian Bureau of Meteorology wind record statistics spanning a 45 year period indicate that the strongest surface winds occur in the summer months during mornings. A separate Australian Bureau of Meteorology analysis for winds recorded at Oodnadatta during November and January over a 26 year period show that strongest winds occur around 9:00 AM and are predominantly south to southeast winds [BURROWS, pers. comm., 1984]. A study of Australian Bureau of Meteorology weather balloon observation records shows that a low level jet stream (above 300 m) most frequently occurs over central Australia in the early morning approximately between 4:00 AM and 8:00 AM [ALLEN, 1981]. These statistics at least superficially seem to relate strong summer winds in central Australia and low level jets.

To summarize the proposed sequence of events indirectly relating low level inversions to roll vortices, late evening low level inversions precede and thereby help instigate the descent of jets. The resultant low level jets give rise to strong sand- moving surface winds. Wind sheer and other factors create instability, which prompts formation of roll vortices.

3.2.15   Soaring

Seagulls soar with wings held straight and rigid in order to take advantage of air currents that either carry them upwards in a spiral or along a straight line nearly parallel to the mean winds and at a fixed elevation. Spiral soaring is executed during relatively still conditions and is taken as evidence of convection cells not unlike the polygonal Bénard cells in bottom- heated or top-cooled fluids without horizontal shearing [WOODCOCK, 1940]. Linear soaring is taken as evidence of roll vortices (lower portion of Figure 10).

Soaring could possibly be due to descent [WOODCOCK, 1940]; however, observed seagulls were clearly ascending during spiral soaring and flight times of the order of tens of minutes were maintained during linear soaring [WOOD-COCK, 1940]. Soaring could also be maintained through utilization of differences of horizontal velocity in the air [WOODCOCK, 1940]. While using differences in velocity in flow for soaring, a bird must, upon entering a zone or stratum of different velocity, turn around "until his direction is so reversed as to be with the wind of that stratum and contrary to the wind of the other stratum" [RAYLEIGH, 1901]. In spiral soaring, observed seagulls turned both clockwise and counter-clockwise in the same area at the same time, and in linear soaring, the seagulls did not turn at all but maintained an apparently straight flight path [WOODCOCK, 1940].

Both spiral and linear soaring in the flight of wedge-tailed eagles in the Lake Frome area of the Strzelecki Desert, South Australia, have been observed. During continuous strong winds on the initial day of an intense early autumn surface high pressure system, eagles soared in a straight line more or less parallel to the mean winds at an elevation of perhaps 20 m and for a distance of approximately 100 m. In the late morning of the second day of the surface high pressure system, eagles soared up in wide spirals to the bases of large cumulus clouds, which may have been thermally induced. These observations lend credence to the testimony of stockmen and oil workers who claim to have witnessed wedge-tailed eagles soaring above and in line with linear dunes. Linear soaring over linear dunes may indicate roll vortices centered on the dunes.

3.2.16   The logical feasibility
                         of roll vortices in deserts

In summary, there is much indirect evidence of the existence of roll vortices in the desert and their possible role in the ordering of longitudinal dune fields.

First, the common claim that roll vortices cannot affect longitudinal dune development because they cannot exist close to the surface due to the prohibitive effects of surface drag has been refuted by empirical evidence.

Second, the shallow rotation basin trials using water over beds of soft China clay and the deep rotation basin (rotation canister) trials using gel and water over loose sand may be valid laboratory models of roll vortice production, longitudinal dune genesis and longitudinal dune ordering.

Third, the meteorological conditions associated with planetary boundary layer roll vortices at least superficially seem to match the meteorological conditions that prevail in longitudinal dune deserts during windy periods.

Fourth, periodic transverse notches of certain linear dunes in certain linear dune fields in the world may be evidence that couples of mutually-orthogonal roll vortices affect sand transport and dune structuring.

Fifth, stability criteria indicate that roll vortices that occur amongst linear dunes must orient themselves such that dune crests lie within the zones of surface flow convergence and dune building is enhanced.

Sixth, longitudinal dune assymetry and the slight angular divergence of longitudinal dunes from mean winds might be explainable by roll vortices assymetry and the slight angular divergence of roll vortices from the geostrophic wind.

Seventh, phenomena in the desert such as the linear soaring of eagles and the migration of air funnels (Sec. 5.21) along linear dune crests are difficult to explain without resorting to roll vortices.

Eighth, the common criticism that roll vortices could not contain the energy necessary for transport and deposition of the vast amounts of sand necessary to form longitudinal dunes is unfounded. Clearly, the moderate to high winds in which roll vortices may exist are strong enough for the transport and deposition of large quantities of sand. The flow velocity at any point in roll vortices would be comparable to that of the mean flow, and the direction of sand

transportation due to the flow at any point in roll vortices will reflect the flow tendency at that point. Thus, the overall pattern of transport, deposition and erosion due to roll vortices will reflect the overall pattern of flow in roll vortices. It is entirely conceivable that roll vortices give rise to ordered longitudinal dune fields.

Chapter Four: Assessment of empirical methods for roll vortices observation

Of the three possible mechanisms for longitudinal dune ordering discussed in this thesis, roll vortices is the only one commonly known at this juncture, and it is widely contested.

From a dynamical point of view, roll vortices is the most observable of the three mechanisms. This is ironic in light of the fact that within the discipline of meteorology, there are relatively few workers involved in roll vortices study simply because, in comparison to macroscale and microscale flows, mesoscale secondary flows such as roll vortices are difficult to detect and measure.

The hypothesis that roll vortices act as a mechanism for longitudinal dune ordering is empirically testable for refutation. That is, if roll vortices cannot be detected and measured in active longitudinal dune fields of uniform wavelength, then the conjecture that they are responsible for the ordering of these dune fields would be demonstrated unviable. For this reason it is important to consider the various possible methods for roll vortice observation and distinguish the most suitable ones for desert work.

4.1   Neutral buoyancy balloons

Released neutral buoyancy balloons can be tracked to observe secondary flow and measure its wavelength. Unfortunately, a great number of trials is usually required, and even then results are often incomplete and widely interpretable. In no case can circulation intensity be gauged and without radar, several wavelengths of secondary flow can be observed simultaneously only with two theodolites per wavelength and, of course, the same number of trained personel. These are all difficult contraints for summer trials in deserts.

4.2   Instrumented towers

Secondary flow can be observed using instrument mounted towers. Plate 22 shows a typical array in which cup anemometers and temperature sensors in metal housings (to shield them from solar radiation and fast currents) are mounted at the ends of horizontal rods on a 30 m tower at logarithmically increasing intervals to measure vertical wind profiles, which vary logarithmically. The extended horizontal boom carries a hygrometer,

a temperature sensor, a wind vane and propellor anenometer for horizontal wind component measurement and a propellor anemometer for vertical wind component measurement. Roll vortices can be observed using any of the boom instruments. Regardless of the parameter, observations must be made very frequently and over long intervals. Collected data must be safely stored and eventually digitized and analyzed.

The results of data analyses may be in the form of frequency spectra graphs, which plot secondary flow intensity versus secondary flow frequency, and intensity maxima on the graphs correspond to dominant secondary flow frequencies and wavelengths. Figure 27 displays spectra of horizontal wind velocities u and v, vertical wind velocity w, temperature T and absolute humidity ρ_v characteristic of roll vortices. These specific spectra, though similar to those for tower measurements, derive from airplane measurements.

As an example of how spectra may be used to measure roll vortices, take the v spectra of Figure 27 for which the predominant frequency is $\sim 10^{-2}$ s^{-1}. Frequency is related to wavelength by the expression

$$f\lambda = \varsigma$$

where $f \equiv$ frequency, $\lambda \equiv$ wavelength and $\varsigma \equiv$ velocity. In this case, the relevant velocity ς is that of the observation aircraft. Using 20 m/s as a typical value, $(10^{-2}$ s$^{-1})\lambda \simeq 20$ m/s and $\lambda \simeq 2000$ m. The predominant secondary flow is roll vortices of wavelength approximately 2 km. Incidentally, the observation aircraft was traveling in a direction nearly transverse to the longitudinal axes of the roll vortices and about 15° off normal to the direction of the mean winds (Fig. 31). More will be said on airplane measurements in Section 4.7.

Although frequency spectra derived from tower measurements can be used to detect roll vortices, they cannot be used to determine roll vortices wavelengths. This is because the lateral velocity of the roll vortices relative to the measuring instruments ς cannot be measured using only fixed instruments. In theory, ς can be found if it is assumed constant and the y−direction perturbation velocity components of the roll vortices are known. Recall that perturbation velocity is the secondary flow velocity superposed on the main stream velocity. For roll vortices the y−direction perturbation velocity component at any given point would be the lateral flow component at that point additional to the lateral migration rate of the roll vortices as a system. In practise, the y−direction perturbation velocity at any given point is calculated from a known ς, and this can be done only for airplane measurements obtained during cross- vortices flights

conducted at a constant speed. Airplane speed is so much greater than the lateral migration rate of roll vortices that any variability in the lateral migration rate would be inconsequential. Hence, the velocity of the instruments with respect to the vortices ζ would be essentially constant.

Vortices must move laterally in order for the lateral variation in perturbation velocity to be detected by fixed instruments. Stability criteria for roll vortices within linear dune fields requires them to be stationary (Sec. 3.2.11); therefore, instrumented towers within linear dune fields are useless for roll vortices observation. At least two instrumented towers situated in an interdune corridor and at wide separation along a line transverse to the longitudinal axis of the linear dunes would be required to derive information on the lateral structure of stationary secondary flow.

Hypothetically, two instrumented horizontal booms set at different levels on a single tower could be used to measure the depth of roll vortices. For planetary layer scale roll vortices, however, depth measurements would require horizontal booms separated by hundreds of meters, and the tallest meteorological towers are in the area of a mere 100 m.

From a purely practical viewpoint, tower investigations of roll vortices are unsuitable for desert work. In deserts, either high heat tolerance solid state components must be used in circuitry, or electronic instruments must be partially refrigerated. General instruments maintenance in the field requires a great deal of time, and this coupled with the infrequency of meteorologically ideal observation conditions protracts field trials. For example, during single tower turbulence studies in Eyre Pennisula, South Australia, conducted in April and May, 1984, only three out of 23 days could be devoted to actual data acquisition.

4.3   Acoustic radar

Acoustic radar or sodar (*sound detection and ranging*) utilizes acoustic waves to detect and range turbulent regions in the atmosphere. Sodar is used to investigate such things as the top of the planetary boundary layer and inversion layers. It can conceivably be used to study roll vortices, for the air uplift zones of roll vortices would appear on sodar as turbulent regions just below the top of the boundary layer. Unfortunately, other forms of secondary circulation that may occur close to the top of the boundary layer, such as gravity waves, may exhibit similar images on sodar. Also, sodar, though cheaper than radar, would

still be very costly even if purchased as military surplus equipment. For these reasons, sodar would be a poor choice for desert work.

4.4   Doppler radar

On either single or double Doppler radar, roll vortices would appear as alternating colored bands. The longitudinal bands in roll vortices in which the air flow were towards the radar installation(s) would be blue shifted, and the longitudinal bands in roll vortices in which the air flow were away from the radar installation(s) would be red shifted. Lateral movement of roll vortices as a system would also indicated by double or dual Doppler radar.

The air motion vectors at discrete points throughout the depth of secondary flow can be obtained from Doppler radar data, and a large enough set of discrete vectors will provide a vivid picture of the circulation (Fig. 17). The effectiveness of Doppler radar imagery depends upon the particulate content of the air. Favorable particulate density is usually provided by water vapor, cloud droplets, rain, hail, or snow. In clear dry air such as in deserts, high particulate content can be induced artificially by airplane dispersal of chaff. The considerable expense of radar and the obvious logistic difficulties of its use in the desert makes it an impracticable method for desert air flow investigation.

4.5   Smoke trails

Smoke has been used to detect and trace leeside flow separation vortices or rotors around longitudinal dunes [TSOAR, 1978] and to detect the larger scale motion of breaking gravity waves in the lower boundary layer (wavelengths of the order of hundreds of meters) over the ocean [SETHURAMAN, 1977]. Smoke released near and from loci on the crests of linear dunes during parallel winds have not revealed roll vortices [TSOAR, 1978; WASSON, pers. comm., 1982; SPRIGG, pers. comm., 1982]; although, the pattern formed by airplane released smoke over the ocean and parallel to prevailing winds has been interpreted as evidence of roll vortices [WOODCOCK and WYMAN, 1947] (Pl. 23).

It is unlikely that smoke released from a single point (on, for instance, the crest of a linear dune) will reveal the presence of planetary boundary layer scale roll vortices, for the smoke will disperse before it can trace the circuit of even a single vortex. Smoke released from several points along a line transverse to roll vortices might reveal their presence by marking air uplift and downdraught

zones. In the air uplift zones, smoke should be advected upwards, and in the downdraught zones, it should be advected downwards and then horizontally dispersed. However, for the fulfilment of momentum conservation, small scale turbulent eddies must occur at both the tops and bottoms of the air uplift and air downdraught zones in roll vortices (Fig. 28), and smoke trails cannot pass through such zones without disruption. Incidentally, though intuitively unrealistic, polygonal vortices would fit perfectly and thereby eliminate eddy zones (Fig. 28). Air flow does not execute right angle turns because curved turns require much less energy. There is some potential for smoke tracing of roll vortices where the smoke is released in a line rather than from a single point.

4.6   Electrical field measurements

Roll vortice measurement by instrumented plane detection of electrical field presents an interesting possibility. In theory, electrical charge is transported upwards from near the ground in the air uplift zones of roll vortices. These regions of increased charge flux are detectable as bands of increased vertical electrical potential gradient. The average distance between bands is therefore the mean wavelength of the roll vortices.

In Figure 29 are examples of vertical potential gradient charts obtained at various levels above the ocean. The charts are for both parallel and crosswind measurement flights, and the wind was 10 to 20 m/s near the water surface. The spikes in the chart for crosswind flight at a height of $\sim$ 5 m have been interpreted to indicate roll vortice air uplift zones [MARKSON, 1975]. In Figure 30 is an example of vertical potential gradient and relative humidity charts taken simultaneously. There seems to be a correlation. The air uplift zones are regions of moisture advection as well as enhanced electrical flux.

Upon initial consideration, vertical potential gradient measurements may seem to offer a good alternative for roll vortices observation. However, serious shortcomings to this method come to light upon closer examination. Electric potential at any point in the atmosphere is determined by the number of charged ions in that vicinity, and the potential gradient is determined by the number and distribution of ions. A probe coated with radioactive material produces ionization in a thin sheath of air enveloping it. If potential difference exists between the ambient air and the probe, the ions will move in the electric field in such a pattern and until such time that the probe potential is sufficiently changed to eliminate the imbalance. It is the change of the probe potential that allows the electric potential and consequently the potential gradient to be measured.

The vertical potential gradient, which has units of volts per meter, may be assessed through electric potential measurements using two radioactive probe antennas mounted at different heights and a differential solid state electrometer to ascertain the voltage difference between them [CHALMERS, 1957; VONNEGUT and McCRAIG, 1960; VONNEGUT, MOORE and MALLAHAN, 1961; MARKSON, 1975]. "In order to avoid measuring the electric field resulting from charge on the airplane, the probes [are to be] positioned in the same equipotential surface arising from aircraft charge" [MARKSON, 1975], and this may be done by mounting the probes symmetrically above and below the airplane wing tip (Pl. 24). If the probes are radioactively too strong (i.e. if its alpha ray emission is too intense) then the electric potential to a considerably further distance from them will be affected, and the measured ambient potential will not provide a good approximation for the true ambient potential. A radioactive coating substance producing beta and gamma ray emissions will affect the electric potential even farther away than coating substances producing only alpha rays. A weak probe does not affect the air around it enough, thereby increasing the amount of time required to attain potential equilibrium. Finally, there is the factor of aircraft charge. Its potential detrimental affects are not necessarily avoided simply by judicious placement of the probes. These measurement difficulties make electrical field detection far less desireable for   field work than it might otherwise seem.

4.7   Other airplane techniques

Roll vortices may be detected and measured through airplane monitoring of the most common meteorological parameters of the three wind speed components, temperature and humidity. By flying a course slightly off perpendicular to the geostrophic wind so as to cut transversely across potential roll vortices, horizontal fluctuation profiles of v, w, T and ρ_v can be obtained, and from these, roll vortices wavelengths are deriveable (Figs 31 and 32).

All the charts in Figure 32, with the exception of the u profile, display a periodicity in their peaks of approximately half a minute. This is the mean time interval between encounters of the sensing devices of the various parameters and the regions of maximum fluctuation of these parameters. Presumably, this is also the mean time interval between encounters of the plane and zones of air uplift in roll vortices. By multiplying this mean time interval, which is the period of the secondary-flow/plane system, by the velocity of the plane relative to the air, which for a cross-vortices flight would be adequately approximated by the

speed of the plane relative to some fixed point on the ground, a secondary flow wavelength is calculated. For example, using the period of ~ 30 s and assuming a typical small plane speed of ~ 70 m/s, a roll vortice wavelength of ~ 2100 m is obtained. This value is a reasonable typical value both for roll vortice wavelength and for linear dune spacing. It is also close to the wavelength value obtained from calculations using the frequency spectra of Figure 27, which must be so, for the frequency spectra of Figure 27 derive from the same original data as the profiles of Figure 32.

In Figure 32, the v profile varies in inverse proportion to the w, T and ρ_v profiles. It is anticipated of roll vortices that where v is at a maximum, w, T and ρ_v are at a minimum and vice versa. Approaching zones of air uplift, v decreases and w increases. T and ρ_v also increase because of the upward advection of air of greater T and ρ_v from below.

Measurements for the charts of Figure 32 were obtained at ~ 175 m above the surface, which is an optimal level for roll vortices observation. Close to the bottom and top of roll vortices, v fluctuations would be particularly pronounced, but w, T and ρ_v variations would be damped. At a level close to the middle of roll vortices, distinct variations in w, T and ρ_v might be obtained, but changes in v would be comparatively small. It is only at levels one quarter roll vortice thickness from the top and bottom of roll vortices that yields substantial variations in all four relevant parameters.

Each set of observational cross-wind flights must be accompanied by a set of observational flights parallel with potential roll vortices (Fig. 33). Any strong, non-random periodicity in u, w, v, T or ρ_v detected during these flights more or less aligned with the mainstream would rule out roll vortices. Parameter flux both across and along the wind would be evidence of discrete circulation cells not unlike Bénard cells.

For airplane measurements of the three wind speed components, it is necessary to know the velocity of the plane relative to a fixed point on the ground at all times, at any elevation and in any orientation. To do this, the observation plane must either be equipped with an inertial navigation system or tracked by double Doppler radar. An inertial navigation system is an advanced type of navigation system, which is not standard equipment for most small planes, and if both double Doppler radar and a plane were available for research, emphasis would not be on the sensing of wind vector components but rather on the monitoring of air circulation marked by airplane-released chaff. In conclusion, the sensing of wind vector components is not a viable alternative for the observation

of roll vortices in deserts. Incidentally, large meteorologically-instrumented planes that have inertial navigation capability are owned and operated by various scientific research organizations around the world. Unfortunately, none of these are stationed close to active desert linear dune fields.

Of the two remaining parameters – temperature and absolute humidity – humidity is discarded as a possibility for desert roll vortices observations for the simple fact that deserts are usually dry, particularly during summers. Temperature stratification close to the ground, on the other hand, is maximal in deserts during summers. This is attested to by the occurrence of optical phenomena, such as inferior mirages, that require relatively large vertical temperature gradients [FRASER, 1979] (Sec. 4.17). Consequently, the potential for vertical temperature advection is great. Before it can be concluded that temperature sensing is indeed a practical alternative as well as a physically desireable one, it must be determined that adequate temperature sensing devices for plane monitoring exist and are purchasable at relatively low cost.

In past empirical studies of roll vortices [LEMONE, 1973; LENSCHOW, 1970], simple resistance wire thermometers mounted on a special aircraft foremast were used to sense temperature [LENSCHOW, 1972] (Pl. 25). The sensing element of one of these thermometers was a meter long length of 0.0025 cm diameter tungsten wire directly exposed to the airstream [LENSCHOW, 1972]. Care was taken to insulate the supports so as to reduce heat conduction that would otherwise affect the accuracy of readings. One possible shortcoming of this system, despite its simplicity, is that it may require the fairly sophisticated mounting that is the foremast. For a small plane with a nose propeller, an instrumented foremast cannot be used. Some small planes have diagonal struts under the wings, and these struts may possibly provide a frame for mounting. However, if this alternative were chosen, care would have to be taken that the instrument were mounted beyond the flow region directly affected by the wing.

The attributes of a good thermometer for use in roll vortice observation in deserts are as follows: (i) It must shield its sensing element from solar radiation (and terrestrial radiation where extreme precision is demanded), which would heat it and raise readings. (ii) It must isolate its sensing element from moisture and solid particles. The former would lower readings through evaporation and the latter, in the case that enough particles came to be attached to the sensing element so as to coat it, would raise readings through insulation. (iii) It must protect the sensing element from damage. And finally (iv) It must be small enough and of a suitable form such that it can be mounted to a small plane without detracting from its operational efficiency. It would appear that to meet

the above criteria, a thermometer known as a reverse-flow temperature probe is best (Fig. 34) [RODI and SPYERS-DURAN, 1971] .

In this device, a platinum sensing element is contained in a cylindrical or bullet-shaped encasement that only opens to leeward of the air flow relative to the plane in flight. As air streams passed the end of the encasement, a considerable negative pressure gradient directed towards the interior of the encasement arises, and a reverse flow results. In the course of the 180° turn executed by the air in reverse flow, water droplets and solid particles are lost or 'thrown off.' The greater momentum of droplets and particles due to their greater density, causes them to continue in a fairly straight trajectory as the flow around them curves. Subsequently, they are advected away by the mainstream. Thus, the air encountered by the sensing device is comparatively pure. In the improved reverse-flow temperature probe, air exits through exhaust tubes.

If this probe is to be mounted onto the diagonal support struts of a wing, it must as with the resistance wire thermometer, be positioned far enough away from the body of the wing and especially its tips so that the sensing device is not in contact with the turbulence generated by the wing. The design of either reverse-flow temperature probe is such that the mounting of this device to the wing of a small air plane would be feasible. In conclusion, aircraft temperature sensing as a means for roll vortices observation is practicable as well as physically advantageous.

4.8   Recommendation for empirical research

Because roll vortices as an ordering mechanism for longitudinal dune fields with uniform spacing is testable for refutation, it deserves priority in empirical investigation of longitudinal dune field study. The mode of observing roll vortices in longitudinal dune fields should be by measurement of horizontal temperature profiles from continual temperature sensing using a reverse-flow temperature probe mounted onto the wing of a small plane and during flights at one quarter of the potential roll vortex depth (150-300 m). Moreover, observational flight paths must be (i) approximately 15° off mainstream to the left in the northern hemisphere and to the right in the southern hemisphere and (ii) approximately 15° off-normal to the mainstream, again, to the left in the northern hemisphere and to the right in the southern hemisphere.

Care must be taken to choose a field site where the linear dunes are active. The winds in relic linear dune fields may be considerably different to

the formative winds with regards to intensity, frequency, duration, direction and structure. For these reasons, the relic Australian linear dune fields would be poor choices for roll vortices studies. It has been suggested that a linear dune field, which is quite possibly a longitudinal one as well, about 100 km to the south of Cairo would be the most suitable site for dynamical study [BAGNOLD, pers. comm., 1983]. This recommendation was probably made mindful of logistic convenience and availability of fairly relevant long-term meteorological records. Libyan and Saudi Arabian sites may be similarly suitable.

Chapter Five: Empirical field results

One of the main thrusts of the field trials was to ascertain the nature of flow and secondary flow around a linear dune. Secondary flow in the form of windwardside rotors, leeside rotors and longitudinally aligned roll vortices were detected; however, circulation wavelengths of these secondary flows could not be measured due to lack of instrumentation. Several techniques were tried for the monitoring of deposition/erosion, sand firmness changes and topographic changes over a linear dune, and these yielded some useful information. The results and methods developed form the focus of this chapter.

Field experiments were carried out from December 7, 1982 to February 11, 1983, in the Strzelecki Desert of central Australia, and in September, 1982, in the littoral dune fields of the northeast Tasmanian coast adjacent to Bass Strait. One predominantly bare desert linear dune was found ~ 15 km south of the main Moomba gas camp (of SANTOS oil and gas company) in the northeastern part of the Strzelecki Desert (Fig. 35 and Pl. 26). It was on this dune and in its immediate vicinity that the most extensive and successful field trials were conducted.

5.1   Orientation and morphology
of the linear dune studied

The longitudinal axis of the study linear dune close to its northern end is oriented almost due north-south (Fig. 36). In the central Australian linear dune fields, Y junctions predominantly open towards the south, indicating propagation towards the north. Therefore, the northern end of the study dune is called the 'head' of the dune in this thesis. At ~ 2.5 km south of its head, the longitudinal axis of the study dune is oriented NNE-SSW at ~ 5° left of a north-south axis (Fig. 36). The longitudinal axis of the study dune remains in this orientation until ~ 3.3 km south of the head (Fig. 36). To the south of this point, the longitudinal axis of the dune is oriented NNE-SSW or ~ 10° left of a north-south axis. The linear dune has two bends of ~ 5° in its plan form.

The linear dune seems to rest upon a very broad, linear base of fairly firm material. Both flanks of this base has very slight slopes. The eastern flank of the dune proper is considerably less steep (Pl. 27) and more vegetated (Pl. 28) than the western flank at all points. As a whole, the study dune is sparsely vegetated and nearly bare from the head to ~ 1.7 km south of the head. Past ~ 1.7 km, the flanks, especially the western one, is covered by patches of brush, and from

past ~ 2.1 km, there are bunches of small trees at intervals along the western flank. Past ~ 2.7 km, the entire dune is covered by sparse vegetation, mostly grasses and small shrubs.

From the dune head to ~ 0.8 km south of it, the dune is comprised of a series of rounded summits at a uniform separation of ~ 0.1 km. Each summit has a small slip face in the form of an avalanche slope on the western flank, and each slip face is oriented such that the normal to the plane tangent to its center is directed towards the general direction of NNW. From ~ 1.1 km south of the dune head to ~ 2.7 km south of the dune head, the subsidiary dune summits are peaked and remain at a mean separation of ~ 0.1 km (Pls 29 and 30).

Where the dune surface is bare there are surface ripples, which are perpendicular to the direction of the prevailing winds. The ripples in the middle section of the dune are particularly important (Pl. 31). Because these surface ripples advance along an axis normal to their own longitudinal axes, the ripples in Plate 31 are moving towards the observer and out of the plane of the picture. Also, because their direction of advance is parallel to the prevailing winds that control them, they seem to indicate a wind that is nearly aligned with the longitudinal axis of the dune. Note that in the background (or to windward) a portion of a surface layer has begun to slide down the slope. The boundary of the sliding layer portion is quite discrete, and the breakage was set off during a hike along the crest just above it.

From ~ 2.7 km southward, the subsidiary summits lose their peakedness once again. This may be due to the greater vegetative cover over the dune from this point onwards. From ~ 3.0 km onwards the summits are no longer at uniform intervals; summits occur at ~ 3.0 km, ~ 3.3 km and ~ 3.5 km. Beyond ~ 3.5 km, there are no discernible summits.

The transition from dune to interdune corridor is quite abrupt in many places on the western side but obscure all along the eastern side. In places on the western side, the loose sand of the slip face meets the firm material of the corridor with no intermediate stage (Pls 32 and 33). Over much of the western side however, the avalanche slope meets an intermediate slope of much lesser inclination. It is this intermediate slope that rests directly upon the broad, firm base spoken of earlier (Pl. 34). On the eastern side, the gentler sloping flank merges with the interdune corridor very gradually, so no clear boundary between the dune and the interdune corridor exists (Pl. 28).

The most curious features of the eastern side of the dune were grassy, sandy rises in the flank and more or less circular clay flats along the flank on the

interdune corridor. Both features occurred periodically at ~ 0.1 km intervals, and past ~ 1.4 km south of the dune head, nearly every summit, whether peaked or smooth, was associated with either a grassy, sandy rise or a clay flat. Each clay flat was situated between two grassy, sandy rises and was populated by shallow clay mounds. Both in their plan shape and in the venation pattern of the shallow grooves to either side of their crests, these clay mounds resemble elongate leaves with slightly convex flanks. These clay mounds and their surface features are possibly the products of water erosion (Pl. 35).

During the study period, the area around the dune was variable in vegetative cover. Some areas were fairly uniformly grassed; some had low, woody vegetation and small trees. Some areas were quite sandy, whilst others were pebbly (Pls 36, 37, 38 and 39).

The study dune divides at ~ 7.5 km south of its head (Pl. 26). It also approaches coalescence with its eastern neighbor at ~ 12.5 km south of its head and again at ~ 15 km south of its head. The predominant winds in the area are from the south; therefore, either of the two above potential coalescences would have resulted in a Y junction whose fork opened to leeward, which is contrary to the general trend.

There is evidence that the core of the study dune was wet during the observation period. On December 9, 1982, wet sand was found at a depth of ~ 35 cm on the dune crest ~ 4 km south of its head. On January 28, 1983, wet sand was found at a depth of 50 cm ±10 cm on the dune crest at ~ 33 m north of the northern perimeter of the study site. Wet sand was found at a depth of 25 cm ±10 cm near the foot of the western flank of the dune at ~ 33 m north of the northern perimeter of the study site.

5.2   The study site

A small section of the dune was chosen as a study site with dimensions of ~ 30 m along the longitudinal axis of the dune and ~ 65 m transversely across it. The study site was in that sector of the dune aligned ~ 5° NNE-SSW. It included two small adjacent rounded summits, the saddle-shaped trough between them and the small but distinct avalanche face to leeward of the larger and more southerly of the two summits. Because some attention is paid to the monitoring of deposition and erosion over the study site, the inclusion of two adjacent summits allowed for the observation of a complete wavelength of the

periodic variation of the dune along its longitudinal axis. The larger summit is centered at $\sim$ 0.3 km from the head (Fig. 36).

Figure 37 is a form line sketch of the study site, for which the height difference between form lines is probably a little less than 0.5 m. The grid points represented by dots, circles and dot crosses are related to two experiments (Secs 5.11 and 5.15). It is interesting to note that the elongated avalanche face close to the southern summit was ephemeral and appeared twice between December 9, 1982 and December 24, 1982 and between January 29, 1983 and February 1, 1983. Topographic change in general is discussed in Section 5.14.

The western side of the study site was, throughout the observation period, nearly bare to the base, and the eastern side had sparse vegetative cover in the form of patches of mostly dried grass and dried small woody plants (Pl. 28). The study dune is parallel with its two neighboring linear dunes, which are more densely vegetated. From the study site, the next dune to the west is $\sim$ 3 km away, and the next dune to the east is $\sim$ 1.7 km away.

Erosion/deposition, change in surface firmness, colored sand transport and wind vector variation over the study site were monitored. Tethered kite trials were conducted in the immediate vicinity of the study site, and balloons were released from the study site in an attempt to track their movement.

5.3   Leeward side rotors

On December 13, 1982, two rectangular patches of different colored sand were laid out to either side of the high point of the larger, southern summit of the study site. These patches were placed $\sim$ 1 m south of the periphery of the study site, and their dimensions were $\sim$ 0.5 m $\times$ $\sim$ 3 m $\times$ 0.015$\pm$0.005 m. The green patch was $\sim$ 6 m west of the summit peak, and the blue patch was $\sim$ 1 m east of the summit peak.

The sand was colored using a pigment and a polymer binder in solution. Once dried, the colored sand conglomerated into cakes, which were pulverized manually. Consequently, a small but significant proportion of the sand remained as aggregates ranging in size from large grains to small pebbles (App. 10).

On the morning of December 16, the winds were of mean speed 11 knots ($\sim$ 5.6 m/s or $\sim$ 20 km/hr) and directed from the SSE at $\sim$ 150°. Sand movement was relatively vigorous. At 8:00 AM sand was streaming from the peaked summits in plumes. That afternoon, winds were fairly calm at 3 to 4 knots,

and on the avalanche or lee slope, an arc of green and blue sand had formed. This arc at its highest point was about one third distance up the avalanche slope, which was itself $\sim$ 2 m in depth. Notably, a considerable proportion of the colored sand particles in the arc were the large aggregates, which would have required considerable wind energy to move against gravity up a steep slope. This arc is taken as evidence of a strong leeward side rotor (Fig. 38).

Subsequently, the colored arc disappeared under the influence of moderate winds and reappeared only during easterly winds such that the avalanche slope was to leeward. When the arc was not in existence, the colored particles that had partially comprised the arc lay at the foot of the avalanche slope. Bits of burnt material and dried material, both presumably of vegetative origin, had also partially comprised the arc*.

It is interesting to note that during strong winds the colored patches, which in large measure consisted of the big aggregates, became raised surfaces. This is in keeping with the conjecture that large particles will shelter the smaller particles in their vicinity from the wind such that the smaller particles are stabilized and not transported away [BAGNOLD, 1941]. During moderate winds, the colored patches sometimes became completely covered over by fresh uncolored sand drift, and this terminated transport of colored sand.

5.4   Windward side rotors

In the late afternoon (5:00 PM), on December 17, 1982, the wind was blowing at $\sim$ 13 knots ($\sim$ 6.7 m/s or $\sim$ 24 km/hr) and from $\sim$ 220° SSW, which made it slightly oblique to the dune and incident upon the western flank. These wind measurements were, as were all other general wind measurements, taken at $\sim$ 40 m west of the study site. It was a clear, hot day, and inferior mirages, indicative of vertical temperature gradient close to the ground were visible in the distance (Sec. 5.16).

A kite tethered to a vehicle, which was parked $\sim$ 10 m to windward of the study site, flew such that, along an axis transverse to the longitudinal axis of the dune, its flight component was contrary to that of the mainstream. A ribbon beneath the kite fluttered in the same direction as the mainstream. During strong gusts (over 15 knots), the kite's departure from the mainstream along the

---

* Particles of burnt material found all over the dune suggested that the dune may have been more heavily vegetated only recently.

transverse axis was about twice the magnitude as its departure during moderate gusts (Fig. 39). This flight behavior is taken as evidence of a windward side rotor. No evidence of a leeward side rotor was found at this time.

The kites during all kite trials were of the delta wing type with a wing span of ~ 160 cm and a head to end length of ~ 75 cm (Fig. 40). They are made of cotton cloth with a frame of light wood. In all instances, an ~ 50 m cord of ~ 50 kg strength was used to tether the kites. The plastic kite tails were each originally ~ 6 m long, but are now, after flight, stretched to ~ 6.5 m long. The flaps on the underside of the kites are ~ 15 cm deep and are used for attaching the kites to their tethering lines. In constant winds, the kites flew steadily without attendance, typically for ten minutes or so.

It should be noted that all given inclination angles of the tethering cord, which were taken at the point of tethering, are slightly smaller than the inclination angles of straight lines connecting the kites and their tethering points. This is due to the sags in the tethering lines due to their weight, which caused them to be slightly parabolic rather than perfectly straight. The differences between the given inclination angles and the ideal inclination angles are not great.

5.5   Kite flight

Because of their inclined orientation in the wind, kite flight may be sustained by purely horizontal flows. Therefore, kite flight, though good for indicating the lateral tendencies of the wind, should not be considered too similar to linear soaring of birds, which can occur only in rising air.

It has been suggested that lighter-than-air balloons may be preferable to kites. Because of their nearly spherical form their tethered flights would presumably offer less directional bias than those of kites. In actuality, the opposite is likely to be true. Tethered balloons would rotate at the end of their lines and possibly at such a rate that Magnus effect, which is a force normal to the direction of fluid flow that acts upon rotating cyclindrical and spherical objects , would cause the balloon to mislead the observer as to the flow direction. Depending upon the rotation and flow rates, Magnus effect can be an important force. From a purely practical point of view, kites trials, without the recurring high cost of gas, would be more economical.

5.6   Roll vortices

In the afternoon (3:00-4:00), on December 18, 1982, the wind was moderate at ~ 10 knots (~ 5.14 m/s or ~ 18.5 km/hr), gusting at ~ 14 knots and from ~ 164° SSE. This made it ~ 15° obliquely incident upon the study dune. There was some shifting in the winds between a slight SSE orientation to a slight SSW orientation. There were cirrus clouds in the sky, and this indicated upper air moisture. Other than high clouds the sky was clear. There were inferior mirages in the distance. It was a relatively hot and windy day.

Four kites were flown simultaneously. One was tethered ~ 10 m to the west of the dune's western periphery, and one was tethered ~ 15 m to the east of the dune's eastern periphery. Two were tethered to the east of the dune beyond the first kite on that side. These were set ~ 50 m apart. The kite furthest east would not sustain flight. This was possibly due to turbulence as a result of the low woody vegetation (1-2 m in height) in the area.

The kites to either side and adjacent to the dune sustained flight contrary to one another for several minutes. That is, the one to the west of the dune flew towards the east, and the one to the east of the dune flew towards the west. They indicated flow with oppositely directed wind velocity components along an axis transverse to the dune. The second kite to east of the dune flew with a similar orientation to that of the first kite (Fig. 41). During the observation of contrary flight between adjacent kites, the wind seemed aligned to the dune. This overall flight pattern is taken as evidence of the occurrence of roll vortices about the dune.

In the early afternoon (2:00-2:30PM), on December 23, 1982, the winds were variable both in magnitude and direction. For the most part they were from the north or NNE and moderate at ~ 7 knots (~ 3.60 m/s or ~ 13 km/hr). It was a hot, overcast day. Mirages were visible, and dust devils were observed.

Two kites were flown simultaneously with one to either side of the dune. Their locations with respect to the dune are the same as those of the adjacent kites in the last trials described. During northerly, moderate winds, the two kites flew in opposition to one another, similarly as did the two adjacent kites in the last trials (Fig. 42). This flight pattern was sustained for several minutes, and it is also taken as evidence of roll vortices.

5.7   On kite trials

Although evidence of certain forms of secondary circulation were obtained during kite trials, wavelengths of these secondary circulations could not be measured.   Working alone, no more than four kites could be maintained simultaneously at $\sim$ 50 m separation. This limited the line of observation to at most $\sim$ 200 m, which is far too small for measurement of secondary circulation estimated to be in the area of 2000 m in wavelength.

To observe roll vortices in linear dune fields, 22 kites tethered at $\sim$ 100 m separations along a line transverse to the direction of the the dunes would be adequate. Twenty of the kites would lie between two adjacent dunes, and two of them would be set just beyond the outer flanks of the two dunes (Fig. 43). This should allow the marking of one wavelength of the phenomenon. During roll vortices, kites in the zones of surface convergence and air uplift, should be observed to fly in opposition to one another along the transverse axis to the mainstream, and kites in the zones of surface divergence and downdraught, should be observed to have extreme difficulty in staying aloft.

Tethered kites offer a simple yet elegant and relatively inexpensive means by which to observe secondary circulation.   However, the great number of workers necessary for the observation of larger scale motions may diminish its practicability. There is also the problem of coordinating workers who are spread out over a substantial distance, for measurements of tethering cord angles should be made simultaneously. For roll vortice observation specifically, tethered kite trials are not as desirable as airplane monitoring of air temperature, which allows for measurement of many wavelengths of the secondary circulation activity.

5.8   Quasi-laminar flow

Throughout the day on December 19, 1982, the winds were at $\sim$ 13 knots ($\sim$ 6.70 m/s or $\sim$ 24 km/hr) and from between 150° and 160° SSE, which meant that winds were between 25° and 35° obliquely incident upon the eastern flank of the dune. It had been windy the night before, and in the morning, which was cool, there were cirrus clouds and middle level clouds. Cloud cover dissipated somewhat as the day wore on and the temperature rose. In the afternoon, sand plumes towards the west were seen streaming from the peaked summits, and mirages became visible.

In the afternoon, the flight patterns of four tethered kites were observed. Two were located to the west of the study site and two were located to the east.

The kites furthest east and west would not stay aloft. Here, as at all other times during the trials, when a kite would not stay aloft, it was replaced by another kite. This was done to reduce the possibility that the inability to sustain flight was due to any defect of the particular kite in question. The kite furthest to the east was tethered in an area of low, woody vegetation, which might possibly have caused the air flow in the vicinity to be turbulent. The kite just east and to windward of the dune flew at a higher elevation than the kite just west and to leeward of the dune (Fig. 44). This pattern in which the flow velocity had a slight increase in its vertical component over the dune is the pattern intuitively expected when the wind is more than 15° oblique to the dune and empirically suggested by discrete wind speed and direction measurements made over the body of the dune (Sec. 5.9).

In the early morning of December 18, 1982, the winds were nearly aligned with the dune at the study site. By 9:30 AM, the wind had shifted to $\sim 160°$ SSE, making it $\sim 25°$ oblique to the dune. Wind speed was ~ 12 knots (~ 6 m/s or ~ 22 m/hr), and there were sand plumes directed towards the west from the peaked summits. The air was warm, and there were a few faint cloud streaks in the sky.

The configuration of the kites was such that wind velocity had the greatest vertical component some short distance (50-60 m) east and to windward of the dune (Fig. 45). The wind flow pattern suggested by the flight of the kites seems to indicate that the dune affected the flow to windward of it. Although the above form of flow is turbulent, it is without any prominant secondary circulation and has, for this reason, been labelled quasi-laminar.

A different and somewhat peculiar kite flight configuration was observed on the morning of December 18 and on the afternoon of December 19. The kite east and just to windward of the dune was lower than the kite to west and just to leeward of the dune (Fig. 46). During the December 19 occurrence of this flight configuration at least, the winds seemed more than usually oblique to the dune at $\sim 35°$ to its longitudinal axis. This kite flight configuration is peculiar in that it is difficult to imagine what sort of air flow pattern it may correspond to.

5.9   Wind velocity over the dune

Surveys of wind speed and direction variation over the dune were conducted on average twice a day, on certain days between December 9, 1982 and

February 1, 1983. Before considering the survey procedure, which is not straight forward, a brief discussion of the measurement techniques, which influenced the form survey procedures is warranted.

The wind direction in the horizontal plane was obtained at any given point by standing to leeward of a pole or stake planted in the sand with a nylon ribbon tied to it at ~ 1 m above the surface and measuring the direction exactly opposite that towards which the suspended ribbon was directed. For these direction measurements an orienteering compass was used.

The vertical wind direction was obtained using a custom built electronic wind vane (*see* Acknowledgements), whose design and operation require some attention. An aluminum rod 885 mm in length and 5 mm in diameter forms the wind vane shaft. At the head is attached an aluminum weight whose purpose is to counterbalance the the tail wing, which is cut from a 11 mm thick styrofoam sheet and has a shape similar to that of the tail of an arrow (Pl. 40). The pivot point of the shaft coincides roughly with the center of a solid brass cylinder through which it passes and to which it is fixed by a grub screw. The shaft is so set that the tail wing is normally fairly level with the ground, which makes the tail wing sensitive to vertical air motion. It is this capacity that allows the device to detect and gauge the vertical component in the wind velocity vector.

The pivot point cylinder is directly attached to the shaft of a variable resister, so that the vertical orientation of the vane is registered on a current meter with DC 100 microampere range. There is a plastic protractor attached to the fixed mounting encasement of the variable resistor, and there is a straight, thick, red aluminum wire attached to the pivot point cylinder. The red wire may be adjusted at its base so that when the vane is level, it lines up with the 90° mark on the protractor. This indicator allows for the calibration of the electronic orientation meter.

The relationship between degrees and microamperes is linear, and a change in vane orientation of one degree illicits a response in the current meter of 1 milliampere shift. Normally, 100 ma corresponds to 106° and 0 ma corresponds to 2°. The precision of the meter and the variable resistor are not a very high standard, and slight departures from linearity in the relationship between angle and current occurred at random points over the angle and current ranges. The measurements made with this devise could therefore only be used as fair estimates. However, considering the variability of even a steady wind, the degree of accuracy provided by this wind vane is probably adequate.

The head of this device, where the moving elements are all located, may itself be rotated and fixed at various orientations. For example, it may be turned 90° such that the tail wing of the vane is perfectly vertical. This converts the instrument to a wind vane for the horizontal plane of air motion. The mountings of the device are all made of hard plastic, and below the joint for the head is a short solid plastic shaft, which is fixed to a steel pipe. For measurements, the instrument is mounted on top of a ~ 2.4 m wooden pole by inserting the head of the wooden pole into the hollow end of the steel pipe. The distance from the pivot point to the end of the wooden pole is a little more than 2.5 m. During measurements, when the pole is planted up to 0.3 m into the sand, the pivot point will be between 2.5 and 2.2 m above the surface (Pl. 41).

The measurement technique was very simply to plant the wooden pole into the sand at the point of interest and to read the current intensity. The angle of wind vane inclination and therefore the vertical angle of flow could be directly calculated from the amperage registered on the meter. Care was taken during measurements to hold the pole so that it was as nearly vertical as possible, and this was aided by a bubble attachment to the wooden pole in some later measurements.

Wind speed measurements at all points were made using standard hand held cup anemometers held at arms length (at a height of ~ 1.4 m) into the wind. Measurements of wind speed as well as various other parameters were not very accurate, and all measurements were necessarily discrete. That is, simultaneous measurements at two or more points were not possible as these observations were taken singlehandedly. However, for the most part, prevailing winds were fairly steady, and this allowed for reasonable assessments of the relative magnitudes of various parameters over the body of the dune.

Relative wind speed measurements were conducted along the same transverse line across the dune as that for the wind direction measurements. In this procedure, this line was traversed from west to east three times and from east to west three times for each survey. During each traverse, an anemometer was held to windward and relative wind speed values were noted at various points on the dune. In this way, the general characteristics of flow over the dune were identified. Figure 49 is an example of a survey record for relative wind speeds over the dune.

Surveys were conducted once in the morning and once in the afternoon on Decembers 9, 11, 12, 14-19, 22 and 23, 1982, January 29, 1983 and February 1, 1983. On certain days only two of the three parameters were measured.

The initial step of each survey was to measure the wind direction both in the horizontal and vertical planes using the methods described above at 4 m intervals across the southern transverse perimeter of the study site.

Horizontal-plane directional flow vectors – horizontal plane vectors indicating flow divergence only – across the dune were successfully surveyed 12 times during the 13 observation days (Fig. 47). Analyses revealed that in 7 instances flow divergence occurred to windward of the crest and flow convergence to leeward of it. These instances occurred during winds more than $\sim 30°$ obliquely incident upon the dune at the study site. In the remaining 5 instances, there was no discernible pattern. Of these 5 instances, two occurred during oblique, shifting winds, two occurred during winds nearly parallel to the dune at the study site and one occurred during oblique winds that were not shifting. It is concluded that generally during oblique winds flow divergence occurs to windward of the crest and flow convergence occurs to leeward of it (Fig. 50).

Vertical-plane directional flow vectors were successfully surveyed 11 times during the 13 observation days (Fig. 48). In 8 instances of the 11, the flow had its greatest vertical upwards component to windward of the crest. These instances occurred during oblique winds. In one instance, there was no discernible organized configuration of vertical-plane directional flow vectors over the dune. This took place during nearly parallel winds. In two instances, the flow had a general vertical downward component over the dune. Both these instances were observed on December 18, the day that roll vortices were evidenced during kite trials. The air may have been unusually stable on that day. It is concluded that generally the wind attains its greatest upward component just to windward of the crest when the wind is obliquely incident upon the shallow sloped flank, and just to leeward when the wind is obliquely incident upon the avalanche slope (Fig. 51).

Wind speed over the dune was successfully surveyed 11 times during the 13 observation days. In four instances, greatest relative wind speed occurred to windward of the crest. In another four instances, maximum wind speed occurred either just to windward of the crest or at the crest. These first eight instances occurred both during winds that were oblique and winds that were within 30° of the dune and both during steady and shifting winds. In one instance, maximum wind speed occurred to leeward of the crest, and in one instance, there was no discernible pattern. Finally, in the last remaining instance, maximum wind speed occurred to leeward of the crest on three of the six survey traverses across the dune and to windward of the crest on three of the six survey traverses across

the dune. It is concluded that maximum wind speed generally occurred in the vicinity of the crest and usually to windward of it.

Though measurements were not made simultaneously during any of the surveys, there is some confidence in the general conclusions drawn for horizontal-plane flow vector divergence and convergence over linear dune during oblique winds and for the vertical-plane flow vector variation over linear dunes during oblique winds. This confidence is inspired by the fair degree of uniformity in survey results. The general conclusion for wind speed variation over the dune is much more doubtful. Both the survey technique and the analysis of survey results were to a degree necessarily subjective. The value of the general conclusions lies in their potential usefulness in the mathematical analysis of linear dune genesis and evolution (Sec. 6.3.6).

5.10   Form drag

It would seem that dunes act directly upon flow to cause variation in the horizontal-plane flow vector during oblique winds, or in other words, form drag offered by linear dunes to oblique flows influence the structure of these flows. It may be easier to see that form drag is responsible for variation in the vertical-plane flow vector over linear dunes. Quite simply, oblique flows encounter the slopes of linear dunes and are deflected upwards. Mass conservation compels the flow to descend again beyond the crests of linear dunes and conform to the leeward dropping slopes.

5.11   Deposition and erosion

Deposition and erosion over the study site were closely monitored on a daily basis through a simple technique using a grid of 148 ~ 2.5 cm × 2.5 cm × 1.225 m wooden stakes (Pl. 42). Eightysix stakes were first planted over the part of the study site that was bare of vegetation. These stakes are designated by dots on Figure 37 and were set on December 8, 1982. Each one was ~ 4 m away from each of its adjacent stakes and protruded ~ 65 cm vertically above the surface. By measuring the length of the stakes above the surface regularly the height of sand accumulation or the depth of sand evacuation around each stake could be calculated. Additional stakes were subsequently added to the grid in the partially vegetated areas: 15 on December 10, 1982 and 47 on December 11, 1982. Of these stakes all had an original protrusion above the surface of ~ 62 cm

except for the 16 stakes that formed the eastern- and western-most complete columns, and these were each ~ 72 cm above the surface. The two western-most individual stakes were each ~ 92 cm above the surface. These 18 exceptions were not set as deep as the rest of the stakes because the ground they occupied was firm and difficult to drive stakes into.

Stake measurements were made once in the morning and once in the afternoon for as many days as possible between December 9, 1982 and December 24, 1982. Stake measurements were also made on December 29, 1982, January 14, 27, 29 and 30, 1983, February 1, 11 and 23, 1983, March 3 and 23, 1983 and April 10, 1983. A total of 28 surveys was conducted. Relative deposition and erosion over the study site could be assessed for the interval between any two surveys by calculating the height of sand accumulation or depth of sand evacuation around each stake. For days on which both a morning and afternoon survey were conducted, the interval between these two surveys was on average about seven hours. This period proved too short for a discernible deposition/erosion pattern to emerge. However, for periods on the scale of days, some idea of the areas of deposition and erosion over the dune can be ascertained, provided of course, that winds during the period were vigorous enough to cause sand transport. Figure 52 is a typical deposition/erosion record. Positive values indicate height accumulation (deposition) around stakes in cms, and negative values indicate depth of sand evacuation (erosion) around stakes in cms.

Winds on the afternoon of December 16, 1982 – the time of commencement for the assessment interval associated with Figure 52 – and on the morning of December 17, 1982 were ~ 4 knots. On the afternoon of December 17, the winds increased to about 13 knots, and on the morning of December 18, 1982 – the end of the assessment interval – the winds were ~ 12 knots. Therefore, the deposition/erosion pattern of Figure 52 is the result of less than 24 hours moderately strong winds.

For periods on the scale of weeks, a clear pattern of deposition and erosion emerges (Fig. 53). Yellow regions of the chart correspond to areas on the dune where substantial erosion – sand evacuation greater than or equal to 5 cm – occurred. Light blue regions correspond to areas where substantial deposition – sand accumulation greater than or equal to 5 cm – occurred. Darker blue regions correspond to areas where greater deposition of sand took place ($\geq$ 25 cm). During the 10 day assessment interval between December 14, 1982 and December 24, 1982, wind measurements were made on 8 days. On 5 of the 8 days mean winds were from either SSE or ESE, and on 4 of these 5 days of southeasterly winds, mean wind speed was above that of sand transport. On

one day, mean winds were incident upon the western flank of the dune and also above sand transport threshold. On one day, winds were more or less aligned with the dune, and on one day, there were no significant winds whatsoever. It is concluded that sand transporting winds were generally from the southeast. The deposition/erosion pattern of Figure 53 shows maximum deposition to lee of the crest and, significantly, to southeast of the the larger summit. This is what was expected for the southeasterly winds during the assessment interval.

To a point, the longer the assessment interval, the more information is contained in the deposition/erosion pattern for it (Fig. 54). Orange regions of this chart correspond to areas on the study site where greater erosion of sand ($\geq$ 25 cm). Wind measurements were only taken for a few days during the 49 day assessment interval between December 24, 1982 and February 11, 1983, so it is not known whether the deposition/erosion pattern of Figure 54 is what might be expected of the sand transporting winds during the assessment interval or not. The deposition/erosion pattern seems to suggest a southeasterly wind.

In Figure 54, a secondary deposition maximum appears to the west of the main deposition maximum. It fits well with the approximate topographic contour lines of the western flank, which are included in the figure, and apparently corresponds to the foot of a westward extension at the southern end of the study dune's western flank. This secondary deposition maximum is also situated in a sparsely vegetated area. The erosion maximum on the southern summit is perhaps due to the exposure of that area to most winds, particularly quasi-laminar winds. The occurrence of the various other erosion maxima are difficult to explain. Of greatest interest are the three maxima that are situated to the west of the crest in an area interpreted as leeward for mean winds throughout the assessment interval. Leeward side rotor activity during southeasterly winds may be a viable mechanism for the formation of these erosion maxima.

The deposition/erosion pattern for the 59 day assessment period between December 14, 1982 and February 11, 1983 is remarkably simple and clear considering the length of time involved (Fig. 55). Deposition maximum lies to NNW of the primary summit, and the secondary deposition maximum lies to NNW of the western flank extension. An erosion maximum just to SSE of the primary summit is implied, and the erosion maximum that actually appears in the plot is located on the western flank extension directly to SSE of the secondary deposition maximum. These features imply fairly uniform mean winds from SSE.

The deposition/erosion pattern for the 58 day assessment period between

February 11, 1983 and April 10, 1983 seems to indicate dominant winds diminished in magnitude and different in orientation from those of the previous example, whose assessment period was of similar length (Fig. 56a). The deposition maximum in Figure 56 lies directly between the two summits, which strongly suggests nearly parallel winds. A limb of high deposition extends east from the southern extent of this maximum and is almost normal in orientation to the form lines that it intersects. This local deposition occurred very uniformly along the gradient of the slope. To either side of this tongue of deposition are parallel strips of fairly uniform erosion along the slope gradient. Though these striking features suggest a mechanism, no form of secondary flow readily suggests itself. These features may be manifestations of maximum local deposition under the wind conditions during the assessment interval and local topographic conditions.

Interestingly, these fairly even deposition and erosion strips along the slope gradient are aligned at nearly 45° to the longitudinal axis of the dune at the study site. They would also be at ∼ 45° with respect to winds nearly aligned with the dune. Finally, the slope on which they occur is locally rounded; in their vicinity, the form lines are approximately elliptical (Fig. 56b). Winds nearly aligned with the dune at the study site would be nearly aligned with the long axis of the elliptical contours that describe the local topography, and the deposition and erosion strips happen to occur in the regions of maximum curvature in these contours. It is possible that flow aligned with the long axis of an elliptical sand knoll results in maximum deposition and erosion obliquely or even nearly orthogonally across contours, to leeward of the summits and along the axis of maximum contour curvature. Over any elliptical mound, maximum deposition and erosion will probably also occur in the zone of surface flow convergence during parallel winds (Fig. 56b). This surface flow convergence is associated with flow separation and would not be unlike the flow separation in flow past spherical objects (Fig. 56c).

The pattern of Figure 56a suggests that the sand transporting winds during the assessment interval were mainly nearly aligned with the dune at the study site. In this case, the erosion maximum that corresponds to the shifted avalanche face might be due to the action of leeward side rotors. It is recognized, however, that the perimeter of the shifted avalanche face, which is demarcated in the plot by a line of open dots, was determined 12 days before the assessment interval commenced. Previously, the center of the avalanche face had moved ∼ 5 m in 53 days (between December 8, 1982 and January 30, 1983). Therefore, by the end of the presently considered assessment interval, the avalanche face may

have shifted again such that its placement and perimeter as of January 30, 1983 does not correspond well with the erosion maximum of the assessment interval in question. The diminished sand transport during the assessment interval, however, makes the above possibility less likely. In Figure 56a singularities, symbolized by question marks, exist in the field of deposition/erosion values. These singularities are points that can have no deposition/erosion value and arise because the stakes with which they are associated were removed sometime during the assessment interval.

The deposition/erosion pattern for the 117 day assessment interval between December 14, 1982 and April 10, 1983 seems to indicate southerly winds in general with the slight predominance of southeasterly winds (Fig. 57) An analysis performed by the personnel of SANTOS gas and oil company at Moomba camp actually indicate a predominance of southerly and southeasterly winds during summers [SANTOS, 1979]. Figure 57 may be taken as one sample of the local summer deposition/erosion pattern.

Two transverse rows of five stakes each were planted near the head of the dune. Stake separation was again ~ 4 m, and initial stake protrusion above the surface was ~ 65 cm. Both short term (December 17, 1982 to December 22, 1982 and January 14, 1983 to January 27, 1983) and long term (December 17, 1982 to February 11, 1983) analyses of the deposition and erosion in the staked area show erosion on the eastern side and deposition on the western side. This is interpreted to indicate windward erosion and leeward deposition (Fig. 58).

The method adopted in this study of deposition/erosion monitoring is both simple and relatively inexpensive. It can provide insight into the nature of predominant winds and their interaction with the dune forms they encounter. Also, it may be the only effective means available for deposition/erosion monitoring. Sand trap experiments measure sand transport rather than erosion or deposition.

It has been suggested that a grid of a large number of wooden stakes, even thin ones, may affect the air flow in its immediate vicinity by increasing the surface drag in that area [BAGNOLD, pers. comm., 1983]. This increased surface drag may, in turn, influence the deposition/erosion pattern over the observation area. This is a valid criticism of the method used. A slight trough was wind excavated around the base of each stake; therefore, local erosion was certainly increased by the presence of the stakes. The mechanism responsible for these troughs was probably small scale vortices in the air flow just above the surface due to encounter between local flow and the stakes (Sec. 8.2.1).

5.12   An apparent paradox

Analyses of the variation of the horizontal-plane flow vector over the study site showed divergence to windward of the crest and convergence to leeward of it. Flow divergence would normally be associated with sediment deposition and flow convergence with sediment erosion; however, deposition/erosion monitoring over the study site indicates the opposite tendencies.

Pure flow divergence causes deposition, but in this instance, horizontal-plane flow divergence was accompanied by an increase in flow speed to windward of the crest (Sec. 5.9). This horizontal flow divergence may have coincided with vertical flow convergence. When flow encountered the dune's windward flank, it is compelled to ascend the slope and converge with the overlying layers of flow. Such a flow convergence just above the slope surface might have induced sand transport. Therefore, the coincidence of horizontal flow divergence and erosion is possible.

5.13   Firmness

Linear dunes in the Strzelecki and Simpson Deserts, as with linear dunes in many other deserts, are not only asymmetric in transverse profile, but are asymmetric with regards to the firmness of the sand packing in the two flanks. This asymmetry in firmness can be related to the profile asymmetry in that the steeper flanks tend to have avalanche faces, which would naturally have the loosest packed sand in a dune. It has been shown that for dunes in the Strzelecki and Simpson Deserts loose sand accumulates on the eastern flanks [BREED and BREED, 1979] while wind erosion and the exposure of older material occurs on the far less steep western flanks [WOPFNER and TWIDALE, 1967]. As with the profile asymmetry, this asymmetry in firmness has been taken to indicate the lateral migration of the dune eastward, in the direction towards which the steeper less firm flank faces [RUBIN, 1985]. A distinct asymmetry in firmness was ascertained in the study dune, though the sense of this asymmetry, as with the profile asymmetry of the study dune, is opposite to that of Strzelecki and Simpson Desert dunes in general. For the study dune, the steeper and less firm flank was the eastern flank. Because the study dune was shown to migrate laterally eastward (Sec. 5.14), the idea that firmness asymmetry may be taken to indicate direction of lateral migration is in this instance supported.

Firmness was determined using a simple pole penetrometer. In the vicinity of each stake, a ∼ 2 cm diameter wooden pole of ∼ 2.4 m length was

inserted into the sand as far as it would go under a certain approximate force. For each measurement, the pole was initially held above head height and pulled down upon, allowing body weight to hang. Therefore, the force applied was the constant force of body weight, which in this case was ∼ 70 kg. The depth of penetration into the sand was taken as a relative measure of tightness of sand packing or firmness.

Firmness patterns for the study area were established for December 22, 1982 and for January 30, 1983 (Figs 59 and 60). The uncolored regions are areas of greatest firmness with penetration less than 20 cm. Regions in the lightest shade of green are areas of penetration greater than or equal to 20 cm, and regions in the middle shade of green are areas of penetration greater than or equal to 50 cm. Regions in the darkest shade of green are areas of greatest looseness, with penetration greater than or equal to 100 cm.

In Figure 59, the two firmness minima on the western flank occur over or in the immediate vicinity of avalanche faces. This is to be expected, for deposition due to avalanching is known to result in sand lamina of very loose packing [BAGNOLD, 1941]. Interestingly, the western firmness minima more to the south exists even when the shifting, ephemeral avalanche face it occurs close to vanishes. Apparently, firmness minima can indicate areas where avalanche deposition takes place periodically. Furthermore, firmness minima may occur where avalanche deposition took place in the past. That is, firmness minima may occur in an area that had been formed due to advance of an avalanche face but where no surface topographical manifestation of that avalanche face persists. Finally, the occurrence of firmness minima in any area is not necessarily evidence of an ephemeral or past avalanche face. For example, the firmness minima on the eastern flank of the study site in Figure 59 is inexplicable. It is also ephemeral and does not occur in the subsequent firmness pattern of Figure 60.

In Figure 60, it is worth noting the detailed firmness survey conducted along the "L" shaped line shown in enlargement to the left of the main plot. Along the transverse branch of the survey line, firmness varies from ∼ 13 cm penetration depth to ∼ 111 cm over a horizontal distance of only ∼ 8 cm. This is a surprisingly abrupt transition.

For the assessment interval from December 22, 1982 to January 30, 1983, some correspondence was found between the patterns of change in firmness and deposition/erosion (Figs 61 and 62). The primary firmness increase maximum occurs on the western flank and coincides fairly well with the erosion maximum, as was expected. The secondary firmness increase maximum occurs in an area of

slight deposition. This is contrary to expectation, but because the deposition was only slight, its coincidence with the increase in firmness is possible. The most minor of the firmness increase maxima occurs in an area of slight erosion. The only firmness decrease maximum coincides with a small area of slight erosion, and the elongated deposition maximum coincides with part of an elongated area of slight increase in firmness. These final two instances are again slight contradictions to expectation.

The deposition/erosion pattern of Figure 62 displays a degree of symmetry. The deposition and erosion maxima lie on virtually the same transverse axis across the study site and at more or less equal distance from the crest. They also have much the same shape and the same area. Their respective magnitudes of deposition and erosion are also similar except for in the region of the western avalanche face, which seems to be an area of significantly greater erosion. There seems to be about the same area of erosion on the western flank as there is deposition on the eastern flank although the shapes of these two regions are not similar. It would appear reasonable to assume that the deposition/erosion pattern of Figure 62 results from easterly winds with perhaps a slight predominance of ESE winds. In this case, deposition would occur just to windward of the crest, and erosion would occur to leeward of the crest due to strong rotor action.

There is an alternative wind regime possibility for the the plot of Figure 62. Westerly winds could cause erosion on the windward flank and deposition just to leeward of the crest. However, the relative rarity of observed westerly winds before and after the assessment interval leads to the idea that a predominance of westerly winds during the assessment interval would be too coincidental to be probable.

In conclusion, sand firmness patterns are potentially useful indicators of local seasonal winds and of the sand transport trends these winds produce. In this study, however, lack of wind data throughout the periods over which observed firmness patterns developed disallowed the proper interpretation of the relationship between the firmness patterns and wind conditions. A more complete study would have greatly reduced the conjectural nature of firmness pattern interpretation.

5.14   Topographic change

Topographic contour along two transverse lines and one longitudinal line across the study site was assessed on December 8, 1982 and January 29, 1983.

The $\sim$ 27 m longitudinal line connected the peaks of the two summits and ran along the crest. Each of the $\sim$ 50 m transverse lines intersected one of the two peaks of the summits (Fig. 63).

The topographic line surveys were carried out using a straight, narrow piece of wood $\sim$ 1 m in length, a meter stick and a small level. For any topographic line survey, the piece of wood was initially set down upon the sand at one end of the survey line. Then the height of its downslope end was adjusted until the level placed on its upper surface indicated that it was horizontal, and the height above the sand surface of the elevated end was measured using the meter stick and recorded as the first increment of the slope. Next, the piece of wood as moved down the survey line one of its lengths, and the second slope increment was measured by the above method. This procedure was repeated again and again until the entire survey line had been covered. For the transverse topographic surveys, increments on the western flank were mostly positive, indicating a slope rising towards the east. Increments on the eastern flank were mostly negative, indicating a slope declining towards the east. By graphically juxtaposing the topographic traces for each of the survey lines taken at the beginning and end of the assessment interval, a good idea of the deposition and erosion along each line over the assessment interval was obtained (Figs 64, 65 and 66).

It should be noted that each of Figures 64, 65 and 66 is slightly elongated with respect to the actual topographic profiles along the lines of survey. In Figure 64 for example, it would seem that the survey line ran between two points separated by a horizontal distance of exactly 50 m. In fact, the survey line ran between two points separated by $\sim$ 50 m as measured over the dune. Hence, the horizontal separation of the two points would necessarily be less than 50 m. In the instance of Figure 64, the distortion of the configuration amounts to about a 1.2 m elongation. That is, the figure represents a horizontal section of $\sim$ 51.2 m width rather than one of $\sim$ 50 m width. The distortions were too minor to adjust for them in the plotting of the profiles.

Figure 64 indicates that the northern transverse profile has shifted towards the west with relatively little change in profile area; there is no substantial net deposition or erosion along this line. This is taken as evidence that linear dunes can migrate laterally, and this has important consequences for longitudinal dune stratigraphy (Sec. 2.2.4).

Another significant feature of Figure 64 is the apparent stationary height of the dune at point A_1, which is at the leading edge of the dune section in its lateral migration westward. That it is stationary implies that deposition across

this point has not occurred. This seems to support the earlier empirical finding that sand transport over a longtudinal dune does not depart the body of the dune [TSOAR, 1978]. Deposition beyond the dune is difficult to achieve unless as the result of avalanching. Saltation intensity and effectiveness is diminished over sandy surfaces as compared with sand free surfaces; therefore, saltating sand will tend to converge upon the sandy areas [BAGNOLD, 1941]. With regards to the boundaries of longitudinal dunes, this means that sand carried beyond the dune and onto the interdune corridor where saltation potential is increased would probably be transported away. Also, there is the constricting role of secondary circulation to retard sand deposition beyond the dune.

In Figure 65, the southern transverse profile is not shifted significantly, but its area is increased. This indicates net deposition. It is interesting to note that a net deposition along the windward transverse survey line rather than along the leeward survey line is in keeping with the conjecture that surface drag was increased over the study site because of its grid of wooden stakes. The increase in surface drag would be accompanied by a decrease in surface sand transport. This would result in a zone of transport divergence just to leeward of the gridded area and a zone of transport convergence just to windward of it. In a zone of transport divergence, more sediment enters than exits, and hence, erosion occurs. In a zone of transport convergence, more sediment enters than exits, and deposition occurs (Fig. 67). In Figure 67, change in velocity vector magnitude is accompanied by relatively much greater change in transport vector magnitude. This is due to the cubic relationship between flow speed and transport intensity.

In Figure 66, the crestal trough of the longtudinal profile has shifted $\sim$ 13 m in the 52 day period, and the windward peak , assuming southerly winds, has shifted $\sim$ 14 m. As a sinusoidal wave, this profile line has shifted while it has remained fairly constant in wavelength and amplitude. It is interesting to speculate that steady longitudinal profile migration may apply to linear dunes in general.

5.15   A sand capture experiment

To each stake of the study site grid, three 10.1 cm x 15.2 cm (4" x 6") file cards were attached at different levels such that each card was adjacent to at least one other card and the top of the top card was flush with the top of the stake (Fig. 68). Each card was wrapped around the stake and fastened using either staples or a rubber band, and each card was color coded so that once removed, it could be ascertained by inspection of its color marking at which level on the

stake it had been positioned. Also, every side of every card was marked with the general direction towards which it faced. Finally, on December 12, 1985–the commencement day for the experiment – vaseline was smeared onto all exposed surfaces of all the cards.

On December 12, the patches of colored sands were set out to either side of the southern summit of the study site (Sec. 5.2). The intention was to capture colored grains on the vaseline-coated cards. By tabulating the number of grains of each color on each face of each card, it was hoped that certain characteristics of the colored sand flow over the study site could be learned. These characteristics would have included direction of colored sand flow over the study site both to windward and to leeward of the crest and the relationship between transport intensity and height above the surface.

On December 12, wind conditions were calm. Sand transporting winds did not occur until 4 days later on December 16. After several hours of vigorous sand transport, the cards were removed and stored separately in plastic sample bags, which were then sealed. The bags were carefully packed away and transported out of the field and back to the Department of Geology, University of Adelaide. They were stored until Janurary 23, 1982, when they were analyzed. Analysis of the cards revealed that a total of 3 colored grains had been captured during the experiment. This is insufficient data for any conclusion on colored sand flow.

A similar sand capture experiment was attempted among littoral linear dunes in Tasmania. In this instance a grid of 77 stakes (11 stakes by 7 stakes) was used, and file cards were attached to horizontal wooden platforms set on top of the stakes. Also, 10 kg of sand of each color was used rather than 20 kg of sand of each color. During the trial, a total of 24 grains of colored sand were captured. Again, this is insufficient data for any conclusions on colored sand flow. Earlier similar sand capture experiments using horizontal-plane adhesive surfaces have yielded results good enough for the assessment of colored sand flow over desert linear dunes [TSOAR, 1978].

Colored grain aggregates were found in some of the trenches excavated around the bases of the stakes (Fig. 69). This pattern was produced by winds of ∼ 11 knots (∼ 5.05 m/s or ∼ 20.4 km/hr) and from ∼ 155° SSE. The colored patch of green sand on the western side of the southern summit was, subsequent to December 16, 1982, wholly covered over by fresh blown sand and then partially reexposed on December 19, 1982. The blue patch on the eastern side of the summit remained exposed throughout the same interval. Colored grain aggregates were dispersed over elliptical areas to windward of both patches

(Fig. 69), and this was caused by winds of ~ 12 knots (~ 6.13 m/s or ~ 22.2 km/hr) from ~ 150° SSE.

5.16   Vertical temperature gradients

Inferior mirages, which are the couples of the normal images and the inverted images of objects above the optical horizon, are phenomena due to quasi-parabolic vertical temperature gradients close to the ground (Figs 70 and 71). They are common in such places as deserts and over large, placid bodies of warm water (i.e. lakes during the summer), where the surface heat flux is directed upwards. They occur under conditions that would seem to favor the generation of strong thermal buoyancy force, and this, as already discussed, would in turn help sustain and intensify roll vortices.

The quasi-parabolic vertical temperature gradients that are associated with inferior mirages can be obtained through relatively simple calculations involving a set of parameters requiring only six measurements [FRASER, 1979]. The most difficult of these are the angular elevations of the optical horizon and the caustic, which is the axis dividing the upper and lower portions of the mirage image. To measure these, a surveyor's theodolite capable of accuracy to within about 4 seconds of arc must be used. The other parameter values needed are the height of the theodolite telescope, the air temperature at that level, the ambient pressure and the distance from the observer to the mirage object. This last can be estimated from an aerial photograph or a topographical map, The calculations for obtaining a vertical temperature gradient can be done in situ using a programmable calculator (App. 11). Optically obtained quasi-parabolic vertical temperature gradients compare favorably with those obtained from thermocouple measurements [FRASER, 1974] and are faster to obtain.

Throughout the period of the field trials, inferior mirages were routinely observed on clear, hot days. A relatively simple program was written to calculate values for the quasi-parabolic vertical temperature profile using the expression given in Appendix 11, and this program was successfully tested using a set of accurate measurements [FRASER, 1974]. Attempts to make optical vertical temperature gradient assessments near the study site however were unsuccessful. Errors may have been committed in the taking of the optical measurements using the surveyors' theodolite. A programmable calculator was not then available therefore barring the immediate checking of angular elevation values.

5.17   Balloon trials

On February 1, 1983, during winds between 7 and 13 knots ($\sim$ 3.6 to $\sim$ 6.7 m/s or $\sim$ 13 to $\sim$ 24 km/hr) and fairly steady from $\sim$ 305° WNW, it was attempted to track balloons released from various sites in the western interdune corridor of the study dune. The balloons, whose diameters were of the order of tens of centimeters, were filled with a gas mixture of helium and nitrogen, and they were ballasted with small lead fishing weights. Two tracking theodolites set at $\sim$ 200 m separation on a line approximately normal to the wind direction constituted the tracking system. Plates 43 and 44 are images of the theodolites close to the dune and more than 200 m to the west of it respectively. Tracking from two theodolites simultaneously was made possible by the help of Mr. Updesh Singh (*see* Acknowledgements). Prior to departing for the field, a procedure for synchronized tracking was established and practised. Two custom-built electronic timers (*see* Acknowledgements) emitting high pitched sound signals approximately every 30 seconds were synchronized before tracking and then placed with each theodolite. Position readings were spoken into cassette tape recorders.

None of the balloon trials was successful, for several reasons. It was impossible under the conditions to establish neutral buoyancy for the balloons. Ballasting had to be done in the partially enclosed back space of a land cruiser, so the air was never still. Usually, too many weights were attached, and these balloons were driven into the ground by the wind and burst amongst the woody vegetation. When a balloon was successfully launched, it was advected beyond the leeward side adjacent dune so quickly that view of it was blocked by the neighboring dune. Trials did not have the advantage of tracking from an elevated vantage point.

5.18   Qualitative observation
                      on the movement of wet sand

When this study was first undertaken, it was assumed that the winds responsible for longitudinal dune genesis and ordering necessarily had to be dry winds that probably occurred during periods of high incoming solar radiation. It was reasoned that winds during rain storms could not contribute to dune formation or development, for wet sands with increased surface cohesion would require winds of extreme strength for saltation. However, in the littoral linear

dunes of northeastern Tasmania winds believed to be about 20 knots were observed to cause considerable saltation during rain. Wet dune cores may not be the stabilizing factor they are widely believed to be.

5.19   Air funnels

While conducting field experiments in the vicinity of the Moomba gas camps at the northeastern corner of the Strzelecki Desert in South Australia, funnels of air made visible by their suspended load of dust were frequently observed during relatively calm days (App. 12). These funnels are popularly known as "dust devils" or "willie willies", and many of them travelled along the crests of linear dunes, one of which was the study dune. Recall that the study dune is slightly curved in the horizontal plane and comprised of a series of summits.

It seems strange that the path of least energy expenditure should be curved and uneven. It is possible that the funnels are confined to their paths along linear dune crests by the surface flow convergence zones of Bénard cells or weak roll vortices centered about the linear dunes. Furthermore, because surface flow convergence zones are also air uplift zones, convection cells probably promote funnel growth.

An unlikely alternative explanation for funnel confinement to linear dune crests is that zones of unequal vertical wind velocity occur over the flanks of the dunes. These zones of unequal vertical wind velocity over the flanks would be due to uneven surface heating of the flanks, and this uneven heating would in turn be due to uneven incidence of solar radiation upon the flanks. This would occur when the sun was in such a position in the sky relative to the dunes that solar rays were more directly incident upon the flanks facing the sun than the flanks facing away from the sun (Fig. 72). In this case, flank slope becomes an important factor.

5.20   Horizontal pressure gradients

Measurement of several relevant field parameters were not sought because of logistic difficulty, unavailability of equipment or lack of funds. Horizontal pressure gradients around linear dunes were assessed but later discounted when the measurement technique was shown invalid. Hollow plastic tubing was laid between points two hundred meters apart in an interdune corridor; one end of the

tubing was left open and the other end connected to an alcohol-filled manometer. Care was taken to orient the open ends of the tubing and the manometer such that the flow was across them with a reduced component into them. This reduced component would not have been negligible however, and nothing was done to minimize eddy effects around the rims of the opening, which would have further influenced readings.

Chapter Six: Simple flow model

6.1 **Energy optimalization**

The patterning of dune fields, as with the meandering of rivers and streams, is an expression of energy conservation. These are, in essence, the "easiest" – most convenient or energy optimal – ways for sand to accumulate under the influence of wind and for channels to bend and twist under the influence of water. All possible mechanisms of longitudinal dune ordering operate presumably by working towards minimalization of energy expenditure. In fact, it is only assuming energy optimalization that any of the possible ordering mechanisms can be quantitatively described. This will become more clear as actual quantitative models are considered.

6.2 **River meanders**

River meanders serve as an initial illustration of the principle of energy optimalization. The ideal river exists in conception only as a perfectly straight channel; in nature, ideal rivers cannot exist, either now or in the distant past [LEOPOLD and LANGBEIN, 1966]. For any river, meander development must have complemented channel development from it earliest stages.

River meanders take "the form in which a river does the least work in turning; hence they [exhibit] the most probable form a river can take" [LEOPOLD and LANGBEIN, 1966]. The mathematical family of curves that typify river meanders is known as the "sine-generated curves," and they are distinguished from other families of curves, such as parabolic curves, connected semicircles and sine curves by their peculiar quantitative definition (App. 13). Qualitatively, the sine-generated curves are the curves that require the "smallest variations of the changes of direction" [LEOPOLD and LANGBEIN, 1966]. That is, if all periodic curves were divided into minute straight line segments of equal length, it would be seen that the number of segments that experience a change in the rate of change in direction would be least for the sine-generated curves. In a way, they are a compromise between curves such as the parabolic and sine curves, whose turns are too abrupt, and curves such as connected semicircles, whose turns are too gradual (Fig. 73). Figure 74 and Plate 45 show images of sine-generated curves as manifested in actual river meanders.

There seems to be a degree of universality in the manifestation of the sine-generated curve in phenomena in which lengths of material must bend. Rods of

spring steel that are bent by the application of force to its ends naturally assume the form of a sine-generated curve. More dramatically in one instance, a train hauling track rails in a long string of freight cars folded under the terrific force of a collision to form what is in configuration a sine-generated curve. Photographs of bent rods of spring steel and the folded train are given in LEOPOLD and LANGBEIN, 1966.

Being forced at its ends, the rod of spring steel, as with the long train of freight cars loaded with steel rails, tended naturally towards the uniform distribution of its internal strains as expressed in a sine-generated curve. It could accommodate a shape change because of its elasticity. With rivers, it is the turbulence and therefore resistance to smooth flow that is minimalized by the assumption of a sine-generated curve configuration. A degree of crosschannel asymmetry is established in flow around a bend (Fig. 76). As the magnitude of asymmetry is increased, so too is the proportion of the flow energy diverted into turbulence. This turbulence may act as a channel's self-regulatory mechanism in that it may contribute to channel restructuring through bank erosion and thereby reduce energy loss into flow asymmetry and also, ironically, turbulence. In this case, turbulence would be both the result of channel configuration instability and the mechanism by which stability is regained. In any case, the sine-generated curve is the unconditional stability configuration for river meanders in which flow asymmetry is minimal.

Interestingly, the secondary flow of the current as it rounds bends is in the form of a single helix (Fig. 76). Transverse flow components may be eliminated, but this requires that the channel broadens downflow to the point of commencement of channel curvature (Fig. 77). Streams do not naturally broaden downflow perhaps because the elimination of transverse flow is not tantamount to the achievement of least energy expenditure. From Figure 77, it is apparent that a considerable amount of shearing occurs in flow rounding a bend that broadens downflow. Helical secondary flow in a current as it rounds a bend should reduce internal shear.

From the consideration of rivers and bending materials, it is apparent that analogous though not necessarily similar circumstances can breed similar results in natural phenomena. This should be borne in mind as the next example of energy optimalization is discussed.

6.3   **Linear sand banks**

Linear sand banks in shallow tidal seas is a case not far removed from that of longitudinal dunes in the desert. Though the one sand form occurs beneath water and the other beneath air, the topographic and dynamic similarities between the two are striking.

"Tidal current ridges or linear sand banks are quasi- periodic bed-forms roughly aligned with the tidal currents and occurring widely on continental shelves [OFF, 1963], apparently where tidal currents are strong and sand is in good supply. They are large – up to 80 km long, typically 1 to 3 km broad and tens of meters high – usually a large fraction of water depth. Their dimensions and spacing (several kilometers) vary between examples but tend to increase together [ALLEN, 1968]" [HUTHNANCE, 1982a] (*see* Fig. 78). The above description of linear sand banks in the southern North Sea not far off the coast of southeastern England shows that they and longitudinal dunes are similarly fairly evenly spaced, mutually parallel and aligned with the formative currents. Their direct proportionality between ridge height and ridge spacing is a characteristic shared by longitudinal dunes [TWIDALE, 1981]. Finally, linear sand banks are also asymmetric across their transverse profile.

Linear sand banks may be produced by roll vortices in the tidal current [HOUBOLT, 1968]; however, this idea is widely contested. In linear sand bank study and longitudinal dune study, even the controversies are similar. Incidentally, for roll vortices in sea currents, surface winds may be a major forcing agent [LANGMUIR, 1938].

For two-dimensional flow – flow with disturbance or perturbation periodic in the transverse direction to the mainstream – it has been proved that two-dimensional instability will occur at Reynold's number lower than those for three-dimensional instability [SQUIRE, 1933]. Hence, within two-dimensional flow, two dimensional instability will predominate, and the resultant secondary flow will be longitudinal or periodic laterally. In light of this, instability in a sediment/flow/sediment transport system in which the flow regime is unidirectional and the flow at any particular time is two- dimensional may also be longitudinal [HUTHNANCE, pers. comm., 1985]. The emergence of ordered linear sand banks in shallow tidal seas was analysed through application of this hypothetical principle by assuming that these linear sand banks are manifestations of one primary predominant longitudinal instability of the system

[HUTHNANCE, 1982a]. The wavelength of the linear sand banks was taken to correspond to the wavelength of the longitudinal instability. It was later quantitatively shown using numerical means that low, parallel depositional forms do indeed grow fastest and are therefore most likely to develop under conditions of a unidirectional tidal current flow regime [HUTHNANCE, 1982b].

In a unidirectional flow regime, mean flow is confined to a narrow range of directions although actual flow, especially secondary flow, may occur in any orientation. Therefore, flow may be obliquely incident upon the linear sand banks. Oblique flow over a sand bank is deflected, and speed of the lower flow layer – that layer in which flow experiences momentum deprivation due to saltation – is diminished. Sediment transport is similarly deflected, but because of the cubic relationship between flow speed and sediment transport intensity, its decrease in magnitude is proportionately much greater than that of the lower flow layer (Fig. 79). This is similar to what was found to happen over the linear study dune although no conclusion could be made on the change of speed in the lower flow layer (Sec. 5.9, Fig. 50). Variation of the sediment transport vector over sand banks governs their growth. Quantification of this variation allows for the numerical analysis of linear deposition forms.

The quantitative treatment of linear sand banks is highly instructive, both in its general approach and its details, with regards to the problem of longitudinal dunes. Indeed, if longitudinal dune ordering is to be considered in the context of simple flow – flow without secondary circulation – a quantitative analysis virtually identical to that of linear sand banks in its basic assumptions and incorporated physical principles must be used. The remainder of this chapter is devoted to a discussion of the linear sand banks model, and the quantitative expressions comprising the analysis and their underlying physical relationships will be discussed first.

6.3.1 The equation of momentum conservation

In the context of linear sand banks, water may be considered a homogeneous fluid; its density may be taken as constant at all times and throughout the shallow water layer. Air in the context of longitudinal dune fields – air in the lower planetary boundary layer – may also be considered as homogeneous.

For the quantitative treatment of linear sand banks, horizontal fluid velocity is considered depth uniform. In other words, the $x-$ and $y-$direction flow

components are taken to be functions independent of height above the sea floor. The horizontal velocity U_h is defined by the expression

$$U_h \equiv \left[u(y,t), v(y,t)\right]$$

where $u \equiv$ the horizontal flow velocity aligned with the topographic corrugations, $v \equiv$ the horizontal flow velocity transverse to the topographic corrugations, $y \equiv$ horizontal distance transverse to the topographic corrugations and $t \equiv$ time. The three basic parameters not included in the above definition are w, x and z, where $w \equiv$ the vertical flow velocity component, $x \equiv$ horizontal distance parallel to the topographic corrugations and $z \equiv$ height above the surface.

It is taken that there exists a uniform "far" current, which is to say that at some unspecified distance from the area of interest, the sea floor is flat and the flow velocity uniform and constant. The magnitude of the far current at any time is given by $U_{max}I(t)$, where $U_{max} \equiv$ the far current maximum speed and $I(t) \equiv$ the far current time dependence.

Flow momentum must be conserved at all points; hence, within the area of linear sand banks, the product of the mass of a water column of unit area in the horizontal plane at any given point and the fluid velocity at that point must be constant and equal to the far current momentum. Quantitatively,

$$hU = HU_{max}I(t) \tag{1}$$

where $h \equiv$ fluid depth or column height at any point, $H \equiv$ far fluid depth and $U \equiv$ fluid velocity magnitude (Fig. 80).

Of greater relevance to the analysis is the $y-$direction component of (1), namely

$$hv = HU_{max}I(t)\sin\alpha \tag{1a}$$

where $\alpha \equiv$ angle between the mean flow and the longitudinal axis of the topographic corrugations. For completeness sake, the $x-$direction component of (1) is

$$hu = HU_{max}I(t)\cos\alpha$$

(Fig. 81). It should be noted that symbol definitions in this thesis do not coincide completely with those of HUTHNANCE. For instance, U_{max} is used here instead of simply U.

By (1) and its component expressions, a decrease in depth is accompanied by an increase in fluid velocity. This means that over a sand bank, flow speed

must increase. This is not necessarily in contradiction to the decrease in flow speed in the lower flow layer affected by saltation, for the mean flow speed as assessed for the entire depth of the fluid may increase while at the same time, the flow speed in the lower flow layer may decrease. In the context of the analysis however the decrease of the flow speed in the lower flow layer must be ignored; a depth uniform flow has been assumed for the sake of mathematical convenience. In any case, increase of flow speed over sand banks in shallow water is reasonable. Recall that for desert linear dunes, flow speed similarly increases over the study dune (Sec. 5.10).

6.3.2   The equations of fluid motion

The set of equations governing the motion of fluids, usually known as the "Navier-Stokes" equations of motion, are

$$\frac{\partial u}{\partial t} + u\frac{\partial u}{\partial x} + v\frac{\partial u}{\partial y} + w\frac{\partial u}{\partial z} = -\frac{1}{\rho}\frac{\partial P}{\partial x} + X + \nu\nabla^2 u - 2(\omega_y w - \omega_z v) \quad (i),$$

$$\frac{\partial v}{\partial t} + u\frac{\partial v}{\partial x} + v\frac{\partial v}{\partial y} + w\frac{\partial v}{\partial z} = -\frac{1}{\rho}\frac{\partial P}{\partial y} + Y + \nu\nabla^2 - 2(\omega_z u - \omega_x v) \quad (ii),$$

and

$$\frac{\partial w}{\partial t} + u\frac{\partial w}{\partial x} + v\frac{\partial w}{\partial z} = -\frac{1}{\rho}\frac{\partial P}{\partial z} + Z + \nu\nabla^2 w - g - 2(\omega_x v - \omega_y u) \quad (iii)$$

where $\rho \equiv$ fluid density, $P \equiv$ fluid pressure, $\nu \equiv$ kinematic viscosity, $\nabla^2 \equiv \frac{\partial^2}{\partial x^2} + \frac{\partial^2}{\partial y^2} + \frac{\partial^2}{\partial z^2}$, $\omega_i \equiv$ the i-direction component of the angular velocity of the earth's rotation at any given point on the earth's surface, X, Y and Z$\equiv$extraneous forces in the $x-$, $y-$ and $z-$directions excluding Coriolis force and gravity and g =gravitational acceleration [NAVIER, 1823; POISSON, 1831; SAINT-VENANT, 1843 and STOKES, 1845]. ω_i are functions of latitude.

It is assumed that v and w are steady or constant in all directions and over time. That is,

$$\frac{\partial v}{\partial t} = \frac{\partial v}{\partial x} = \frac{\partial v}{\partial y} = \frac{\partial v}{\partial z} = 0$$

and

$$\frac{\partial w}{\partial t} = \frac{\partial w}{\partial x} = \frac{\partial w}{\partial y} = \frac{\partial w}{\partial z} = 0$$

This is the same as saying that only the current component parallel to the topographic corrugations is not constant, which may or may not be true in nature. However, by adopting this condition for the analysis, (i) and (ii) are eliminated, and the mathematical complexity of the treatment is greatly reduced.

Steady *v* and *w* are reasonable for flows without either secondary circulations or significant random turbulence. Also, that this analysis is ultimately successful in predicting linear sand bank spacing does not necessarily go to prove the validity of the assumptions used. In fact, the quantitative analysis is an entity or phenomenon quite independent of the phenomenon in nature it is meant to describe. It is perhaps more appropriate to speak of an analogy between the theoretical phenomenon and the physical one. The quantitative analysis, as will become apparent, is actually a topic in its own right and one requiring some investigation.

Of (i), the remaining equation of motion, it is again assumed that there is no vertical variation in the flow. Furthermore, horizontal variation is confined to the *y*–direction. That is

$$\frac{\partial u}{\partial z} = \frac{\partial u}{\partial x} = 0.$$

Because the major topographic variation occurs in the *y*–direction, it is sensible to assume that the mechanism responsible for this is connected to flow variation in the *y*–direction. The change of u with respect to *y* becomes important.

The flow is considered irrotational, which is to say the fluid is assumed inviscid ($\nu = 0$). Therefore,

$$\nu \nabla^2 u = 0,$$

and a particularly complicated term in the equation is eliminated. Irrotationality may not be a good assumption for either shallow tidal seas or deserts in that rotationality would seem to be a salient characteristic of the flow in both settings. For example, the desert kite trials clearly demonstrated the rotationality of air flow around dunes (Ch. 5). However, rotationality must be retained only if secondary flow plays a major role in the phenomena in question. Though secondary flow probably controls the ordering of longitudinal dunes of uniform spacing, it may be of minor importance for the ordering of longitudinal dunes of variable spacing. Moreover, secondary flow is assumed largely irrelevant with regards to the genesis and ordering of linear sand banks; hence, irrotationality becomes a pivotal assumption in the analysis of linear sand banks. This condition greatly simplifies calculations, yet leads to fairly accurate results. Again, that results are good does not show that secondary flow cannot occur around linear sand banks. Incidentally, because the linear sand banks are separated by distances more than one hundred times greater than the depth of the water, formative roll vortices would have to be very much wider than they would be deep, and such shallow roll vortices have never been observed in any fluid and therefore seem highly unlikely.

Resuming the discussion of (i), because the vertical component of flow w is very small in comparison to the horizontal components, the first term of the Coriolis quantity – the product of the y–direction component of the earth's angular velocity at any given point on the earth's surface ω_y and w – is negligible in comparison to the second term – the product of ω_z and v. Quantitatively, since

$$w \ll v,$$

$$\omega_y w \ll \omega_z v.$$

At mid-latitudes, ω_y and ω_z are of comparable magnitude. What is left of the Coriolis terms in (i) is only $2\omega_z v$. This is replaced by fv, where f, known as the "Coriolis parameter", is defined by $2\omega_z$.

Besides Coriolis force, the only other external force is the drag due to surface friction. This is written as

$$-C_m |\vec{U}|^{m-1} u/h$$

where $|\vec{U}| \equiv U_{max}|I(t)| \equiv$ magnitude of vector $\vec{U}$ and $C_m \equiv C/U^{m-2}$. C is the usual drag coefficient in the drag law for turbulent flow

$$\vec{\tau} \equiv \rho C |\vec{U}| \vec{U}$$

where $\vec{\tau} \equiv$ shear vector. The parameter m is a power whose value may vary but is widely favoured as 2. The surface friction term is always negative, for it is a force always opposed to the direction of motion. There is no form drag upon u, for u is by definition aligned with the topographic corrugations.

The negligible terms of (i) are eliminated, fv is replaced for the collective Coriolis quantity and $-C_m|\vec{U}|^{m-1}u/h$ is replaced for the extraneous forces X. After some further algebraic manipulations utilizing (1a) and (1b), it is obtained that

$$\frac{\partial u}{\partial t} + v\frac{\partial u}{\partial y} - fv + C_m|\vec{U}|^{m-1}\frac{u}{h} = -\rho\frac{\partial P}{\partial x} = U\cos\alpha\frac{dI}{dt} - fUI\sin\alpha \qquad (2)$$
$$+ C_m U^m |I|^{m-1} I \cos\alpha/H.$$

This is the equation of motion that is used in the analysis. It will later be changed during calculations, but for the time being it will be left in this form. It is understood that $U \equiv U_{max}$ and $I = I(t)$.

6.3.3   The sediment transport equation

Equation (1), equation (2) and boundary conditions appropriate for the description of the surface topography and the free upper boundary are adequate for the description of flow around linear sand banks. However, these things are not sufficient for a description of linear sand bank evolution. For this task, a third fundamental relationship is required, and that is the sediment transport equation. From this an expression for sediment deposition and erosion may be derived.

Several sediment transport relationships have been derived [BAGNOLD, 1941; EINSTEIN, 1950; YALIN, 1963; ENGELUND and HANSEN, 1967b; ACKERS and WHITE, 1973] (App. 14). The features and relative advantages of these different relationships have been considered, and a comparative study was made of measured sediment transport rates and those calculated using various sediment transport relationships [HEATHERSHAW, 1981]. Of the existing relationships, those of BAGNOLD and EINSTEIN are most widely favored by workers in the field for their general applicability and accuracy. The latter derives from a probabilistic treatment, and the former from a consideration of simple physical principles. A BAGNOLD-type sediment transport relationship is used in this analysis, and it is

$$Q = \gamma |\vec{U}|^n \left(u, \; v + \Lambda |\vec{v}| \frac{dh}{dy} \right) \tag{a}$$

where $\gamma \equiv$ non-dimensional scaling factor, $n \simeq 2$, $1 + \Lambda \frac{dh}{dy} \equiv$ "an enhancement factor" for the downslope component of transport and $\vec{v} \equiv y-$direction component of the fluid velocity vector. A "downslope" is defined as any surface over which the fluid layer depth increases with increasing y, the positive $y-$direction being defined as that direction towards which the mean flow is directed (Fig. 82). Consequently, the downslope is always the leeward slope, and sediment transport over the downslope is en hanced by gravity. Conversely, sediment transport over the "upslope" is decreased by gravity. The downslope slope enhancement parameter Λ may be expressed as a function of the friction angle. Specifically,

$$\Lambda \simeq 2\pi H/L \tan(\text{friction angle})$$

where $L \equiv$ characteristic length scale. Λ diminishes with increasing suspension load, for the transport of suspended load is not enhanced on the downslope.

Note that the sediment transport equation for this derivation does not take into account a threshold fluid velocity. This probably simplifies calculations without significantly affecting them.

6.3.4 An equation for sediment erosion, deposition and pure transport for linear sand banks

A substantial derivative of the sediment transport equation yields the conditions for sediment erosion, deposition and pure transport. These are as follows:

(i) $\frac{dQ}{dt} > 0$ erosion

(ii) $\frac{dQ}{dt} = 0$ pure transport

(iii) $\frac{dQ}{dt} < 0$ deposition

where $\frac{d}{dt} \equiv$ "the total or substantial derivative of". If over any control area, sediment transport increases with time, then the control area loses material, and erosion occurs. If sediment transport decreases with time, then the control area gains material, and deposition occurs. Finally, if sediment transport neither increases or decreases, then material is neither gained or lost, and pure transport occurs.

Expanded, the substantial derivative for sediment transport is

$$\frac{dQ}{dt} = \frac{\partial Q}{\partial t} + u\frac{\partial Q_x}{\partial x} + v\frac{\partial Q_y}{\partial y} + w\frac{\partial Q_z}{\partial z}$$

where $Q_i \equiv$ the $i-$direction component of the sediment transport vector $\vec{Q}$. This is a completely general expression (App. 15). Because $w \simeq 0$, the final partial derivative component on the right-hand side is negligible.

It is assumed that the substantial derivative is very nearly zero, which is to say that a parcel of fluid moving over the surface (at a velocity not necessarily the same as that of the mean flow) experiences no net change in sediment transport. The parcel may pass over many regions of erosion, deposition and pure transport, but overall, there is neither erosion or deposition within, simply pure transport. Another way to approach this assumption is to imagine a comparatively large

area for which there is neither the introduction or substraction of, the creation or destruction of sediment. The assumption is tantamount to the condition of sand conservation. For relatively short intervals of time, this is reasonable; however, for longer periods, it would seem that a large region such as a dune field would either gain or lose sand. Assuming sand conservation, the derivative equation becomes

$$\frac{dQ}{dt} = \frac{\partial Q}{\partial t} + u\frac{\partial Q_x}{\partial x} + v\frac{\partial Q_y}{\partial y} \simeq 0$$

or after rearranging terms

$$-\frac{\partial Q}{\partial t} = u\frac{\partial Q_x}{\partial x} + v\frac{\partial Q_y}{\partial y}. \tag{b}$$

The local time derivative of sediment transport $\frac{\partial Q}{\partial t}$ is the change in sediment transport over time at a specific locus. Change in sediment transport, as already discussed, determines erosion and deposition; and erosion and deposition, in turn, determine change in topography. Consequently, $\frac{\partial Q}{\partial t}$ relates directly to change in topography, and for linear sand banks, change in topography is inversely proportional to change in water depth. That is

$$\frac{\partial h}{\partial t} \propto -\frac{\partial Q}{\partial t}.$$

For the moment, the above direct inverse proportionality will be left as is.

In the derivative equation for erosion, deposition and pure transport (b), Q is replaced with the left-hand side of the sediment transport equation (a). The expression obtained is

$$-\frac{\partial Q}{\partial t} = u\frac{\partial}{\partial x}\Big(\gamma|\vec{U}|^n u\Big) + v\frac{\partial}{\partial y}\Big[\gamma|\vec{U}|^n v + \Gamma|\vec{v}|\frac{dh}{dy}\Big].$$

The $\frac{dh}{dx}$ term of the u component of sediment transport is missing because $\frac{dh}{dx} = 0$ There is no change in surface slope in a field of topographic corrugations in the direction parallel to the longitudinal axis of the corrugations.

Both $\frac{\partial|\vec{U}|}{\partial x}$ and $\frac{\partial u}{\partial x}$ are equal to zero because all flow velocity components are constant in the x-direction. The above equation becomes

$$-\frac{\partial Q}{\partial t} = v\frac{\partial}{\partial y}\Big[\gamma|\vec{U}|^n\Big(v + \Gamma|\vec{v}|\frac{dh}{dy}\Big)\Big].$$

6.3.5   An equation for topographic
                          change for linear sand banks

Returning to the direct inverse proportionality between $\frac{\partial Q}{\partial t}$ and $\frac{\partial h}{\partial t}$, an explicit expression is attainable through judicious selection of a proportionality constant. The parameter $\frac{\partial h}{\partial t}$ has units kg/s; whereas, $\frac{\partial Q}{\partial t}$ has units kg-m/s^2. The dimensional difference between the two is m/s, which are the dimensions of velocity. Therefore, $\frac{\partial h}{\partial t}$ may be expressed in terms of $\frac{\partial Q}{\partial t}$ divided by some velocity parameter or characteristic velocity. In other words, $\frac{\partial h}{\partial t}$ is inversely proportional solely to the divergence of sediment transport $\frac{\partial Q}{\partial x_i}$, for $\frac{\partial Q}{\partial t}/U_i = \frac{\partial Q}{\partial t}/\frac{\partial x_i}{\partial t} = \frac{\partial Q}{\partial x_i}$. Consequently, the equation for topographic change becomes

$$\gamma' \frac{\partial h}{\partial t} = \frac{\partial}{\partial y}\left[\gamma|\vec{U}|^n\left(v + \Gamma|\vec{v}|\frac{dh}{dy}\right)\right]$$

where $\gamma' \equiv$ some constant coefficient.

The parameter γ', being a constant, is taken out of the bracketed differentiated quantity to become a factor for the partial derivative with respect to y, and as it turns out, γ' is a function of sand bed porosity [HUTHNANCE, 1982a]. The derivative equation now becomes

$$(1-p)\gamma'' \frac{\partial h}{\partial t} = \gamma\frac{\partial}{\partial y}\left[|\vec{U}|^n\left(v + \Gamma|\vec{v}|\frac{dh}{dy}\right)\right]$$

where $p \equiv$ porosity and $\gamma'' = \frac{\gamma'}{1-p}$. Finally, both sides of the above equation are divided by $(1-p)\gamma''$ to obtain

$$\frac{\partial h}{\partial t} = \frac{\gamma'''}{(1-p)}\frac{\partial}{\partial y}\left[|\vec{U}|^n\left(v + \Gamma|\vec{v}|\frac{dh}{dy}\right)\right] \tag{3}$$

where $\gamma''' = \gamma/\gamma''$. This is an equation of topographic change based upon the condition of sand conservation.

6.3.6   An equation for fluid flow velocity
                          over a corrugated surface

The variation of the $x-$direction component of the fluid flow velocity over a corrugated surface is expressed by the equation

$$u = I\cos\alpha + \delta\left[a(t)\cos y + b(t)\sin y\right] \tag{4}$$

where $\delta \equiv$ magnitude of the perturbation of u, $\delta \ll 1$ and $a(t)$ and $b(t)$ are the time dependence of δ. Also, for future reference, $\varpi \equiv a(t) + b(t)i$. The factors $\cos y$ and $\sin y$ assure that maximum perturbation and therefore maximum u occur just flowward of the crest whichever way the positive y-direction is directed (Fig. 83). This happens to agree well with observed flow velocity behavior over desert linear dunes (Sec. 5.9). Expression (4) assumes topographic corrugation sinusoidal in the y-direction, and a and b will hereafter be understood to mean $a(t)$ and $b(t)$.

6.3.7   Expansion of the topographic change equation

The sinusoidal bottom topography has wavelength L and is expressed by the relationship

$$h = 1 + \delta \sin y \qquad (5).$$

Because the topographic relief is small compared to the fluid depth above it, $\delta \ll 1$.

Replacing (5) and the fluid velocity expression (4) into the topographic change equation (3), it is obtained that

$$\frac{\partial h}{\partial t} = \frac{1}{1-p} \frac{SU^3 T}{gHL} \frac{\partial}{\partial y} \left\{ \left[I \cos \alpha + \delta(a \cos y + b \sin y) \right]^2 \right.$$

$$+ \left. (1 - \delta \sin y)^2 I^2 \sin^2 \alpha \right\}^{n/2} \left[(1 - \delta \sin y) I \sin \alpha \right. \qquad (3a)$$

$$\left. + \Gamma | (1 - \delta \sin y) I \sin \alpha | \frac{dh}{dy} \right]$$

The parameters u, v, h, y, t and f have been non-dimensionalized using the characteristic scaling dimensions U, U, H, $\frac{l}{2\pi}$, $\frac{T}{2\pi}$ and $\frac{2\pi}{T}$ respectively.

Briefly, each quantity must be non-dimensionalized individually. For example,

$$\frac{\partial u}{\partial t} = \frac{U(\partial u/U)}{T 2\pi \delta(2\pi t/T)} = \frac{2\pi U}{T} \frac{\partial u^*}{\partial t^*}$$

where $u^* \equiv u/U$ and $t^* \equiv t/T$. In (3a), as with equations throughout this dissertation incorporating normalized quantities, the superscript stars have been dropped. Also in (3a), the parameter γ''' of (3) has been replaced by S/g where $S \equiv$ scaling coefficient and $g \equiv$ gravitational constant. The gravitational constant must be included for the complete normalization of (3). That is, after all quantities other than γ''' in (3) have been non-dimensionalized, the right-hand

side still has the dimensions of acceleration, and this is eliminated through the division by g.

For flow as described by (4), the zero identities $\overline{I|I|^s} = 0$ and $\overline{b|I|^s} = 0$ where $s \equiv$ any integer can be shown to hold true. Using these two identities as well as the conditions $\frac{\partial y}{\partial t} = 0$, $\frac{\partial \delta}{\partial t} = \frac{d\delta}{dt}$ and $\frac{\partial h}{\partial t} = \delta \cos y \frac{\partial y}{\partial t} + \sin y \frac{\partial \delta}{\partial t} = \sin y \frac{d\delta}{dt}$ and simplifying greatly, (3a) becomes

$$\delta^{-1} \frac{d\delta}{dt} = \frac{1}{1-p} \frac{SU^2}{Hg} Fkn \left[\overline{|I|}^n a \sin \alpha \cos \alpha + \overline{|I|}^{n+1} \frac{\Gamma}{n} |\sin \alpha| \right] \qquad (3b)$$

where $k = \frac{2\pi H}{CL} \equiv$ corrugation wavelength and $F \equiv \frac{CUT}{2\pi H} =$ friction parameter.

Relationship (3b) expresses deposition/erosion as a function of the three variables a, α and k only. Once a function is found expressing a as a function of α and k, the final form of the deposition/erosion relationship can be obtained.

6.3.8 Possible flow cases

Incorporating the fluid velocity equation (4) into the chosen form of the equation of motion (2) it is obtained after considerable manipulation

$$F^{-1}(\varpi') + \left(|I|^{m-1}q - iIl \right)\varpi = iI\left(|I|^{m-1} r \cos \alpha - f/F \sin \alpha \right) \qquad (2a - i)$$

where $q \equiv m\cos^2 \alpha + \sin^2 \alpha$, $l \equiv k\sin \alpha$ and $r \equiv m\sin^2 \alpha + \cos^2 \alpha$. This is a first order differential equation of ϖ for the case of unsteady flow with significant Coriolis infuence. Three other flow cases of diminishing complexity are possible. They are as follows:

$$F^{-1}(\varpi') + \left(|I|^{m-1}q - iIl \right)\varpi = iI\left(|I|^{m-1} r \cos \alpha \right) \qquad (2a - ii)$$

for unsteady flow with negligible Coriolis influence,

$$\left(|I|^{m-1}q - iIl \right)\varpi = iI\left(|I|^{m-1} r \cos \alpha + f/F \sin \alpha \right) \qquad (2a - iii)$$

for quasi-steady flow with significant Coriolis influence and

$$\left(|I|^{m-1}q - iIl \right)\varpi = iI\left(|I|^{m-1} r \cos \alpha \right) \qquad (2a - iv)$$

for quasi-steady flow with negligible Coriolis influence. Quasi-steady flow is defined by $\frac{\partial \varpi}{\partial t} \neq 0$, and Coriolis influence by $f \neq 0$.

For both the cases of linear sand banks and longitudinal dunes, flow varies with time and is therefore unsteady. The significance of Coriolis influence is

determined by the ratio f/F, which compares Coriolis force to frictional drag. Because $F = CU/H$, in terms of dimensional quantities, $f/F = fH/CU$. Approximate characteristic values of f, C, U and H for linear sand banks in mid-latitudes are 10^{-4}s^{-1}, 3×10^{-3}, 1 m/s and 30 m respectively, and $f/F \simeq 1$. Hence, for linear sand banks Coriolis influence is significant. Approximate characteristic values of f, C, U and H for longitudinal dunes in mid-latitudes are 10^{-4} s^{-1}, 10^{-3}, 10 m/s and 1000 m, and $f/F \simeq 1$. Again, Coriolis force is significant. Therefore, for the analysis of both cases, equation (2a-i) must be used.

6.3.9
The final expression
for maximum deposition

Assuming a square wave time-dependency for flow, which is the simplest time variation, equation (2a-i) is solved analytically for the parameter a, and this is replaced into (3b) to obtain the expression of maximum deposition

$$\sigma(k, \alpha) = \frac{SU^3}{(1-p)gJ} nk^2 \left\{ \cos\alpha \sin^2\alpha \frac{Fr\cos\alpha - f\sin\alpha}{q^2 + l^2} \right.$$
$$\left. \times \left[1 - 2q\frac{\cosh\pi Fq - \cos\pi Fl}{\pi F(q^2 + l^2)\sinh\pi Fq}\right] - \frac{\hat{\Gamma}}{n}|\sin\alpha| \right\} \qquad (3c)$$

where $\sigma(k, \alpha) = \delta^{-1}\frac{d\delta}{dt} \equiv$ deposition rate and $\hat{\Gamma} = C/\tan((\text{friction angle}). \, .$

For every value of σ, there is a unique set of α and k values. Maximum σ therefore corresponds to a set of optimal α and k. Maximum σ can be found either analytically or numerically. Analytically, the σ function is differentiated with respect to both α and k. Where these first derivatives are equal to zero, either maxima or minima. Second derivatives are taken, and where these are less than zero, maxima occur. Quantitatively, where $\frac{\partial\sigma}{\partial\alpha} = \frac{\partial\sigma}{\partial k} = 0$ and $\frac{\partial^2\sigma}{\partial^2\alpha} = \frac{\partial^2\sigma}{\partial^2 k} = 0$, σ is a maxima with respect to α and k. If there is only one loci where the above criteria are met, then the system has only one maxima, and the α and k values associated with it are the optimal values.

Numerically, σ values are computed for combinations of different α and k values over wide ranges, and the highest σ is the maximum. Again, the α and k values associated with the maximum are the optimal values.

6.3.10   Optimal spacing

Because k for the system is directly related to the wavelength L of the system and because L for the system is the same as L for the topographic corrugations, optimal L, which corresponds to equilibrium sand bank spacing, is directly calculable from optimal k. From the definition of k, the equation expressing optimal L as a function of optimal k is

$$L_{opm} = 2\pi H / C k_{opm}$$

where $L_{opm} \equiv$ optimal L and $k_{opm} \equiv$ optimal k.

In the analysis of linear sand banks, optimal α and k were found numerically, and graphical deposition rate contours were constructed using α as the y−axis dimension and k as the x−axis dimension (Fig. 84). These calculations were performed assuming characteristic values for f, F, Λ, m and n of 0, 1, 0.005, 2 and 2 respectively. As can be seen from the contour graph, $\alpha_{opm} \simeq 28°$ and $k_{opm} \simeq 10$ where σ is maximum. This corresponds to $L_{opm} \simeq 7.5$ km, which agrees fairly well with the observed mean sand bank spacing of ~ 9 km.

It is interesting that the final expression was derived assuming significant Coriolis force though a reasonably accurate mean sand bank spacing was obtainable through the final expression using the assumption of negligible Coriolis force.

6.3.11   The applicability of the analysis
                       to longitudinal dunes in deserts

The application of the present analysis to the aeolian case of longitudinal dune fields, whether of uniform or variable dune spacing, can be assessed quickly by using the expression for optimal sediment ridge spacing to predict dune separation. Before this can be done, appropriate values for C and H must be obtained.

For wind over sand there exists the expression

$$C = \left[0.4 / \ln 9300 / D \right]^2$$

where $D \equiv$ mean surface roughness dimension (i.e. mean sand grain diameter for smooth sand surfaces or mean ripple height for rippled sand surfaces)

[DONELAN, 1982]. All linear dunes observed during the course of this investigation have had rippled surfaces, but this is not a very significant factor so far as the calculation of the optimal spacing is concerned. Taking a typical ripple height to be $\sim$ 5 mm, $C \simeq 1.32 \times 10^{-3}$, and taking a typical grain diameter to be $\sim$ 0.2 mm, $C \simeq 2.99 \times 10^{-3}$. These C values are of the same order of magnitude; therefore, L_{opm}, which is inversely directly proportional to C, will be of comparable magnitude assuming either rippled or smooth dune surfaces. For the present calculation of L_{opm}, $C = 1.3 \times 10^{-3}$ will be used for a rippled surface. This value is quite reasonable in light of a review of drag coefficients over oceans and continents in which a C value of 1.03×10^{-3} was calculated for a 1.43×10^{7} km^2 region in northern Africa that was 17% forest and 66% desert [GARRATT, 1977].

Using a convenient planetary boundary layer thickness approximation of 1 km for H and the value derived in the linear sand bank analysis of 10 for k, it is obtained that $L_{opm} \simeq 480$ km. Using a low level inversion height approximation of 250 m for H instead, it is obtained that $L_{opm} \simeq 120$ km. Both values are two orders of magnitude greater than most observed mean spacings in linear dune fields. Clearly, the analysis as it stands, does not provide a good model for longitudinal dune field evolution although its component assumptions and physical relationships were all shown to be relevant to the eolian case. A simple flow approach may still be valid, and with increased sophistication, a simple flow analysis may yield accurate dune spacing predictions.

Note that the C values for the aqueous and aeolian cases were of the same order of magnitude. Because the density of water is three orders of magnitude greater than that of air, one might be led to expect a substantial difference between the C values of the two. However, C is a function of the ratio between fluid density ρ and viscosity μ. The viscosity of water is two orders of magnitude greater than that of air; hence, the ratios between ρ and μ for water and air and are comparable. Subsequently, the C values for water and air are comparable.

6.3.12   Qualitative rationalization of energy optimalization in linear sediment ridge systems controlled by simple flow

Linear sand ridge system ordering is not so easily demonstratable by mechanical analogy as river meanders were using bendable rods of spring steel. One way in which to gain an intuitive physical understanding of the expression of energy optimalization in the ordering of linear sediment ridges is the qualitative consideration of extreme instances.

Maximum ridge spacing would be infinite separation – a plain of firm material swept clean of sediment. Approaching this limit would be the instance of very large ridges separated by very great distances. This would be an extremely inefficient state, for a great amount energy would be necessary to transport sediment over vast distances then drive it up extensive slopes against gravity.

Minimum ridge spacing would be infinitesimal separation – a flat bed of sediment. Approaching this limit would be the instance of a series of very small corrugations, each of which is positioned immediately next to its adjacent corrugations. Here flow would experience momentum deprivation everywhere over the ridge system due to saltation. Again, this mode of sand transport is highly inefficient.

In nature, some optimal ridge configuration between the limiting cases must develop. In the optimal configuration, the ridge spacing must be such that the expenditure of energy is minimalized, which occurs when sediment transport is confined to relatively short distances on firm material and up slopes of moderate extent.

6.3.13 Evolutionary timescale

Included in the analysis of linear sand banks is a parameter called the evolutionary timescale [HUTHNANCE, 1982a]. This is an estimate of the minimum interval of time necessary for the formation of an ordered sand bank system.

In the expression for topographic change (3b), the dimensionless constant coefficients of the two sides must be equal. That is, $1 = \frac{SU^3T}{gHL(1-p)}$, where $T \equiv$ timescale. Therefore, by simple algebraic manipulation, $T = \frac{gHL(1-p)}{SU^3}$. Using the typical values for p, H, L, S and U of 0.4, 30 m, 6 km, 1.6×10^{-3} and 1 m/s, $T \simeq 21$ years. Because this is a minimum value, it is reasonable that to develop linear sand bank systems may require several times this minimum interval or up to several hundred years.

The equation for topographic change of longitudinal dunes would almost certainly take a very similar form as (3b) whether simple flow or complex flow with secondary circulation is assumed. Therefore, it is likely that the above expression for evolutionary timescale also applies to longitudinal dune fields. Using the typical values for p, H, L, S and U of 0.4, 1 km, 2.5 km, 1×10^{-6} and 10 m/s, $T \simeq 470$ years. Subscribing to the same mode of interpretation as before, longitudinal dune fields could require several thousand years to develop.

Note that S for the aeolian case is three orders of magnitude less than S for the aqueous case. This ultimately arises from the density difference between air and water. Finally, it is interesting that the evolutionary timescale for longitudinal dune fields is small enough that Holocene formation and ordering of the Australian linear dunes is possible (Sec. 2.1).

6.3.14 Modification of the simple flow model

Minor modifications to the analysis of linear sand banks were made to see if slight adjustments would be adequate for fitting it to the case of longitudinal desert dunes. First, Coriolis force was taken to be 10^{-4}, a mid-latitude approximation, and appropriate values for F and $\hat{\Lambda}$ were calculated for the case of longitudinal dunes. These could be installed into (3c) for the numerical assessment of α_{opm} and k_{opm} without changes to the values of any of the remaining coefficients. This is because only F and $\hat{\Lambda}$ have a direct effect upon the first and second derivatives of σ, which in turn determine α_{opm} and k_{opm}.

Recall that $F \equiv \frac{CUT}{2\pi H}$ and $\hat{\Lambda} \equiv C/\tan(\text{friction angle})$. Taking characteristic values for C, U, H, T and friction angle of 1×10^{-3}, 10 m/s, 1 km, 3 days (wind storm duration) and 32°, it was found that $F \simeq 0.5$ and $\hat{\Lambda} \simeq 0.002$ for longitudinal dunes. These values were used to obtain $\alpha_{opm} \simeq 29°$ and $k_{opm} \simeq 10$, which are virtually the same as the optimal values calculated for linear sand banks. Hence, slightly refined characteristic parameter values have little effect upon the outcome. For a prediction of $L_{opm} \simeq 2.5$ km, a realistic mean longitudinal sand dune spacing, k_{opm} would have to be about 2.5×10^3.

6.3.15 Sand budget

A more sophisticated attempt was made to modify the existing simple flow model by replacing the condition of sand conservation within a dune field with the assumption that either a constant rate of net gain or a constant rate of net loss of sand occurred. Quantitatively, this is taking $\frac{dQ}{dt} \neq 0$ or

$$\frac{dQ}{dt} = \frac{\partial Q}{\partial t} + u\frac{\partial Q_x}{\partial x} + v\frac{\partial Q_y}{\partial y} + w\frac{\partial Q_z}{\partial z} = \vartheta$$

where $\vartheta \equiv$ some constant coefficient, which may be either positive or negative.

The above form of the transport equation results in a topographic change equation of the form

$$\frac{\partial h}{\partial t} = \frac{SU^3 T}{gHL(1-p)}\frac{\partial}{\partial y}\left[|\vec{U}|^n\left(v + \Lambda|\vec{v}|\frac{dh}{dy}\right)\right] - \frac{SU^3\vartheta}{gT(1-p)}$$

where $\vartheta > 0$ corresponds to a net gain in sand, $\vartheta < 0$ a net loss and $\vartheta = 0$ sand conservation. Quite obviously from the form of the above relationship, the quantity ϑ has no effect upon k and therefore also no effect upon sediment ridge spacing L. Only the magnitudes of deposition rate σ and angle α are affected. These assertions have been verified through calculation. Hence, the assumption of net sand gain or loss has no significant bearing upon the question of longitudinal dune ordering at least so far as this simple flow model is concerned.

The formulation of a topographic change equation not assuming sand conservation was inspired by the recent theory that longitudinal dune fields represent areas of net sand loss or "negative sand budget" [MAINGUET, 1984a].*

---

* By this same scheme, transverse dune fields would be areas of net sand gain or "positive sand budget."

Chapter Seven: Complex flow model

A model of secondary circulation during complex flow is reviewed, and its implications on longitudinal dune genesis and ordering are discussed. The particular secondary flow model considered assumes an inviscid and compressible fluid. Although flow in the planetary boundary layer in general (and around dunes in particular) is essentially incompressible (footnote of Section 1.2) an inviscid, compressible model may still be applied to planetary boundary layer phenomena. Compressibility enhances precision in lower layer models.

7.1   The secondary flow model
                and longitudinal dune ordering

7.1.1   The basic equations

At this point it becomes necessary to examine in slightly greater detail the planetary boundary layer secondary flow model [BROWN, 1970] introduced in **Chapter Three.**

The model assumes small perturbations of the quantities u, v, w, P, T and ρ such that $u = \overline{u} + U'$, $v = \overline{v} + v'$, $w = \overline{w} + w'$, $P = \overline{P} + P'$, $T = \overline{T} + T'$ and $\rho = \overline{\rho} + \rho'$ where the barred quantities are mean values and the primed quantities are perturbation values. Mean flow within the boundary layer is taken to be two-dimensional. Quantitatively, this means that $w \ll u$ and $w \ll v$ or $\overline{w} \simeq 0$. The mean values $\overline{u}$ and $\overline{v}$ are taken to be constant in the $x-$ and $y-$directions. The basic non-dimensionalized equations used are those for a compressible, viscous, rotational fluid, and they include the Navier-Stokes equations of motion, the continuity equation (mass conservation), the energy equation and the equation of state. The last three of these are as follows:

$$\frac{\partial \rho}{\partial t} + \mathrm{div}\big(\rho \vec{U}\big) = \frac{\partial \rho}{\partial t} + \rho \nabla \cdot \vec{U} + \vec{U} \cdot \nabla \rho$$

$$= \frac{\partial \rho}{\partial t} + \rho \left(\frac{\partial U}{\partial x} + \frac{\partial v}{\partial y} + \frac{\partial w}{\partial z} \right) + u \frac{\partial \rho}{\partial x} + v \frac{\partial \rho}{\partial y} + w \frac{\partial \rho}{\partial z}$$

$$= 0,$$

$$\frac{\partial T}{\partial t} + u \frac{\partial T}{\partial x} + v \frac{\partial T}{\partial y} + w \frac{\partial T}{\partial z} + \frac{P}{\rho c_H} \left(\frac{\partial u}{\partial x} + \frac{\partial v}{\partial y} + \frac{\partial w}{\partial z} \right) - K_h \nabla^2 T = 0$$

where $c_H \equiv$ specific heat and $K_h \equiv$ coefficient of head diffusion and

$$P = \rho RT$$

where $R \equiv$ gas constant. Note that non-dimensionalization in this case has been carried out by simply redefining parameters as their dimensional quantities divided by their characteristic values. For example T(non-dimensional)$\equiv$ T(dimensional)/some characteristic T.

Making use of Squire's proof, as was done in the simple flow model, a two-dimensional secondary flow is assumed [SQUIRE, 1933]. The equations describing the complete flow are divided into two sets – those taking into account a horizontally homogeneous mean flow and those taking into account a perturbed flow that is periodic and whose magnitude is independent of the longitudinal coordinate. BROWN [1970] concisely outlines the manipulation of the mean flow equations and the perturbation flow equations in deriving the flow instability equation (discussed in Sec. 7.1.2).

From the accepted condition of a longitudinal instability arises the assumption that the resultant secondary flow will be longitudinal as well. Perturbation velocity components and temperature are taken to be periodic laterally. That is

$$\Psi = \Phi(z) \exp\left[i\eta(y - \chi t)\right],$$

$$u' = u(z) \exp\left[i\eta(y - \chi t)\right],$$

and

$$T = T(z) \exp\left[i\eta(y - \chi t)\right]$$

where $v' \equiv \frac{\partial \Psi}{\partial z}$, $w' \equiv \frac{\partial Psi}{\partial y}$, $u' \equiv \left(\frac{\partial \overline{u}}{\partial z}/\overline{v}\right)\Psi$, $\eta \equiv$ instability wavenumber and $\chi \equiv$ a coefficient encompassing both the real wave speed and the instability growth factor.

7.1.2　　The stability equation　　and inflection points

The coupling between u' and Φ in the perturbation equations is weak except for when Coriolis force is large or Re is small. Also, it has been shown that for negligible temperature-density perturbation, the effect of Coriolis force on secondary flow growth rate is insignificant [LILLY, 1966] (Sec. 3.2.4). For a neutral, horizontally homogeneous atmosphere, the perturbation equation becomes

$$(\overline{v} - \chi)\left(\frac{\partial^2 \Phi}{\partial z^2} - \eta^2 \Phi\right) - \frac{\partial^2 \overline{v}}{\partial z^2}\Phi = \left[\frac{1}{i\eta Re}\right]\left[\frac{\partial^4 \Phi}{\partial z^4} - 2\eta^2 \frac{\partial^2 \Phi}{\partial z^2} + \eta^4 \Phi\right].$$

This is the *fundamental differential equation for disturbance (stability equation)*, widely known as the *Orr-Sommerfield equation*, and it is dependent upon the lateral mean velocity component and the vertical variation of the lateral mean velocity component. For large Re (high wind speed), viscous force becomes insignificant in comparison with inertial force, and the right-hand side of the stability equation goes to nought. The new equation

$$(\overline{v} - \chi)\left(\frac{\partial^2 \Phi}{\partial z^2} - \eta^2 \Phi\right) - \frac{\partial^2 \overline{v}}{\partial z^2}\Phi = 0$$

is the *inviscid Orr-Sommerfield equation* or *frictionless stability equation*.

Near surface vertical velocity profiles for which the change of wind speed with height $\frac{\partial |\vec{U}|}{\partial z}$ reaches a maximum where $\partial\left(\frac{\partial |\vec{U}|}{\partial z}\right)/\partial z = 0$ and $\partial^2\left(\frac{\partial |\vec{U}|}{\partial z}\right)/\partial z^2 < 0$ are known as inflection point profiles. Through the inviscid Orr-Sommerfield equation, it was shown that an inflection point is a necessary instability condition [RAYLEIGH, 1880, 1887 and 1913] (Fig. 85). Later it was shown that an inflection point is also a sufficient instability condition [TOLLMEIN, 1935]. Hence, from a purely mathematical point of view, two-dimensional instability and consequently longitudinal secondary flow within two-dimensional flow may arise in an inviscid and therefore irrotational fluid provided an inflection point occurs in the near surface vertical velocity profile. For real fluids, an inflection point results from shear, and shear of course, requires internal friction. In conclusion, viscosity is an inescapable prerequisite for instability.

Where an inflection point exists, vorticity, which is dependent upon $\frac{\partial |\vec{U}|}{\partial z}$, reaches a maximum where $\frac{\partial |\vec{U}|}{\partial z}$ does. This low level vorticity maximum causes amplification of any flow disturbances that happen to be brought down to near the surface (Fig. 85). Also, according to boundary layer theory, vertical velocity profiles in intervals of pressure decrease do not have inflection points whereas those in intervals of pressure increase invariably have them. The occurrence of an inflexion point therefore gives some information on pressure gradient conditions [SCHLICHTING, 1960]. Both these points will be made use of in the discussion of longitudinal dune genesis in the next chapter.

Returning to the full Orr-Sommerfield equation for viscous flow, $\chi = \chi_r + i\chi_i$ where $\chi_r \equiv$ real wave speed and χ_i determines whether the instability wave grows ($\chi_i > 0$), remains unchanged ($\chi_i = 0$) or diminishes ($\chi_i < 0$). Assuming longitudinal secondary flow has the same space and time periodicity as the instability that prompted it, the secondary flow wavelength is expressible in the following simple function of η:

$$\lambda = 2\pi/\eta$$

where $\lambda \equiv$ secondary flow wavelength. The question of stability now becomes an eigenvalue problem, and for any set of values for Re, λ and ε, the angle between the two- dimensional waves and the geostrophic wind velocity, there is a specific complex eigenvalue χ associated with the eigenfunction $\Phi(z) = |\Phi(z)|e^{i\varrho}$ where $\varrho \equiv$ perturbation phase angle, which is a parameter that helps determine the shape of the instability and the resultant secondary flow.*

Plotting χ values for both the inviscid and viscid forms of the stability equation together in a Cartesian plane where Re is the absissa coordinate and $\eta\varrho$ is the ordinate coordinate reveals two important features. The region of viscous instability lies entirely within the region of frictionless instability, and the critical Re of viscous instability is higher than that of frictionless instability. Figure 86 which compares the instability regions associated with viscous and inviscid instability derives from a slightly simpler stability equation, one whose eigenfunctions do not depend upon ϱ.

Line a of Figure 86 defines the boundary of the region of inviscid instability and corresponds to $\chi_i = 0$. Line b of Figure 86 defines the boundary of the region of viscid instability, and curiously, viscid instability occurs where the vertical velocity profile does not have an inflection point.

Growth rate plots as a function of the growth factor $\eta\chi_i$ and ε were constructed for various Re, and critical χ_i and ε of ~ 0.5 and $\sim 20°$ respectively were found [BROWN, 1980].

7.1.3   The form and magnitude of secondary flow

The secondary flow solutions to the complete stability equation are

$$v' = \frac{\partial \Psi}{\partial z} = \frac{\partial |\Psi(z)|}{\partial z}(\cos \varrho \cos \eta y - \sin \varrho \sin \eta y)|\Psi|_{max}$$

and

$$w' = -\frac{\partial \Psi}{\partial y} = |\Psi(z)|(\sin \varrho \cos \eta y + \cos \varrho \sin \eta y)|\Psi|_{max}.$$

These give the form and magnitude of the secondary flow components. At any Re, there is one unique pair of η and ϱ values correspondent to maximum

---

* The roll vortices that arise in the model are each individually asymmetric in that they "lean" to one side in their transverse section (Figs 18 and 19), and the degree of this asymmetry is dependent upon ϱ. Roll vortices observed in nature display no such skewness.

perturbation growth, and optimal η determines the secondary flow wavelength through $\lambda = 2\pi/\eta$.

The value of $|\Psi|_{max}$ is found through the energy balance equation

$$|\Psi|_{max}^2 = \int_0^H U_E A(z) dz / \int_0^H \overline{U}' A(z) dz$$

where $U_E \equiv$ Ekman profile (App. 16), $\overline{U}' \equiv$ mean flow velocity modification due to the finite perturbations and $A(z) \equiv$ the shape function $\equiv 2\eta\left[\partial(\frac{\partial \varrho}{\partial z}\Phi^2)/\partial z\right]$. The form of $A(z)$ derives from the solution to the stability equation.

7.1.4 Longitudinal dune genesis and ordering

Let it be assumed that fixed roll vortices occur in a desert area with a supply of loose sand. To learn what type of deposition structures will result from the interaction between the roll vortices and the sand, v' from above is substituted for v in the topographic change equation of form equation (3) of Section 6.3.5. Right-hand differentiation of such an expression with respect to y, would result in a topographic change relationship of form

$$\frac{\partial h}{\partial t} \propto \cos\varrho \sin\eta y - \sin\varrho \cos\eta y.$$

This immediately indicates that given steady roll vortices, well-ordered longitudinal dunes of the same wavelength as the roll vortices will begin to form. The unlikeliness of unconfined, steady roll vortices, however, makes this mode of longitudinal dune genesis seem improbable. As quickly as low sediment ridges are deposited, they would be disrupted by the lateral shifting of the roll vortices.

Once longitudinal dunes of significant height are established, roll vortices, whether responsible for dune genesis or not, will assume an alignment such that their near surface flow convergence zones superpose the dunes (Sec. 3.2.11). Consequently, further building of the dunes will occur. Longitudinal dune fields in which dune spacing is nearly uniform and of wavelengths roughly twice the thickness of the planetary boundary layer would be the expected outcomes (Sec. 1.5.1).

A quantitative description of the entire process of longitudinal dune genesis and growth under the influence of roll vortices should derive from an analysis coupling topographic change and secondary flow while taking into account a corrugated bottom boundary. Though straight forward in conception, such an analysis promises to be a considerable mathematical undertaking.

Chapter Eight: Dune genesis

The formation of linear dunes by the extension of barchans and the growth of subsidiary barchans [BAGNOLD, 1941] or the linkage of extending barchans [SOLOKOW, 1984] has been discussed in Section 2.2.3. Though there exists in the field examples of sand ridges that are in essence barchan chains [LANCASTER, 1980], these forms are linear and oblique rather than longitudinal. Therefore, this type of sand ridge formation mechanism is not examined in this chapter.

As was seen in the last chapter, longitudinal dune genesis is the expected consequence of steady large scale roll vortices close to the ground. The other possibility is that longitudinal dunes begin as sediment ridges deposited by small scale roll vortices generated as a result of the interaction between elongate debris mounds and oblique winds [TWIDALE, 1972a and 1981]. This second possibility for longitudinal dune genesis is, like the dune coalescence mechanism for longitudinal dune ordering, a difficult question to deal with in that no conceptually simple quantitative approach readily suggests itself. Also, there is a general paucity of field information regarding flow around transverse debris mounds. However, the aerodynamic feasibility of such a mechanism may be considered. What follows is an introduction to Australian linear dunes that initiate at transverse debris mounds and a qualitative consideration of the various components of the aerodynamic mechanism of longitudinal dune genesis.

8.1   Central Australian linear dunes

From the air it can be seen that in the deserts of central Australia linear dunes, most of which are not presently but may at one time have been longitudinal dunes as well, often propagate from debris mounds at the leeside boundaries of dried salt lakes, river beds and alluvial flood plains [TWIDALE, 1972a and 1981] (*see* Pl. 12). The debris mounds result from deposition of the deflated material from their associated bare alluvial beds, and they are oriented such that cross flows are usually experienced during strong winds. Figure 35 is a map of the desert regions of central Australia, which features a large number of dried lakes and water courses. Figures 87, 88 and 89 show leeside debris mounds and linear dunes.

The linear dunes that propagate from leeside debris mounds are randomly spaced and of varying heights. Within kilometers downwind, these dunes assume

the low degree of order characteristic of longitudinal dune fields of variable dune spacing. As noted earlier, the transition zone between the random and orderly portions of the dune network is highly significant. It is within this area that the coalescence mechanism operates most intensely to impose organization.

Incidentally, it is possible that longitudinal dunes migrate downwind. This is not simply to say that they lengthen along their longitudinal axis but that they move leeward as a body, presumably once their sediment source is sufficiently depleted. Downwind migration would explain why linear dunes are sometimes observed far from any potential sediment source areas.

8.2   Aerodynamic mechanism

Obstacles at oblique angles to the mean strong winds such as debris mounds may cause several types of air flow instability. These instabilities give rise to paired vortical air currents with individual members of opposite senses of rotation – small scale roll vortices. Longitudinal deposition occurs in the surface flow convergence zones of these roll vortices. With time, longitudinal dunes develop. To appreciate this mechanism, it is necessary to understand the different types of possible air flow instability due to interaction between the flow and debris mounds, and the manner in which these instabilities create vortical currents.

8.2.1   Stagnation pressure instability

Stagnation pressure is the fluid pressure on the flowward surface of obstacles, where flow velocity must be zero. An expression for stagnation pressure as the sum of the ambient fluid pressure and a parameter that is a function of local fluid velocity is

$$P_\mathrm{o} = P + \Gamma(\vec{U})$$

where $P_\mathrm{o} \equiv$ stagnation pressure.

Because flow velocity is a function of height and disappears precisely at the ground, stagnation pressure also diminishes downward (Fig. 90). A vertically downward directed pressure gradient is established over the flowward surface of obstacles. The downward pressure gradient force causes the downward transport of fluid, and this initial displacement results in a vertical mass exchange. An

oscillation is created, and the flow to leeward becomes rotational. Obstacle-scale roll vortices are generated to leeward (Fig. 91).

Alternatively, roll vortices production in this instance can be thought of as due to inflection point instability (Sec. 7.1.2). Along line s in Figure 91, the vertical velocity profile has an inflection point (Fig. 85), which indicates certain pressure gradient characteristics. Namely, to flowward of line s ambient pressure is reduced by flow constriction over and around the obstacle. Just to leeward of line s, flow immediately above the surface has insufficient momentum to pierce the high pressure zone in that vicinity. Leeward flow is turned back upon itself, and both a leeside rotor and leeside roll vortices are produced (Fig. 92). Line s designates the "separation of flow" boundary. Stagnation pressure instability is probably the main mechanism of roll vortices generation to the lee of debris mounds.

8.2.2   Centrifugal instability

Flow along a concave surface is centrifugally unstable. This is due to a gradient in the fluid flow acceleration along lines normal to the surface. That is, a gradient in fluid acceleration occurs over a concave surface, where centrifugal acceleration increases with increasing radial distance from the surface (App. 17). As with the previous instance of stagnation pressure gradient, vortical currents are generated. This type of instability is known as "Görtler instability," and the resultant roll vortices are known as "Görtler vortices" (Fig. 93). An easy but perhaps somewhat simplistic rule for flow over curved surfaces is that flow over convex surfaces is intrinsically stable and flow over concave surfaces is intrinsically unstable (Fig. 93).

8.2.3   Momentum deprivation instability

Momentum deprivation near the surface may induce an inflection point in the flow's vertical velocity profile in which case the flow becomes unstable (Fig. 85). Inflection point instability will cause the generation of roll vortices (Sec. 7.1.2), and one possible cause for near surface momentum is saltation.

8.2.4   Longitudinal dune formation
to the lee of debris mounds

Flow encountering a debris mound at an oblique angle experiences stagnation pressure instability. Descending the leeside slope it experiences the additional minor instability due to centrifugal force imbalance, and during saltation, inflection point instability also contributes slightly to the total instability. Such instabilities are significant around topographic irregularities in the debris mound such as bulges and notches, and roll vortices are generated to leeward of these irregularities. The secondary flow promotes longitudinal deposition to the lee of irregularities and the amplification of these irregularities, particularly bulges, by trenching around them. The more pronounced irregularities create greater instability and more vigorous roll vortices. Longitudinal leeside deposition intensifies, and with time, secondary irregularities are produced, which generate their own secondary flow and develop their own deposition tail. Eventually the deposition tails become recognizeable longitudinal dunes. Figure 94 is a series of sketches depicting the topographic change around a single bulge. Figure 95 shows the genesis of a series of longitudinal dunes from a single debris mound.

8.2.5   Wind tunnel trials

Empirical support for the theory that longitudinal dunes can propagate from debris mounds was sought through wind tunnel trials using scaled plasticene models of debris mounds [TWIDALE, 1972a]. The plasticene obstacles gave rise to roll vortices, which in turn produced longitudinal deposition tails (Fig. 96).

8.2.6   Conclusion

The theory for longitudinal dune genesis to the lee of debris mounds seems fairly well supported by physical argument and laboratory trials, and though debris mounds are associated with the Australian linear dune fields of variable spacing, their relevance with respect to longitudinal dune fields of uniform wavelength remains an open possibility. This can be resolved only after a comprehensive survey of aerial imagery for global linear dune fields.

In closing, it is noted that the same aerodynamic factors that cause longitudinal deposition to the lee of debris mounds may also support longitudinal deposition to the lee of small hills or depressions. It is therefore possible for individual longitudinal dunes to form in isolation.

Chapter Nine

Conclusions

Longitudinal dune ordering and longitudinal dune genesis are two separate phenomena. Furthermore, there are probably two distinct types of ordered longitudinal dune fields – those with variable dune spacing and those with uniform dune spacing. Of the various recorded hypotheses, the only viable mechanism for the ordering of longitudinal dunes of uniform wavelengths is planetary boundary layer scale roll vortices. This conviction is superficially supported by the fact that such dune fields typically display mean wavelengths of about twice the planetary boundary layer thickness. A considerable body of meteorological and fluid dynamical research relevant to roll vortices in the boundary layer indicates the feasibility and likelihood of roll vortices in deserts, especially where uniformly spaced longitudinal dunes exist (Ch. 3).

The roll vortices mechanism can be tested for refutation simply by testing for the occurrence of roll vortices in currently active longitudinal dune fields of uniform wavelength. If roll vortices are not evidenced during typical strong winds, then it becomes unlikely that they could have worked to establish the ordering of the dunes. The various possible methods for roll vortices detection and measurement have been carefully considered, and the best one for desert work with regards to the quality of data obtained, logistical feasibility and cost efficiency, involves the airplane measurement of horizontal temperature variation (Sec. 4.7). A cheaper and simpler method utilizing a network of tethered kites will yield substantially less reliable data and require the coordinated effort of a large number of field workers (Sec. 5.1.8). Australia is unsuitable for wind studies in general and roll vortices observations in particular, for its linear dune fields are currently stabilized by vegetation and are of variable dune spacing (Sec. 5.19). Egypt is recommended as an area for roll vortices observation, for its linear dune fields are active, comparatively simple in form and relatively accessible.

Periodic two-dimensional instability within simple-flow/sand-transport/longitudinal-dunes systems is a possible mechanism for the ordering of longitudinal dune fields, whether of uniform or variable dune spacing (Ch. 6). A model for simple-flow/sand-transport/linear-sandbanks systems is slightly modified to accomodate desert conditions and is shown to be invalid for longitudinal dune ordering. Nevertheless, the simple flow linear sandbanks model is promising, and its details are paid close attention. A more sophisticated simple flow longitudinal dunes model may one day fare better than the current one. Alternatively, the roll vortices mechanism can be tested assuming complex flow. Salient features

of the best available planetary boundary layer secondary flow model and the implications of its results on longitudinal dune genesis and ordering are discussed (Ch. 7).

Dune coalescence may control the low organization of longitudinal dune fields of variable dune spacing (Sec. 3.1.2.). This impression is supported by the high density of Y junctions characteristic of these dune fields. The wide variability of mean dune spacing among these dune fields suggests a mechanism strongly influenced by local conditions, and an aerodynamic dune coalescence mechanism would presumably be partially dependent upon topography and wind conditions. One possible explanation for dune coalescence may be horizontal pressure gradients within longitudinal dune fields due to flow constriction between adjacent dunes (Sec. 3.1). All possible mechanisms for longitudinal dune ordering are considered to be manifestations of the principle of energy optimalization (Ch. 6). Once again, ordered longitudinal dune fields result when wind sand transport is maximized in dune/wind/sand-transport systems.

Some central Australian linear dunes propagate to the lee of transverse alluvial debris ridges on fringes of exposed lake and river beds (Ch. 8). Linear sediment ridges to leeward of the debris mounds are probably initiated when flows obliquely incident upon the mounds produce leeward roll vortices that, in turn, result in leeward longitudinal deposition. Vertical pressure gradients over the windward face of the mounds is the most likely main cause for leeward roll vortices generation although centrifugal instability over concave leeward slopes and near-surface momentum deprivation of the flow due to bottom saltation are probably subsidiary contributors to this effect. Essentially the same aerodynamic factors may produce isolated longitudinal dunes to the lee of small hills and depressions. It is highly significant that linear dunes that emerge from debris mounds are random but assume a low degree of organization through coalescences within a distance of tens of kilometers. Clearly, the coalescence mechanism operates very vigorously within a small space. Of great interest is the unresolved possibility that linear dune propagation to leeward of debris mounds may occur to form longitudinal dune fields of uniform wavelength.

Using tethered kites around linear dunes, evidence was found of windward side rotors during oblique flows (Sec. 5.5) and roll vortices during parallel flows (Sec. 5.7). Using colored sand, evidence was found of leeward side rotors during oblique flows (Sec. 5.3). Using simple wind velocity and direction monitoring schemes, the wind velocity vector was found to attain maximum magnitude just to windward of the crest of the study linear dune (Sec. 5.10), and to deflect

such that its directional component transverse to the dune increased while its directional component aligned with the dune decreased (Sec. 5.11).

The periodic summits on the study dune were found to translate to leeward along the longitudinal axis of the dune while altering in spacing only slightly, and the study dune's lateral migration was detected (Sec. 5.15).

Sand firmness patterns over the study dune were quite distinctive and may be related to sand transport trends. For example, it was seen that the sand was relatively very loose over the area in which avalanche faces occurred periodically but were not evident at the time of firmness measurement. It is conceivable that firmness patterns may be related to local seasonal wind patterns, but without long term monitoring, interpretation of firmness patterns will remain highly conjectural.

The monitoring of deposition and erosion over any sandy area and in particular over a dune using a grid of implanted stakes was tested (Sec. 5.12). As alluded to above, various types of flow and secondary flow were observed using tethered kites (Secs 5.5, 5.6, 5.7, 5.8 and 5.9). Various other methods for secondary flow observation and sand transport monitoring, amongst which were tethered balloons, tracked free flight balloons, instrumented towers, instrumented planes, radar, smoke trails and colored sand capture, were assessed for their reliability, logistic feasibility and cost (Ch. 4). Horizontal pressure gradients around linear dunes were assessed but later discounted when the measurement technique was shown to be invalid (Sec. 5.22).

Table One

Morphometry of linear dunes in sand seas

[BREED and GROW, 1979]

[$\bar{W}$, mean width; $\bar{L}$, mean length (*, some or all dunes extend beyond edge of image); $\bar{\lambda}$, mean wavelength (crest-to-crest distance); $\bar{F}$, mean frequency (number of dunes per kilometre) across sample, normal to trend of dunes. All measurements in kilometres]

Region[1]	Latitude, longitude	Desert or sand sea area	Area sampled (km²)	$\bar{W}$	$\bar{L}$	$\bar{\lambda}$	$\bar{L}/\bar{W}$	$\bar{W}/\bar{\lambda}$	$\bar{L}/\bar{\lambda}$	$\bar{F}$	Figure No.
		Simple(?) linear dunes									
1	35°30'-36° N., 111°-111°15' W.	Navajo Indian Reservation (northern Arizona, U.S.A.)--------------------------	625	0.043	3.65	0.15	84.9	0.29	24.3	4.92	168B
2	23°-27°30' S., 137°-140°30' E.	Simpson Desert (Australia)-----------------	30,000	.22	24.0	.90	109.1	.24	26.67	1.44	None.
3	19°30'-23°30' S., 122°30'-128°30' E.	Great Sandy Desert (Australia)------------	35,000	.29	22.7	.90	78.3	.32	25.22	1.06	169B
4	23°30'-25°45' S., 17°30'-19°30' E.	Kalahari Desert (southern Africa)---------	15,000	.29	26.0	.70	89.7	.41	37.14	1.26	169A
5	20°30'-21°30' N., 52°-52°30' E.	Northeastern Rub' al Khali (Saudi Arabia)-	2,500	.38	14.34	1.41	37.7	.27	10.17	.64	241
		Compound linear dunes									
6	21°-22° N., 08°-10° W.	Southwestern Sahara (Mauritania)----------	2,500	0.94	>100.00*	1.93	106.4*	0.49	51.81*	0.48	169D
7	18°-19° N., 13°-14°30' E.	Southern Sahara (Niger)--------------------	7,500	1.06	>40.*	1.90	37.7*	.56	21.05*	.29	None.
8	16°30'-19°15' N., 45°30'-50° E.	Southwestern Rub' al Khali (Saudi Arabia)-	20,000	1.21	>83.*	2.18	68.6*	.55	38.07*	.48	169C
		Complex linear dunes									
9	24°-24°45' S., 14°45'-15°30' E.	Namib Desert (South-West Africa)----------	2,500	0.88	27	2.20	30.7	0.40	12.27	0.47	169E
10	26°30'-28° N., 00°30'-02°30' E.	Northern Sahara (Algeria)------------------	2,500	1.09	30.75	3.24	28.2	.34	9.49	.33	168B
11	19°-19°30' N., 15°-15°30' E.	Southern Sahara (Niger)--------------------	2,500	1.28	65	3.28	50.8	.39	19.81	.30	None.
12	18°45'-19°30' N., 45°15'-46° E.	Western Rub' al Khali (Saudi Arabia)------	2,500	1.48	73	3.17	49.3	.47	23.03	.21	169F

[1]Sources of data--(1) Aerial photographs, National Aeronautics and Space Administration: 236-28-0071, 236-28-0072. Following are numbered Landsat images: (2) E1315-00140, E1227-00264, E1224-00100, E1369-00135, E1369-00141, E1133-00040, E1296-00090, E1367-0025, E1224-00093;(3) E1344-01160, E1127-01111, E1377-00585, E1127-01113, E1415-01091, E1130-01045, E1124-00535, E1130-01051, E1125-00591, E1124-00542, E1344-01165, E1413-00584, E1344-01162;(4) E1147-08160, E1416-08085, E1416-08091, E1145-08052; (5) E1184-06255; (6) E1119-10324; (7) E1192-08553; E1193-09012; (8) E1187-06433, E1132-06380, E1187-06435, E1170-06493; (9) E1383-08270; (10) E1115-10074; (11) E1192-08553; (12) E1189-06550.

Table Two

Flow boundaries, their associated critical
Rayleigh numbers and the dimensional ratios
of the resultant convection cells and bands

Boundaries		Rayleigh number	D/H of square cells	D/H of bands	D/H of hexagonal cells
free, free	$\nu_{x,y} = \nu_z$	658	4.0	2.83	3.28
	$\nu_{x,y} \gg \nu_z$	658	$2.83\left(\frac{\nu_x\nu_y}{\nu_z}\right)^{\frac{1}{2}}$	$2.0\left(\frac{\nu_x\nu_y}{\nu_z}\right)^{\frac{1}{2}}$	
free, fixed		1,100	3.28	2.34	2.7
fixed, fixed		1,708	2.8	2.0	2.32

[KUETNNER, 1965]

In this context, "boundaries" refers specifically to horizontal plane boundaries.

A "free" boundary may be quantitatively defined as any boundary at which $w = \frac{\partial^2 w}{\partial z^2} = 0$, where w is the vertical velocity component. A free boundary at $z = 1$ km may be the top of the Planetary Boundary Layer.

A "fixed" boundary may be quantitatively defined as any boundary at which $w = \frac{\partial w}{\partial z} = 0$. A fixed boundary at $z = 0$ may be the ground.

The set of boundaries relevant to say cloud layers is "free, free", and the set of boundaries relevant to flow over the surface is "free,fixed".

The parameters $\nu_{x,y,z}$ are the three components of eddy viscosity, which is a coefficient that gauges the potential for eddy formation in a fluid. Eddy viscosity is closely tied with the concept of viscosity, for without the internal forces of cohesion (intermolecular binding forces) that manifest themselves in viscosity, a fluid could not turn or rotate and thereby form eddies.

Note that the horizontal components of eddy viscosity $\nu_{x,y}$ may be considerably greater than the vertical component ν_z. This would correspond to the situation of a convection free layer of clear air between layers of clouds.

$H \equiv$ distance between the boundaries

$D \equiv$ salient dimension of resultant convection cells

Assumming "square" convection cells, D is the measure of a side.

Assuming convection "bands", D is the measure of a typical band width.

Assuming "hexagonal" convection cells, D is the measure of the distance between opposite sides.
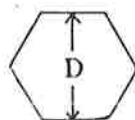
Table Three

Buoyancy and Coriolis terms (ergs gm^{-1})
during roll situations in Oklahoma

	Height	$\overline{w_r T_r g}/T$	$f\overline{u_r v_r}$	$-f\overline{u_r w_r}\cos\phi$	
15 June 1035–1157	$0.55z_I$	-3.7	0.08	0.21	2 rolls
28 June 1049–1137	$0.35z_I$	0.35	-0.06	0.05	1 roll
28 June 1537–1637	$0.20z_I$	2.4	-0.01	0.05	2 rolls
29 June 1412–1509	$0.25z_I$	2.3	0.12	0.21	1 roll

$\overline{w_r T_r g}/T \equiv$ buoyancy term
   where $w_r \equiv$ roll w
   and $T_r \equiv$ roll T

$f\overline{u_r v_r} \equiv$ transverse Coriolis term
   where $u_r \equiv$ roll u
   and $v_r \equiv$ roll v

and

$-f\overline{u_r w_r}\cos\Psi \equiv$ vertical Coriolis term
   where $\Psi \equiv$ stream function defined by
   $u = -\frac{\partial\Psi}{\partial y}$ and $v = \frac{\partial\Psi}{\partial x}$

[LEMONE, 1973]

Table Four

ε versus T_N/L_N and T_W/L_W

ε	T_N/L_N	T_W/L_W
10	0.485	2.06
15	0.850	1.18
20	1.57	0.637
25	3.39	0.295
30	5.31	0.188
35	13.0	0.0769
40	31.9	0.0313
45	86.6	0.0115

[WIPPERMAN, 1969]

$\varepsilon \equiv$ angle between the two orthogonal sets of roll vortices

$T_N/L_N \equiv$ ratio between the wavenumbers of the transverse roll vortices
and the longitudinal roll vortices
$\equiv \nu/\mu$ in WIPPERMAN

$T_W/L_W \equiv$ ratio between the wavelengths of the transverse roll vortices
and the longitudinal roll vortices
$\equiv \lambda_\nu/\lambda_\mu$ in WIPPERMAN

Appendix One

The physics of sand migration

Over a flat surface, the paths of travel of individual sediment grains is only partially determined by the flow that provides most of the transport energy. The random collisions between grains that occur both in the air and on the ground is another factor. On slopes, gravity causes grain paths to depart from the direction of mean flow, and strong secondary circulation also contributes to grain motion divergence. Finally, during oblique winds, grain motion on the leeward slope of linear dunes is aligned not to the flow but to the longitudinal axis of the dunes [TSOAR, 1978]. Clearly, the direction of mean sand transport cannot always coincide with the direction of the mean flow. Hence, gauges of sand migration, such as the annual resultant drift [McKEE, 1979], may not reflect the predominant winds, and it is indeterminant whether linear dunes aligned with sand migration are longitudinal.

Appendix Two

Compound crests

The appearance of compound crests may suggest the lateral overtaking of one linear dune by its neighboring linear dune. Upon careful consideration, however, this idea must be abandoned. If the individual crests of linear dunes with compound crests are of nearly equal height, they would originally have had to belong to individual linear dunes of similar dimensions. It is difficult to understand why the lateral rates of migration for two linear dunes of similar size would have been different enough to allow one dune to overtake the other.

On the other hand, if the individual crests of linear dunes with compound crests are of different heights, then the crests of each dune would presumably have had to originate from individual dunes of different size. It is possible for dunes of different sizes to have different rates of lateral migration, but it is highly unlikely for an entire dune field to consist of pairs of neighboring dunes of significantly different rates of lateral migration.

An alternative explanation for linear dunes with compound crests may be that initially broad, single-crested linear dunes developed dual crests as a result of aerodynamic processes in which the spatial distribution of sand was affected. Possibly, compound crests developed as secondary circulation such as vortices (during parallel winds) and rotors (during oblique winds) excavated sand from the center of the dune and deposited it to either side of the resultant crestal rift. Alternatively, the instability of the dune/wind/sand-transport system may simply manifest itself under certain conditions in the form of compound crests.

Appendix Three

Hypothetical palaeoclimatic conditions

During glacial periods, global mean temperatures would have been lower, with the probable consequence that precipitation dwindled because of inhibited evaporation. Ultimately, reduced moisture would have resulted in extensive hyperarid regions on the continents. It has been hypothesized that much if not most of Australia at this time was hyperarid and therefore suitable for longitudinal dune development [BOWLER, 1976, 1978 and 1982].

Greater glacial period polar ice caps would have induced contraction of the mid-latitudinal cyclones and anticyclones. The more densely packed isobars of these contracted systems would have produced higher mean winds, thereby presumably facilitating dune formation and ordering.

Appendix Four

Comparative Reynold's number analysis
for aqueous bedform features and linear dunes

$R \equiv$ Reynold's number

$R \equiv VL\rho/\eta$ where $V \equiv$ typical relative velocity
of the body with
respect to the fluid,

$\qquad L \equiv$ typical salient dimension
of the body

$\qquad \rho \equiv$ fluid density,

and

$\qquad \eta \equiv$ fluid viscosity.

aqueous bedform features

$V \simeq 0.40$ m/s

$L \equiv$ water depth
$\simeq 0.05$ m

$\rho \equiv \rho$ for water at 20° C and 1 atm
$= 0.99823$ gm/ml
$\simeq 0.998 \times 10^6$ gm/m^3

$\eta \equiv \eta$ for water at 20° C
$\simeq 1$ centipoise
$\simeq 1$ gm/s-m

$$R \simeq \frac{(0.40 \frac{m}{s})(0.05 \text{ m})(0.998 \times 10^6 \frac{gm}{m^3})}{1 \frac{gm}{s-m}}$$

$\simeq 2 \times 10^4$

linear dunes

$V \simeq 40$ km/hr $\simeq 11.1$ m/s

$L \equiv$ typical PBL* thickness
$\simeq 1$ km $= 10^3$ m

$\rho \equiv \rho$ for dry air at 40° C and 1 atm
$= 0.001205$ gm/ml
$\simeq 1.21 \times 10^3$ gm/m^3

$\eta \equiv \eta$ for dry air at 40° C
$= 190.4$ micropoise
$\simeq 190 \times 10^{-4}$ gm/s-m

$$R \simeq \frac{(11.1 \frac{m}{s})(10^3 \text{ m})(1.21 \times 10^3 \frac{gm}{m^3})}{190 \times 10^{-4} \frac{gm}{s-m}}$$

$\simeq 7.07 \times 10^8$

* Planetary Boundary Layer

Appendix Five

Dune coalescence

A linear dune within a certain distance of the next windward linear dune may be sheltered to some extent by this neighbor from the full effects of the flow. Such a wind "shadow" could conceivably cause dune coalescence, and it would explain the instances in which adjacent linear dunes converge but do not coalesce and, in many cases, subsequently diverge (Pl. 46). Possibly, the mainstream "jumps" the gap between the juxtaposed dunes, and a weak rotor in the gap acts to maintain separation (Fig. 97).

Appendix Six

Comparative Reynold's number analysis
for parallel-travelling ships and
longitudinal desert dunes

$R \equiv$ Reynold's number

$R \equiv VL\rho/\eta$ where $V \equiv$ typical relative velocity
of the body with
respect to the fluid,

$L \equiv$ typical salient dimension
of the body

$\rho \equiv$ fluid density,

and

$\eta \equiv$ fluid viscosity.

parallel ships	*longitudinal dunes*
$V \simeq 30$ km/hr $\simeq 8.33$ m/s	$V \simeq 40$ km/hr $\simeq 11.1$ m/s
$L \equiv$ typical ship's length $\simeq 200$ m	$L \equiv$ typical dune's length $\simeq 10$ km $= 10^4$ m
$\rho \equiv \rho$ for water at 20° C and 1 atm $= 0.99823$ gm/ml $\simeq 0.998 \times 10^6$ gm/m^3	$\rho \equiv \rho$ for dry air at 40° C and 1 atm $= 0.001205$ gm/ml $\simeq 1.21 \times 10^3$ gm/m^3
$\eta \equiv \eta$ for water at 20° C $\simeq 1$ centipoise $\simeq 1$ gm/s-m	$\eta \equiv \eta$ for dry air at 40° C $= 190.4$ micropoise $\simeq 190 \times 10^{-4}$ gm/s-m

$$R \simeq \frac{(8.33 \, \frac{m}{s})(200 \text{ m})(0.998 \times 10^6 \, \frac{gm}{m^3})}{1 \, \frac{gm}{s\text{-}m}}$$

$$\simeq 1.66 \times 10^9$$

$$R \simeq \frac{(11.1 \, \frac{m}{s})(10^4 \text{ m})(1.21 \times 10^3 \, \frac{gm}{m^3})}{190 \times 10^{-4} \, \frac{gm}{s\text{-}m}}$$

$$\simeq 7.00 \times 10^9$$

Appendix Seven

Estimated minimum deceleration
for rotation canister fluid

$\omega = V/R$ where $\omega \equiv$ angular velocity
$V \equiv$ velocity
and $R \equiv$ radius of curvature

$V = \omega R$

$a \equiv \frac{\Delta V}{\Delta t}$ where $a \equiv$ acceleration
and $t \equiv$ time

1.) $\Delta V = \Delta(\omega R)$

For any individual canister trial R is constant. Hence, for a hypothetical trial for which all factors assumed mean values, R is taken to be invariant.

2.) $\Delta V = R(\Delta \omega)$

3.) Thus $a = R\frac{\Delta \omega}{\Delta t}$

$\Delta \omega \equiv \omega(\text{initial}) - \omega(\text{final})$
$\Delta t \equiv t(\text{initial}) - t(\text{final})$

4.) For $\omega(\text{initial}) = 0.83 \text{ s}^{-1}$,
$\omega(\text{final}) = 0 \text{ s}^{-1}$,
$t(\text{initial}) = 0 \text{ s}$,
$t(\text{final}) = 10 \text{ s}$,
and $R = 0.10 \text{ m}$,

$$a = -\left(\frac{0.10 \text{ m} \times 0.83 \text{ s}^{-1}}{10 \text{ s}}\right) = -0.0083 \text{ m/s}^2$$

Appendix Eight

Comparative Reynold's number analysis
for rotation canister longitudinal sand
and desert longitudinal dunes

$R \equiv$ Reynold's number (See App. 1)

$R_\omega \equiv$ rotational Reynold's number

$R_\omega \equiv \omega L \rho / \eta$ where $\omega \equiv$ rotation rate

rotation canister longitudinal sand streaks

$\omega \simeq 0.83 \text{ s}^{-1}$

$L \equiv$ canister fluid depth
$\simeq 2$ canister radii $\simeq 0.20$ m

$\rho \equiv \rho$ for water at 20° C and 1 atm
$= 998 \text{ kg/m}^3$
$\simeq 0.998 \times 10^6 \text{ gm/m}^3$

$\eta \equiv 4 \times \eta$ for water at 23° C
$\simeq 1$ centipoise
$\simeq 3.73 \times 10^{-3} \text{ kg/s-m}$

$$R \simeq \frac{(0.83 \frac{m}{s})(0.20 \text{ m})(998 \times 10^6 \frac{gm}{m^3})}{3.73 \times 10^{-3} \frac{kg}{s-m}}$$

$\simeq 4.39 \times 10^4$

desert longitudinal dunes

$V \simeq 11.1 \text{ m/s}$

$L \equiv$ PBL thickness
$\simeq 1 \text{ km} = 10^3 \text{ m}$

$\rho \equiv \rho$ for dry air at 40° C and 1 atm
$= 1.21 \text{ kg/m}^3$
$\simeq 1.21 \times 10^3 \text{ gm/m}^3$

$\eta \equiv \eta$ for dry air at 40° C
$= 190.4$ micropoise
$\simeq 190 \times 10^{-7} \text{ kg/s-m}$

$$R \simeq \frac{(11.1 \frac{m}{s})(10^3 \text{ m})(1.21 \times 10^3 \frac{gm}{m^3})}{190 \times 10^{-7} \frac{kg}{s-m}}$$

$\simeq 7.07 \times 10^8$

Appendix Nine

Comparative Froude number
analysis for rotation canister
longitudinal sand streaks and
desert longitudinal dunes

$F \equiv$ Froude number $\equiv V^2/gL$ where $g \equiv$ gravitational constant

$F_\omega \equiv$ rotational Froude number $\equiv \omega_2 L/g$ where $\omega \equiv$ rotation rate

rotation canister longitudinal sand streaks	*desert longitudinal dunes*
$V \simeq 0.83 \text{ s}^{-1}$	$V \simeq 11.1 \text{ m/s}$
$L \equiv$ canister fluid depth $\simeq 2$ canister radii $\simeq 0.02$ m	$L \equiv$ PBL thickness $\simeq 10^3$ m
$F_\omega = \dfrac{(0.83 \text{ s}^{-1})^2 (0.20 \text{ m})}{9.8 \frac{m}{s^2}}$	$F = \dfrac{(11.1 \frac{m}{s^2})}{(9.8 \frac{m}{s^2})(10^3 \text{ m})}$
$\simeq 1.47 \text{x} 10^{-2}$	$\simeq 1.26 \text{x} 10^{-2}$

Appendix Ten

Sand coloring technique

Of the several procedures tried for sand coloring, some personally developed, the best one was found to be that used in two well known past experiments observing sand transport in tides and over longitudinal dunes [INGLE, 1966; TSOAR, 1978].

For every kilogram of sand, 1 g of Neo-Zapon pigment (manufactured by B.A.S.F.) is disolved in 50 mls of a solvent, for example ethyl alcohol. To the staining solution, 2.5 g of Mowital binder (manufactured by Hoechst) is mixed in slowly and gradually; a sudden inclusion of binder will cause it to coagulate in a polymer wad. The readied staining solution is poured into the clean sand, and this is stirred until all the sand has assumed the color of the stain. The sand is then allowed to dry, and after drying, the resultant sand conglomerations must be pulverized.

Using this procedure has several advantages. Because there is a fairly good selection of Neo-Zapon pigments, sands of various different colors can be produced. Also, Neo-Zapon pigment provides for fairly bright coloration. The presence of the binder in the final pigment adds considerably to the durability of the coloration. It is resistant to fresh and salt water dissolution for at least up to one month under still conditions. The pigment resides in the pits and crevices of grain surfaces and therefore is fairly impervious to the impacts of saltation. The amount of pigment that adheres to each grain is comparatively very little. Thus it is believed that pigmentation does not significantly affect sand density or the aerodynamic properties of each grain.

As briefly discussed in Section 5.3, poor pulverization of the freshly colored sand results in a significant proportion of conglomerated particles. Therefore, care must be taken in this step of the procedure of doing a thorough job. A cement mixer is recommendable for pulverization.

Appendix Eleven

An expression for the calculation of a
quasi-parabolic vertical temperature gradient
using optical measurements of inferior mirages

$$T_h - T_e = A\tau_*\left[1 - (1 - \xi_s/\xi_* - h/\xi_*)^{\frac{1}{2}}\right] + B(h + \xi_s)$$

where $h \equiv$ height above the surface in m

$T_h \equiv$ air temperature at height h in°C

$T_e \equiv T$ at eye level

$\overline{T} \equiv$ mean ambient T

$\overline{P} \equiv$ mean ambient air pressure in mbar

$A \equiv \overline{T}^2/(1.58\text{x}10^{-4}\overline{P})$

$\beta_h \equiv$ angular elevation of the optical horizon in rad

$x_c \equiv$ distance to the object intersected by the caustic

$\beta_c \equiv$ angular elevation of the caustic at the distance x_c in rad

$z_s \equiv$ negative h at eye level

$F_a \equiv 4\beta_h^2 z_s/3\beta_c^3 x_c$

$\tau_s \equiv \frac{2}{3}\left\{2\cos\left[\frac{4\pi + \arccos(1 - 27F_a/16)}{3}\right] + 1\right\}$

$\tau_* \equiv \beta_h^2/\tau_s$

$r_e \equiv$ radius of the earth $= 6.371\text{x}10^6$ m

$R \equiv$ gas constant for dry air

$\gamma_a \equiv g/R = 0.0342°$ C/m

$B \equiv \frac{2A}{r_e} - \gamma_a$

Expression and parameters after FRASER, 1979.

Appendix Twelve

Air funnels

Funnels are instigated at the boundaries between zones of different horizontal air velocity [BYRON-SCOTT, pers. comm., 1983] Such boundaries may occur at the boundaries between surfaces of unequal surface friction. As thermal buoyancy force stretches the funnel, its rate of angular velocity increases coincidentally with the contraction of its diameter because of the need to conserve momentum.

Appendix Thirteen

Sine-generated curves

"The mathematics involved in finding the average, or most probable, path taken by a random walk of fixed length had been worked out in 1951 by Hermanm von Schelling of the General Electric Company. The exact solution is expressed by an elliptic integral, but in our case a sufficiently accurate approximation states that the most probable geometry for a river is one in which the angular direction of the channel at any point with respect to the mean down-valley direction is a sine function of the distance measured along the channel.

"The curve that is traced out by this most probable random walk between two points in a river valley we named a 'sine- generated' curve. As it happens, this curve closely approximates the shape of real river meanders" [LEOPOLD and LANGBEIN, 1966]" (Fig. 98).

Appendix Fourteen

Sediment transport relationships

BAGNOLD's basic sediment transport relationship is in the form

$$Q \equiv \Gamma\left(|\vec{U}| - |\vec{U}_{cr}|\right)^3$$

where $Q \equiv$ sediment transport rate, $\Gamma \equiv$ "function of" and $|\vec{U}_{cr}| \equiv$ critical flow speed below which no sediment transport occurs. A version of BAGNOLD's exact expression in this form has been used in a fairly successful model of barchan dune evolution and equilibrium [HOWARD, MORTON, MOHAMED GAD-EL-HAK and PIERCE, 1978] and to predict sediment transport in tidal flows [STERNBERG, 1972; GADD, LAVELLE and SWIFT, 1978; HEATHERSHAW, 1981 and LANGHORNE, 1982]. It has also been used in the interpretation of ancient tidal deposits [ALLEN 1981a and b].

A recent refinement of the above form is

$$Q = \Gamma\left(|\vec{U}|^2 - |\vec{U}_{cr}|^2\right)\vec{U}$$

[VINCIENT, YOUNG and SWIFT, 1981]. This has been shown to be more accurate than its predecessor [HADISTY, 1983]. It is also more reflective of the physical considerations originally taken into account in deriving a cubic sediment transport relationship [HADISTY, 1983].

Appendix Fifteen

A derivitive form of the sediment transport relationship
as an expression for erosion, deposition and pure transport

Erosion, deposition and pure transport are expressible as the substantial derivative of a sediment transport relationship. Quantitatively

$$\frac{dQ}{dt} = \frac{\partial Q}{\partial t} + u\frac{\partial Q_x}{\partial x} + v\frac{\partial Q_y}{\partial y} + w\frac{\partial Q_z}{\partial z}$$

where $\frac{d}{dt} \equiv$ "total or substantial derivative of", $\frac{\partial}{\partial t} \equiv$ "partial or local time derivative", $\frac{\partial}{\partial x_i} \equiv$ "partial derivative in the x_i-direction" ($x_i = x$, y or z), $Q_{x_i} \equiv$ the x_i-direction component of the vector $\vec{Q}$ and $Q \equiv$ the magnitude of $\vec{Q}$. $\frac{dQ}{dt} > 0$ corresponds to erosion, $\frac{dQ}{dt} < 0$ to deposition and $\frac{dQ}{dt} = 0$ to pure transport. Incidentally, the substantial derivative is the change in a parameter of a conceptual parcel within the fluid moving at a rate not necessarily that of the mean flow ($\frac{D}{Dt}$ is the change in a parameter of a conceptual parcel within the fluid moving at the same rate as that of the mean flow) and the local time derivative $\frac{\partial Q}{\partial t}$ is the change in a parameter at a fixed point.

Each of the four component partial derivatives may be analyzed for its individual contribution to the total derivitive. For example, the second partial derivative $\frac{\partial Q_x}{\partial x}$ may be examined to ascertain whether erosion, deposition or pure transport occurs in the x-direction. This may be done for any control area by determining whether sediment transport is greater or less at the flowward perimeter of a fixed conceptual area than at the leeward perimeter. If as in the right-hand side portion of Figure 67, sediment transport is greater at the leeward perimeter, then more material exits the control area than enters it. Hence, erosion occurs. Similar test charts can be constructed for all cases of all the partial derivatives.

Because the component partial derivatives are independent of each other, a substantial derivative expressing any of the three transport modes – erosion, deposition and pure transport – may be comprised of any combination of component partial derivatives expressing different transport modes. For example, a negative subtantial derivative expressing deposition may have a positive local time derivative expressing erosion, a neutral vertical derivative expressing pure transport and negative horizontal derivatives expressing deposition.

Appendix Sixteen

Ekman flow

The Ekman profile is the turning of the mean flow with increasing height; a curve known as the Ekman spiral is traced by connecting the end points of wind velocity vectors at various heights drawn from a common origin (Fig. 100). The velocity components of Ekman flow are quantitatively expressed by the equations

$$u_E = -U_g \sqrt{2} \cos \iota_o \, e^{-\Omega z} \sin(\Omega z + \iota_0 - \pi/4)$$

and

$$v_E = U_g \Big[1 - \cos \iota_o \sqrt{2} e^{\Omega z} \cos(\Omega z + \iota_0 - \pi/4) \Big]$$

where

$u_E \equiv u$ of U_E,

$v_E \equiv v$ of U_E,

$U_E \equiv$ Ekman profile,

$\iota_o \equiv \tan^{-1}\left(-\frac{v_o}{u_o}\right) = \tan^{-1}\left[-\frac{(\partial v/\partial z)_o}{(\partial c/\partial z)_o}\right]$,

$\Omega = \sqrt{\frac{\rho \omega \sin \phi}{\mu}}$,

$\omega \equiv$ earth's rotation rate,

$\phi \equiv$ latitude,

$U_g \equiv$ geostrophic wind $= \frac{1}{f\rho}\left(-\hat{x}\frac{\partial P}{\partial y} + \hat{y}\frac{\partial P}{\partial z}\right)$,

$\simeq$ wind measured at ~ 500 m

and

$\hat{x}$ and $\hat{y}$ are unit vectors in the x- and y-directions.

Appendix Seventeen

Centrifugal instability

Centrifugal acceleration is expressible as the ratio of the square of velocity to the radial distance of the point of consideration from its center of curvature. Quantitatively,

$$c_{ac} = (U_T)^2/r$$

where $c_{ac} \equiv$ centrifugal acceleration, $U_T \equiv$ tangential flow speed and $r \equiv$ distance from the center of curvature to the point of interest (Fig. 100a).

Radial distance from the center of curvature r decreases linearly with radial distance from a concave surface. Tangential flow speed increases non-linearly as raised to some power greater than one with radial distance from a concave surface, and this holds true whether the radial velocity profile bears an inflection point or a neutral stability configuration. Therefore, from the relationship for centrifugal force and tangential flow speed, it is clear that the centrifugal acceleration increases even faster than tangential flow speed with distance from the surface. See Figure 100b, where the ratio between the centrifugal forces at 2 and 1 is greater than the ratio between the tangential flow speeds at 2 and 1. A gradient in centrifugal force directed towards the concave surface is created.

Bibliography: Geomorphology

ALLEN, J.R.L., 1967, Erosional marks on weakly cohesive mud beds. *Journal of Sedimentary Petrology*, v. 39, pp. 607-623

_____, 1968, The nature and origin of bed-form hierarchies. *Sedimentology*, v 10, pp. 161-182

_____, 1981a, Lower Cretaceous tides revealed by cross-bedding with mud drapes. *Nature*, v. 289, pp. 579-581

_____, 1981b, Paleotidal speeds and ranges estimates from cross-bedding sets with mud drapes. *Nature*, v. 293, pp. 394-396

_____, 1982a, Mud drapes in sand-wave deposits: A physical model with application to the Folkstone Beds (early Cretaceous, southeast England). *Philosophical Transactions of the Royal Society of London*, Series A., v. 306, pp. 291-345

_____, 1982b, *Sedimentary Structures: Their Character and Physical Basis, v. 2 – Developments in Sedimentology, v. 30B* (J.R.L. Allen, editor). Elsevier, Amsterdam, 663 pp.

AUFRÈRE, L., 1930, L'orientation des dunes continentales. *Report on the Proceedings of the 12th International Geographers Congress*, Cambridge, 1928, pp. 220-231

_____, 1931, Le cycle morphologique des dunes. *Annales de Geographie*, v. 40, pp. 362-385

BAKER, V.R., 1981, The geomorphology of Mars. *Progress in Physical Geography*, v. 5, n. 4, pp. 473-513

BAGNOLD, R.A., 1931, Journeys in the Libyan desert, 1929 and 1930. *Geographical Journal*, v. 78, pp. 13-39

_____, 1933, A further journey through the Libyan desert. *Geographical Journal*, v. 82, pp. 211-235

_____, 1941, *The Physics of Blown Sand and Desert Dunes*. Chapman & Hall, London, 265 pp.

BALL, J., 1927, Problems of the Libyan desert. *Geographical Journal*, v. 70, pp. 21-38, 105-128, 209-224

BARNDORFF-NIELSON, O., DALSGAARD, K., HALGREEN, G., KUHLMAN, H., MOLLER, J.T. and SCHOM, G., 1982, Variations in particle size distribution over a small dune. *Sedimentology*, v. 29, pp. 53-65

BEADNELL, H.J.L., 1910, The sand dunes of the Libyan desert. *Geographical Journal*, v. 35, pp. 379-395

————————— , 1934, Libyan desert dunes. *Geographical Journal*, v. 84, pp. 337-340

BEARD, J.S., 1982, Late Pleistocene aridity and aeolian landforms in Western Australia. in: *Evolution of the Flora and Fauna of Arid Australia* (W.R. Barker and P.J.M. Greenslade, editors). Peacock, Frewville, S.A., Australia, pp. 101-106

BESLER, H., 1975, Messungen zur Mobilität Dunensanden am Nordrand der Dune–Namib (Südwestafrika). *Würzberger Geographische Arbeiten*, v. 43, pp. 135-147

BIGARELLA, J.J., 1972, Eolian environments: Their characteristics, recognition and importance. in: *Recognition of Ancient Sedimentary Environments* (J.K. Rigby a.o., editor) – *Special Publication No. 16*. Society of Economic Paleontologists and Mineralogists, pp. 12-62

BLACKWELDER, E., 1930, Yardang and zastruga. *Science*, v. 72, pp. 396-397

————————— , 1934, Yardangs. *Bulletin of the Geological Society of America*, v. 45, pp. 159-166

BLANFORD, W.T., 1876, On the physical geography of the Great Indian Desert with especial reference to the former existence of the sea in the Indus valley, and on the origin and mode of formation of the sand-hills. *Journal of the Asiatic Society of Bengal*, Calcutta, v. 45, n. 2, pp. 86-103

BREED, C.S. and BREED, W.J., 1979, Dunes and other windforms of central Australia (and a comparison with linear dunes on the Moenkopi Plateau, Arizona). *Apollo-Soyuz Test Project Summary Science Report, v. 2 : Earth Observations and Photography* (Farouk El-Baz and D.M. Warner, editors), – *U.S. National Aeronautics and Space Administration SP-412*, 692 pp.

BREED, C.S., FRYBERGER, S.C., ANDREWS, S. McCAULEY, C., LENNARTZ, F., GEBEL, D. and HORSTMAN, K., 1979, Regional studies of sand seas using Landsat (ERTS) imagery. in: *A Study of Global Sand Seas* (E.D. Mckee, editor), – *U.S. Geological Survey Professional Paper 1052*, pp. 305-398

BREED, C.S., GROLIER, M.J. and McCAULEY, J.F., 1979, Morphology and distribution of common 'sand' dunes on Mars: Comparison with the Earth. *Journal of Geophysical Research*, v. 84, n. B14, pp. 8183-8204

BREED, C.S. and GROW, T., 1979, Morphology and distribution of dunes in sand seas observed by remote sensing. in: *A Study of Global Sand Seas* (E.D. Mckee, editor) – *U.S. Geological Survey Professional Paper 1052*, pp. 253-302

BROOKFIELD, M. 1970, Dune trends and wind regime in central Australia. *Zeitschrift für Geomorphologie, Supplementband 10* (H. Mensching, editor),

pp. 121-153

BROOKFIELD, M.E. and AHLBRANDT, T.S., editors, 1983, *Eolian Sediments and Processes – Developments in Sedimentology, v. 38.* Elsevier, Amsterdam, 660 pp.

BOBEK, H., 1959, *Features and Formation of the Great Kawir and Masileh.* University of Tehran Oress, Tehran, 63 pp.

BOSWORTH, T.O., 1922, *Geology of Northwest Peru.* MacMillan, London, 434 pp.

BOWLER, J.M., 1976, Aridity in Australia: Age, origins and expression in aeolian landforms and sediments. *Earth Science Review,* v. 12, pp. 279-310

_____ , 1978, Glacial age aeolian events at high and low latitudes: A southern hemisphere perspective. in: *Antarctic Glacial History and World Paleoenvironments* (E.M. van Zinderen Bakker, editor), Balkema, Rotterdam, pp. 149-172

_____ , 1982, Aridity in the late Tertiary and Quaternary of Australia. in: *Evolution of the Flora and Fauna of Arid Australia* (W.R. Barker and P.J.M. Greenslade, editor). Peacock, Frewville, S.A., Australia, pp. 101-106

BUCKLEY, R.C., 1981a, Central Australian sandridges. *Journal of Arid Environments,* v. 4, pp. 91-101

_____ , 1981b, Parallel dunefield ecosystems: Southern Kalahari and central Australia. *Journal of Arid Environments,* v. 4, pp. 287-298

_____ , 1981c, Soils and vegetation of central Australian sandridges III. Sandridge vegetation of the Simpson Desert. *Australian Journal of Ecology,* v. 6, pp. 405-422

CASTON, V.N.D., 1972, Linear sand banks in the southern North Sea. *Sedimentology,* v. 18, pp. 63-78

China Tames Her Deserts: A Photographic Record, 1977, Desert Department, Institute of Glaciology, Cryopedology and Desert Research, Academia Sinica. Science Press, Beijing

CHUDEAU, R., 1920, Étude sur les dunes Sahariennes. *Annales de Geographie,* v. 29, pp. 334-356

CLARKE, R.H. and PRIESTLEY, C.H.B., 1970, The asymmetry of Australian desert sand ridges. *Search,* v. 1, p. 77

CLOS-ARCEDUC, A., 1967, La direction des dunes et ses rapports avec celle du vent. *Comptes Rendus Académie Des Sciences, Series D,* Tome 264, pp. 1393-1396

_____ , 1968, Emploi des convectures photographiques aériennes pour

la verification des theories relatives à la formation des dunes allongées dans une direction voisine de celle du vent. *XI Congrès International de Photogrammetrie*, Lausanne, July 8-20, 1968, 8 pp.

COOKE, R.U. and WARREN, A., 1973, *Geomorphology in Deserts.* University of California Press, Berkeley, 374 pp.

COOPER, W.S., 1958, The coastal sand dunes of Oregon and Washington. *Geological Society of America Memoirs*, v. 72, 162 pp.

Cooper Basin Liquids Project – Environment Review, 1981. SANTOS Ltd., 183 Melbourne St., N. Adelaide, S.A. 5006, Australia

DZULYNSKI, S. and WALTON, E.K., 1965, *Features of Flysch and and Graywackes – Developments in Sedimentology*, v. 7. Elsevier, Amsterdam, 274 pp.

ENQUIST, F., 1932, The relation between dune-form and wind-direction. *Geologiska Foreningen i Stockholm Forhandlingar*, v. 54, pp. 19-59

FINKEL, H.J., 1959, The barchans of southern Peru. *Journal of Geology*, v. 67, pp. 614-647

FOLK, R.L., 1971, Longitudinal dunes of the northwestern edge of the Simpson Desert, Northern Territory, Australia: Geomorphology and grain size relationships. *Sedimentology*, v. 16, pp. 5-54

FAROUK EL-BAZ, BREED, C.S., GROLLIER, M.J. and McCAULEY, J.F., 1979, Eolian features in the Western Desert of Egypt and some applications to Mars. *Journal of Geophysical Research*, v. 84, n. B14, pp. 8205-8221

FRERE, H.B.E., 1870, Notes on the Runn of Cutch. *Journal of the Royal Geographical Society*, v. 40, pp. 181-207

FRYBERGER, S.G., (assisted by G. Dean), 1979, Dune forms and wind regime. in: *A Study of Global Sand Seas* (E.D. McKee, editor) – *U.S. Geological Survey Professional Paper 1052*, pp. 137-170

FRYBERGER, S.G., ABDULKADER M. AL-SARI, THOMAS J. CLISHAM, SYED A.R. PIZVI and KHATTAB G. AL-HINAI, 1984, Wind sedimentation in the Jafurah sand sea, Saudi Arabia. *Sedimentology*, v. 31, pp. 413-431

FURNES, G.K., 1974, Formation of sand waves on unconsolidated sediments. *Marine Geology*, v. 16, pp. 145-160

GARDNER, R. and PYE, K., 1981, Nature, origin and paleoenvironmental significance of red coastal and desert dune sands. *Progress in Physical Geography*, v. 5, n. 4, pp. 514-534

GEVERS, T.W., 1936, The morphology of western Damaraland and the adjoining Namib desert of southwest Africa. *South African Geographical*

Journal, v. 19, pp. 61-79

GLENNIE, K.W., 1970, *Desert Sedimentary Environments – Developments in Sedimentology, v. 7.* Elsevier, Amsterdam, 222 pp.

—————————, 1972, The Permian Rotliegendes of northwest Europe interpreted in light of modern desert sedimentation studies. *Bulletin of the American Association of Petroleum Geology,* v. 56, pp. 240-263

HACK, J.T., 1941, Dunes of the western Navajo country. *Geographical Review,* v. 31, pp. 240-263

HANNES, G. and HANNES, S.M., 1982, Lake Erie snow dunes. *Weatherwise,* v. 35, n. 6, pp. 278-279

HASTENRATH, S.L., 1967, The barchans of the Arequipa region, Southern Peru. *Zeitschrift für Geomorphologie,* v. 11, pp. 300-331

HEDIN, S., 1904, *Scientific Results of a Journey in Central Asia (1899-1902).* Lithographic Institute Swedish Army, Stockholm, v. I & II

HOLM, D.A., 1953, Dome-shaped dunes of the Central Nejd, Saudi Arabia. *19th International Geological Congress,* Algiers, 1952, C.R., Fasc. 7, pp. 109-112

HUME, W.F., 1925, *The Geology of Egypt. I.* Government Press, Cairo, 408 pp.

HUNTER, R.E., RICHMOND, B.M., and ALPHA, T.R., 1983, Storm- controlled oblique dunes of the Oregon coast. *Bulletin of the Geological Society of America,* v. 94, pp. 1405-1465

HUNTER, R.E. and RUBIN, D.M., 1983, Interpreting cyclic crossbedding with an example from the Navajo Sandstone. in: *Eolian Sediments and Processes – Developments in Sedimentology, v. 38* (M.E. Brookfield and T.S. Ahlbrandt, editors). Elsevier, Amsterdam, pp. 429-454

INMAN, D.L., EWING, G.C. and CORLISS, J.B., 1966, Coastal sand dunes of Guerro Negro, Baja California, Mexico. *Bulletin of the Geological Society of America,* v. 77, pp. 787-802

JACOBI, R.D. and MROZOWSKI, C.L., 1979, Sediment slides and sediment waves in the Bonin Trough, western Pacific. *Marine Geology,* v. 29, pp. M1-M9

JENNINGS, J.N., 1968, A revised map of the desert dunes of Australia. *Australian Geographer,* v. 10, pp. 408-409

KÁDÁR, L., 1934, A study of the sand sea in the Libyan desert. *Geographical Journal,* v. 83, n. 6, pp. 470-478

KING, D., 1956, The Quaternary stratigraphic record at Lake Eyre North and the evolution of existing topographic forms. *Transactions of the Royal Society of South Australia,* v. 79, pp. 99-103

_____, 1960, The sand ridge deserts of South Australia and related aeolian landforms of the Quaternary arid cycles. *Transactions of the Royal Society of South Australia,* v. 93, pp. 99-108

LANCASTER, N., 1980, Formation of sief dunes from barchans. *Zeitschrift für Geomorphologie,* v. 24, pp. 160-167

_____, 1981a, Aspects of Morphometry of linear dunes of the Namib Desert. *South African Journal of Science,* v. 77, pp. 366-368

_____, 1981c, Grain size characteristics of Namib Desert linear dunes. *Sedimentology,* v. 28, pp. 115-122

_____, 1983, Controls of dune morphology in the Namib sand sea. in: *Eolian Sediments and Processes – Developments in Sedimentology v. 38* (M.E. Brookfield and T.S. Ahlbrandt, editors). Elsevier, Amsterdam, pp. 261-289

LEIGHLY, J., 1936, Meandering Arroyos of the dry Southwest. *The Geographical Review,* v. 26, pp. 270-282

LEOPOLD, L.B. and LANGBEIN, W.B., 1966, River meanders. *Scientific American,* v. 214, n. 6, pp. 60-70

LEOPOLD, L.B. and WOLMAN, M.G., 1957, *River Channel Patterns: Braided, Meandering and Straight – U.S. Geological Survey Professional Paper 282-B,* pp. 39-73

LONSDALE, P. and MALFATT, B., 1974, Abyssal dunes of foraminiferal sand on the Carnegie Ridge. *Bulletin of the Geological Society of America,* v. 85, pp. 1697-1712

MABBUTT, J.A. and SULLIVAN, M.E., 1968, The formation of longitudinal dunes: Evidence from the Simpson Desert. *Australian Geographer,* v. 10, n. 6, pp. 483-487

MABBUTT, J.A., WOODING, R.A. and JENNINGS, J.N., 1969, The asymmetry of Australian desert sand ridges. *Australian Journal of Science,* v. 32, n. 4, pp. 159-160

MADIGAN, C.T., 1936, The Australian sand-ridge deserts. *The Geographical Review,* v. 26, pp. 205-227

_____, 1946, The Simpson Desert expedition, 1939. *Transactions of the Royal Society of South Australia,* v. 70, pp. 45-63

MAINGUET, M., 1978, The influence of trade winds, local air- masses and topographic obstacles on the aeolian movement of sand particles and the origin and distribution of dunes and ergs in the Sahara and Australia. *Geoforum,* v. 9, pp. 17-28

_____, 1980, *Utilisation des images mètèosat pour prèciser les trajectoires*

èoliennes au sol, au Sahara et sur les Marges Sahèliennes – *Bulletin No. 78-2.* Sociètè Française de Photogrammètrie et de Tèlèdètection, 13 pp.

——————— , 1982, Les dunes d'érosion: signification morphodynamique et climatique de leur existence. *Würzberger Geographische Arbeiten*, v. 56, pp. 79-92

——————— , 1984a, A classification of dunes based on aeolian dynamics and the sand budget – ch. 2 of *Deserts and arid lands* (F. El-Baz, editor). Martinus Nijhoff, The Hague, pp. 31-58

——————— , 1984b, Space observation of Saharan aeolian dynamics – ch. 3 of *Deserts and arid lands* (F. El-Baz, editor). Matinus Nijhoff, The Hague, pp. 59-77

MAINGUET, M. and CALLOT, Y., 1978, *L'Erg de Fachi-Bilma (Tchad- Niger): Contribution à la connaissance de la dynamique des ergs et des dunes des zones arides chandes* – *Mémoires et documents, 19.* CNRS, Paris, 185 pp.

MAINGUET, M. and CHEMIN, M.-C., 1983, Sand seas of the Sahara and Sahel; An explanation of their thickness and sand dune type by the sand budget principle. in: *Eolian Sediments and Processes* (M.E. Brookfield and T.S. Ahlbrandt, editors). Elsevier, Amsterdam, pp. 353-363

MAINGUET, M., VIMEUX-RICHEUX, M. and CHEMIN, M.-C., 1983, Autochtonie et allochtonie des sables de la zone sahara- sahélienne au Niger. *Revue de Géologie Dynamique et de Géographie Physique*, v. 24, Fasc. 2, pp. 167-175

McKEE, E.D., ed., 1979, *A Study of Global Sand Seas* – *U.S. Geological Survey Professional Paper 1052*, 429 pp.

——————— , 1982, *Sedimentary structures in dunes of the Namib Desert, South West Africa* – *Geological Society of America Special Paper 188*, 64 pp.

McKEE, E.D. and TIBBITTS Jr., G.C., 1964, Primary structures of a sief dune and associated deposits in Libya. *Journal of Sedimentary Petrology*, v. 34, n. 1, pp. 5-17

MEDLICOTT, H.B. and BLANFORD, W.T., 1879, *A Manual of the Geology of India, I.* Geological Survey, Calcutta, 414 pp.

MELTON, F.A., 1940, A tentative classification of sand dunes – its application to dune history in the southern high plains. *Journal of Geology*, v. 48, pp. 113-174

RUBIN, D.M., 1984, Factors determining desert dune type (discussion). *Nature*, v. 309, pp. 91-92

——————— , 1985, Lateral migration, internal structure, and climbing of linear dunes in the Strzelecki Desert, Australia (in press). (For Dr. Rubin's address,

see list of researchers referenced.)

RUBIN, D.M. and HUNTER, R.E., 1985, Why deposits of longitudinal dunes are rarely recognized in the geologic record. *Sedimentology,* v. 32, n. 1, pp. 147-157

RUBIN, D.M. and McCULLOUGH, D.S., 1980, Single and superimposed bedforms: A synthesis of San Francisco Bay and flume observations. *Sedimentary Geology,* v. 26, pp. 207-231

OFF, T., 1963, Rhythmic linear sand bodies caused by tidal currents. *Bulletin of the American Association of Petroleum Geologists,* v. 47, pp. 324-341

SOKOLOW, N.A., 1984, *Die Dunen, Bildung, Entwicklung and innerer Bau.* (Translated from Russian into German by Andreas Arzani.) Springer, Berlin, 298 pp.

SPRIGG, R.C., 1979, Stranded and submerged sea-beach systems of southeast South Australia and the aeolian desert cycle. *Sedimentary Geology,* v. 24, pp. 53-96

_____ , 1980, Alternating wind cycles of the Quaternary Era and their influences on aeolian sedimentation in and around the dune deserts of southeastern Australia. *INQUA Loess Commission Workshop,* Canberra

STEELE, R.P., 1982, A case study of an aeolian sandstone: the Permian yellow sands of N.E. England. *11th International Congress on Sedimentology, Abstracts of Papers,* p. 170

STEIN, M.A., 1909, Explorations in central Asia. *Geographical Journal,* v. 34

SUEH, A. and WEISSBROD, T., 1983, Size-frequency distribution of longitudinal dune rippled flank sands compared to that of slipface sands of various dune types. *Sedimentology,* v. 30, pp. 717-725

SWIFT, D.J.A., 1973, Ridge and swale topography of the middle Atlantic bight North America: Secular response to the Holocene hydraulic regime. *Marine Geology,* v. 15, pp. 227-247

TANNER, W.F., 1965, Upper Jurassic paleogeography of the Four Corners region. *Journal of Sedimentary Petrology,* v. 35, pp. 564-574

TSOAR, H., 1978, *The Dynamics of Longitudinal Dunes.* U.S. Army, European Research Office, London, 171 pp.

TSOAR, H., GREEELEY, R. and PETERFREUND, A.R., 1979, Mars: The north polar sand sea and related wind patterns. *Journal of Geophysical Research,* v. 84, n. B14, pp. 8167-8180

TWIDALE, C.R., 1972a, Evolution of sand dunes in the Simpson Desert, central Australia. *Transactions of the Institute of British Geographers,* v. 56, pp. 77-109

————————, 1981, Age and origin of longitudinal dunes in the Simpson and other sand ridge deserts. *Die Erde,* v. 112, pp. 231-247

TWIDALE, C.R. and WOPFNER, M.W., 1981, Aeolian landforms of central Australia. *Zeitschrift für Geomorphologie,* v. 25, pp. 353-358

VERLAQUE, C., 1958, Les dunes d'In Salah. *Travaux de l'Institute de Recherches Saharienes,* v. 17, pp. 13-57

WALTHER, J., 1924, *Das Gesetz der Wustenbildung.* Leipzig

WARREN, A., 1970, Dune trends and their implications in the central Sudan. *Zeitschrift für Geomorphologie, Supplementband 10,* pp. 154-179

————————, 1972, Observations on dunes and bi-modal sands in the Ténéré Desert. *Sedimentology,* v. 19, pp. 37-44

————————, 1976b, Dune trend and the Ekman spiral. *Nature,* v. 259, pp. 653-654

WARREN, A. and KNOTT, P., 1983, Desert dunes: A short review of needs in desert dune research and a recent study of micrometeorological dune-initiation mechanisms. in: *Eolian Sediments and Processes – Developments in Sedimentology, v. 38* (M.E. Brookfield and T.S. Ahlbrandt, editors). Elsevier, Amsterdam, pp. 343-352

WASSON, R.J., 1983a, The Cainozoic history of the Strzelecki and Simpson dunefields (Australia), and the origin of the desert dunes. *Zeitschrift für Geomorphologie, Supplementband, v. 45,* pp. 85-115

————————, 1983b, Dune sediment typres, sand colour, sediment provenance and hydrology in the Strzelecki-Simpson dunefield, Australia. in: *Aeolian Sediments and Processes – Developments in Sedimentology, v. 38* (M.E. Brookfield and T.S. Ahlbrandt, editors). Elsevier, Amsterdam, pp. 165-195

————————, 1984, *Post-conference excursion notes, Strzelecki Dunefield: Australian-New Zealand Geomorphology Group, 2nd conference,* Broken Hill, Australia, 30 pp.

WASSON, R.J. and HYDE, R., 1983a, A test of granulometric control of desert dune geometry. *Earth Surface Processes and Landforms,* v. 8, pp. 301-312

————————, 1983b, Factors determining desert dune type. *Nature,* v. 304, pp. 337-339

————————, 1984, Factors determining desert dune type (reply). *Nature.,* v. 309, pg. 92

WILSON, I.G., 1972, Aeolian bedforms: Their development and origins. *Sedimentology,* v. 19, pp. 173-210

WINGATE, O., 1934, In search of Zerzara. *Geographical Journal,* v. 83, n. 4,

pp. 281-305

WOPFNER, H. and TWIDALE, C.R., 1967, Geomorphological history of the Lake Eyre basin. in: *Landform Studies from Australia and New Guinea* (J.N. Jennings and J.A. Mabbutt, editors). Australian National University Press, Canberra, pp. 119-143

Bibliography: Fluid dynamics,
sediment transport and related topics

ACKERS, P. and WHITE, W.R., 1973, Sediment transport: New approach and analysis. *Journal of the Hydraulics Division American Society of Civil Engineers*, v. 99, pp. 2041-2060

ALLEN, J.R.L., 1967, Erosional marks on weakly cohesive mud beds. *Journal of Sedimentary Petrology*, v. 39, pp. 607-623

—————— , 1968, The nature and origin of bed-form hierarchies. *Sedimentology*, v 10, pp. 161-182

—————— , 1981a, Lower Cretaceous tides revealed by cross-bedding with mud drapes. *Nature*, v. 289, pp. 579-581

—————— , 1981b, Paleotidal speeds and ranges estimates from cross-bedding sets with mud drapes. *Nature*, v. 293, pp. 394-396

—————— , 1982a, Mud drapes in sand-wave deposits: A physical model with application to the Folkstone Beds (early Cretaceous, southeast England). *Philosophical Transactions of the Royal Society of London, Series A.*, v. 306, pp. 291-345

—————— , 1982b, *Sedimentary Structures: Their Character and Physical Basis, v. 2 – Developments in Sedimentology, v. 30B* (J.R.L. Allen, editor). Elsevier, Amsterdam, 663 pp.

ALLEN, S., 1981, *Australian low level jet climatology – Meteorological Note 119*. Australian Department of Science and Technology, Bureau of Meteorology, 23 pp.

ANGELL, J.K., PACK, D.H., HOLZWORTH, G.C. and DICKSON, C.R., 1966, Tetroon trajectories in an urban atmosphere. *Journal of Applied Meteorology*, v. 5, pp. 565-572

ANGELL, J.K., PACK, D.H. and DICKSON, C.R., 1968, A Lagrangian study of helical circulations in the planetary boundary layer. *Journal of Atmospheric Sciences*, v. 25, pp. 707-717

BAGNOLD, R.A., 1941, *The Physics of Blown Sand and Desert Dunes*. Chapman & Hall, London, 265 pp.

—————— , 1952, The surface movement of blown sand in relation to meteorology. *Proceedings, International Symposium of Desert Research*, Jerusalem, May 7-14, 1952, Research Council of Israel in cooperation with UNESCO

—————— , 1954, Experiments on a gravity-free dispersion of large solid spheres in a Newtonian fluid under shear. *Proceedings of the Royal Society of London, Series A*, v. 225, pp. 49-63

——————— , 1956, The flow of cohesionless grains in fluids. *Philosophical Transactions of the Royal Society of London, Series A*, v. 249, pp. 235-297

——————— , 1960, *Some Aspects of the Shape of River Meanders – U.S. Geological Survey Professional Paper 282-E*, pp. 135-144

——————— , 1963, Mechanics of marine sedimentation. in: *The Sea, v. 3* (M.N. Hill, editor). Wiley, New York, pp. 507-582

——————— , 1966, *An approach to the sediment transport problem from general physics – U.S. Geological Survey Professional Paper 422-I*, 169 pp.

——————— , 1972, The nature of saltation and of 'bed-load' transport in water. *Proceedings of the Royal Society of London, Series A*, v. 332, pp. 473-504

BARCILON, V., 1965, Stability of a non-divergent Ekman layer. *Tellus*, v. 17, pp. 53-68

BARRINGER, L.B., 1940, *Flight Without Power*. Pitman Pub. Corp., New York, 221 pp.

BATCHELOR, G.K., 1967, *An Introduction to Fluid Dynamics*. University Press, Cambridge, 615 pp.

BEARD, J.S., 1982, Late Pleistocene aridity and aeolian landforms in Western Australia. in: *Evolution of the Flora and Fauna of Arid Australia* (W.R. Barker and P.J.M. Greenslade, editors). Peacock, Frewville, S.A., Australia, pp. 101-106

BEGELMAN, M.C., BLANFORD, R.D. and REES, M.J., 1984, Theory of electromagnetic radio sources. *Reviews of Modern Physics*, v. 50, p. 1, pp. 255-351

BÉNARD, H., 1900, Les tourbillons cellulaires dans une nappe liquide. *Revue Générale des Science Pures et Appliquées*, v. 11, pp. 1261-1271, 1309-1328

——————— , 1928 Sur les tourbillons cellulaires les tourbillons en bandes, et la theorie de Rayleigh. *Procès-verbaux et Résumé Communications de la Société Française de Physique*, n. 266, pp. 112-115

BERGER, M.I. and DOVIAK, R.J., 1979, *An Analysis of the Clear Air Planetary Boundary Layer Wind Synthesized from NSSL's Dual Doppler-radar Data -- NOAA-ERL-NSSL-87*. National Severe Storms Laboratory, Norman, Oklahoma, 55 pp. [*NTIS PB-300865/AS*].

BESLER, H., 1975, Messungen zur Mobilität Dunensanden am Nordrand der Dune–Namib (Südwestafrika). *Würzberger Geographische Arbeiten*, v. 43, pp. 135-147

BIGARELLA, J.J., 1972, Eolian environments: Their characteristics, recognition and importance. in: *Recognition of Ancient Sedimentary Environments*

(J.K. Rigby a.o., editor) – *Special Publication No. 16.* Society of Economic Paleontologists and Mineralogists, pp. 12-62

BIJKER, E.W., 1967, The increase of bed shear in a current due to wave action. *Proceedings of the 10th Coastal Engineering Conference,* Tokyo, 1966, (published by the American Society of Civil Engineers), pp. 746-765

BJERKNES, V.F.K. a.o., 1911, *Dynamic Meteorology and Hydrography, Part II– The Kinematics.* The Carnegie Institution of Washington, Washington D.C., 175 pp.

BROOKFIELD, M. 1970, Dune trends and wind regime in central Australia. *Zeitschrift für Geomorphologie, Supplementband 10 (H. Mensching, editor),* pp. 121-153

BROWN, R.A., 1970, A secondary flow model for the planetary boundary layer. *Journal of Atmospheric Sciences,* v. 27, pp. 742-757

——————— , 1972, The inflection point instability problem for stratified rotating boundary layers. *Journal of Atmospheric Sciences,* v. 29, pp. 850-859

——————— , 1974, *Analytic Methods in Planetary Boundary Layer Modelling.* John Wiley, New York, 150 pp.

——————— , 1980, Longitudinal instabilities and secondary flows in the planetary boundary layer: A review. *Reviews of Geophysics and Space Physics,* v. 18, n. 3, pp. 683-697

——————— , 1981, Modeling the geostrophic drag coefficient for AIDJEX. *Journal of Geophysical Research,* v. 86, n. C3, pp. 1989-1994

——————— , 1982, On two-layer models and the stability functions for the PBL. *Boundary-Layer Meteorology,* v. 24, pp. 451-463

——————— , 1983, Review of development of boundary layer theory. in: *Eolian Sediments and Processes – Developments in Sedimentology, v. 38* (M.E. Brookfield and T.S. Ahlbrandt, editor). Elsevier, Amsterdam, 660 pp.

BROWN, E.H., 1975, Applications of propagation parameters to atmospheric echosondes. *Proceedings of the 16th Radar Meteorology Conference,* American Meteorological Society, pp. 272-277

BROWN, E.H. and HALL Jr., F.F., 1978, Advances in atmospheric acoustics. *Review of Geophysics and Space Physics,* v. 16, n. 1, pp. 47-110

BRUNT, D., 1937, Natural and artificial clouds. *Quarterly Journal of the Royal Meteorological Society,* v. 63, n. 271, pp. 277-288

——————— , 1939, *Physical and Dynamical Meteorology.* University Press, Cambridge, pp. 219-220

_____, 1944, *Physical and Dynamical Meteorology.* University Press, Cambridge, 428 pp.

_____ , 1951, Experimental cloud formation. *Compendium on Meteorology*, pp. 1255-1262

BOWLER, J.M., 1976, Aridity in Australia: Age, origins and expression in aeolian landforms and sediments. *Earth Science Review*, v. 12, pp. 279-310

_____ , 1978, Glacial age aeolian events at high and low latitudes: A southern hemisphere perspective. in: *Antarctic Glacial History and World Paleoenvironments* (E.M. van Zinderen Bakker, editor), Balkema, Rotterdam, pp. 149-172

_____ , 1982, Aridity in the late Tertiary and Quaternary of Australia. in: *Evolution of the Flora and Fauna of Arid Australia* (W.R. Barker and P.J.M. Greenslade, editor), Peacock, Frewville, S.A., Australia, pp. 101-106

BUDYKO, M.I., 1982, *The Earth's Climate: Past and Future. International Geophysics Series, v. 29*, Academic Press, New York, 307 pp.

CASTON, V.N.D., 1972, Linear sand banks in the southern North Sea. *Sedimentology*, v. 18, pp. 63-78

CASTON, V.N.D. and STRIDE, A.H., 1970, Tidal sand movement between some linear sand banks in the North Sea off northeast Norfolk. *Marine Geology*, v. 9, pp. M38-M42

CHALMERS, J.A., 1957, *Atmospheric Electricity*, Pergamon, London, 327 pp.

CHANDRA, K., 1938, Instability of fluids heated from below. *Proceedings of the Royal Society of London, Series A.*, v. 164, pp. 231-242

CHANDRASEKHAR, S., 1961, *Hydrodynamic and Hydromagnetic Stability*, The International Series of Monographs of Physics, Clarendon Press, Oxford, 652 pp.

CHIA-SHUN YIH, 1960, Exact solutions for steady two-dimensional flow of a stratified fluid. *Fluid Mechanics*, v. 9, pp. 161-174

_____ , 1965, *Dynamics of Nonhomogeneous Fluids.* MacMillan, New York, 306 pp.

CLARKE, R.H. and PRIESTLEY, C.H.B., 1970, The asymmetry of Australian desert sand ridges. *Search*, v. 1, p. 77

DEAN, W.R., 1928, Fluid motion in a curved channel. *Proceedings of the Royal Society of London, Series A.* v 121, pp. 402-420

DONELAN, M.A., 1982, The dependence of the aerodynamic drag coefficient on wave parameters. *Proceedings of the 1st International Conference on Meteorological and Air-Sea Interaction of the Coastal Zone*, Royal Netherlands

Meteorological Institute, published by the American Meteorological Society, pp. 381-387

DUNCAN, W.T., THOM, A.S. and YOUNG, A.D., 1960, *An Elementary Treatise on the Mechanics of Fluids.* Edward Arnold, London, 714 pp.

DYERS, K.R., 1982, The initiation of sedimentary furrows by standing internal waves. *Sedimentology,* v. 29, pp. 885-889

EINSTEIN, H.A., 1950, *The bedload function for sediment transportation in open channel flows – Technical Bulletin No. 1026.* U.S. Department of Agriculture Soil Conservation Service, 78 pp.

ENGELUND, F. and FREDSØE, J., 1982, Sediment ripples and dunes. *Annual Review of Fluid Mechanics,* v. 14, pp. 13-37

ENGELUND, F. and HANSEN, E., 1967a, Comparison between similarity theory and regime formula. in: *Basic Research-Progress Report No. 13* Hydraulic Laboratory, Technical University of Denmark, pp. 14-16

—————————, 1967b, *A Monograph on Sediment Transport in Alluvial Streams.* Technisk Vorlag, Copenhagen, 62 pp.

ENQUIST, F., 1932, The relation between dune-form and wind-direction. *Geologiska Foreningen i Stockholm Forhandlingar,* v. 54, pp. 19-59

FALLER, A.J., 1961, An experimental analogy to and proposed explanation of hurricane spiral bands. *Proceedings of the 2nd Technical Conference on Hurricanes,* Miami Beach. pp. 307-313

—————————, 1963, An experimental study of the instability of the laminar Ekman boundary layer. *Journal of Fluid Mechanics,* v. 15, p. 4, pp. 560-576

—————————, 1964a, The angle of windrows in the ocean. *Tellus,* v. 16, pp. 363-370

—————————, 1964b, Large eddies in the atmospheric boundary layer and their possible role in the formation of cloud rows. *Journal of Atmospheric Sciences,* v. 22, pp. 176-183

—————————, 1966a, Investigations of stability and transition in rotating boundary layers. in: *Dynamics of Fluids and Plasmas.* Academic Press, New York, pp. 309-329

—————————, 1966b, A numerical study of the instability of the laminar Ekman boundary layer. *Journal of Atmospheric Sciences,* v. 23, pp. 466-480

—————————, 1967, Instability of the Ekman spiral with applications to the planetary boundary layers. *The Physics of Fluids Supplement,* pp. S212-S219

—————————, 1969, Instability of the thermal wind. in: *Clear Air Turbulence and its Detection* (Y.H. Pao and Arnold Goldberg, editors). Plenum Press,

New York, pp. 63-72

FALLER, A.J. and KAYLOR, R.E., 1965, *A Numerical Study of the Laminar Ekman Boundary Layer – Technical Note BN 410.* University of Maryland, Institute of Fluid Dynamics, July 1965, 26 pp.

——————— , 1966, Investigations of stability and transition in rotating boundary layers. in: *Dynamics of Fluids and Plasmas* (S. Pai a.o., editors). Academic Press, New York, pp. 309-329

——————— , 1971, Instability of the stratified Ekman boundary layer and the generation of internal waves. *Journal of Atmospheric Sciences,* v. 29, pp. 497-509

FIELDMAN, H., CONRAD, G. and McFADDEN, J., 1970, ESSA research flight facility aircraft participation in BOMEX. *Bulletin of the American Meteorological Society,* v. 51, pp. 822-834

FRASER, A.B., 1979, Simple solution for obtaining a temperature profile from the inferior mirage. *Applied Optics,* v. 18, n. 11, pp. 1724-1731

FREDSØE, J., 1974, The development of oblique dunes. in: *Progress Report 33,* Institute of Hydrodynamics and Hydraulic Engineering, Technical University of Denmark, pp. 15-22

FREE, E.E., 1911, *The movement of soil material by the wind with a bibliography of eolian geology by S.C. Stuntz and E.E. Free – U.S. Department of Agriculture, Bureau of Soils, Bulletin, v. 68,* 272 pp.

FRENZEL, B., 1973, *Climatic Fluctuations of the Ice Age.* The Press of Case Western Reserve University, Cleveland, 306 pp.

FRERE, H.B.E., 1870, Notes on the Runn of Cutch. *Journal of the Royal Geographical Society,* v. 40, pp. 181-207

FRISCH, A.S., MILLER, L.J. and STRAUCH, R.G., 1974, Three-dimensional air motion measured in snow. *Geophysical Research Letters,* v. 1, pp. 86-89

FRYBERGER, S.G., (assisted by G. Dean), 1979, Dune forms and wind regime. in: *A Study of Global Sand Seas* (E.D. McKee, editor), – *U.S. Geological Survey Professional Paper 1052,* pp. 137-170

FRYBERGER, S.G., ABDULKADER M. AL-SARI, THOMAS J. CLISHAM, SYED A.R. PIZVI and KHATTAB G. AL-HINAI, 1984, Wind sedimentation in the Jafurah sand sea, Saudi Arabia. *Sedimentology,* v. 31, pp. 413-431

FUJIYOSHI, 1950, Theoretical treatise on the meandering of rivers. *Japan Science Review,* v. 26, pp. 270-282

FURNES, G.K., 1974, Formation of sand waves on unconsolidated sediments. *Marine Geology,* v. 16, pp. 145-160

GADD, P.E., LAVELLE, J.W. and SWIFT, D.J.P., 1978, Estimates of sand transport on the New York Shelf using near-bottom current- meter observations. *Journal of Sedimentary Petrology*, v. 48, pp. 239-252

GARRATT, J.R., 1977, Review of drag coefficients over oceans and continents. *Monthly Weather Review*, v. 105, pp. 915-929

GIFFORD, F., 1953, A study of low level air trajectories at Oak Ridge, Tennessee. *Monthly Weather Review*, v. 81, n. 7, pp. 179-192

GRAHAM, A., 1933, Shear patterns in an unstable layer of air. *Philosophical Transactions of the Royal Society London, Series A.*, v. 232, pp. 285-296

GRIBBON, J., ed., 1978, *Climatic Change.* University Press, Cambridge, 280 pp.

GODSKE, C.L. and others, 1957, *Dynamic Meteorology and Weather Forecasting.* American Meteorology Society, Boston, 800 pp.

GÖRTLER, H., 1940, Über eine dreidimensionale Instabilität laminar Grenzschicten an konkaven Wänden. *Nachrichten von der Gesellshaft der Wissenshaft Göttingen Nachrichten, Mathematische-physikalishe Klasse, New Series 2*, No. 1, 26 pp.

——————, 1959, Über eine Analogie zwischen den Instabilitäten laminarer Grenzschictströmungen an konkaven Wänden und an erwärmten Wänden. *Ingenieur-Archiv*, v. 28, pp. 71-78

GREGORY, N., STUART, S.T. and WALKER, W.S., 1955, On the stability of three-dimensional boundary layers with application to the flow due to a rotating disk. *Philosophical Transactions of the Royal Society of London, Series A*, v. 248, pp. 155-199

HADISTY, J., 1983, An assessment and calibration of formulations for Bagnold's bedload equation. *Journal of Sedimemtary Petrology*, v. 53, p. 3

HAILS, J.R. and BENNETT, J.M., 1980, Wind and sediment movement in coastal dune areas. *Proceedings of the 17th International Coastal Engineering Conference ASCE*, Sydney, March 23-28, 1980, pp. 1565-1575

HANNA, S.R., 1969, The formation of longitudinal sand dunes by large helical eddies in the atmosphere. *Journal of Applied Meteorology*, v. 8, pp. 874-883

HANNES, G. and HANNES, S.M., 1982, Lake Erie snow dunes. *Weatherwise*, v. 35, n. 6, pp. 278-279

HANSEN, E., 1967, On the formation of meanders as a stability problem. in: *Basic Research-Progress Report No. 13* Hydraulic Laboratory, Technical University of Denmark,

HAURWITZ, R., 1941, *Dynamic Meteorology.* McGraw-Hill, New York, 365 pp.

HEAPS, N.S., 1972, Estimation of density currents in the Liverpool Bay area of

the Irish Sea. *Geophysical Journal of the Royal Astronomical Society,* v. 30, pp. 415-432

_____ , 1978, Linearized vertically-integrated equations of residual circulation in coastal seas. *Deutsche Hydrographische Zeitschrift,* v. 31, pp. 147-169

HEATHERSHAW, A.D., 1981, Comparison of measured and predicted sediment transport rates in tidal currents. *Marine Geology,* v. 42, pp. 75-104

HILDEBRAND, P.H., 1980, Multiple Doppler radar observations of PBL structure. *Preprints 19th Conference on Radar Meteorology,* Miami Beach, American Meteorological Society, pp. 656-661

HORST, W., 1970a, Experimente zur Untersuchung von Spiralstrukturen in Wirbeln (Experimental study of the spiral structure in vortices). *Annalen der Meteorologie,* Offenbach, a.M., n.s. No. 4, pp. 190-194

_____ , 1970b, Experiments on the vortex structure of an unstable Ekman boundary layer. *Contributions to Atmospheric Physics,* Oxford, v. 43, n. 1, pp. 1-34

HOUBOLT, J.J.H.C., 1968, Recent sediments in the Southern Bight of the North Sea. *Geologie en Mijnbouw,* v. 47, pp. 245-273

HOWARD, A.D., MORTON, J.B., MOHAMMED GAD-EL-HAK and PIERCE, D.B., 1978, Sand transport model of barchan dune equilibrium. *Sedimentology,* v. 25, pp. 307-338

HSU, S.A., 1973, Computing eolian sand transport from shear velocity measurements. *Journal of Geology,* v. 81, pp. 739-743

HUNTER, R.E., RICHMOND, B.M., and ALPHA, T.R., 1983, Storm-controlled oblique dunes of the Oregon coast. *Bulletin Geological Society of America,* v. 94, pp. 1405-1465

HUNTER, R.E. and RUBIN, D.M., 1983, Interpretiang cyclic crossbedding with an example from the Navajo Sandstone. in: *Eolian Sediments and Processes – Developments in Sedimentology, v. 38* (M.E. Brookfield and T.S. Ahlbrandt, editors). Elsevier, Amsterdam, pp. 429-454

HUTHNANCE, J.M., 1973, Tidal current asymmetries over the Norfolk sandbanks. *Estuarine and Coastal Marine Science,* v. 1, pp. 89-99

_____ , 1982a, On one mechanism forming linear sand banks. *Estuarine and Coastal Marine Science,* v. 14, pp. 79-99

_____ , 1982b, On the formation of sand banks of finite extent. *Estuarine, Coastal and Shelf Science,* v. 15, pp. 277-299

INGLE Jr., J.C., 1966, *The Movement of Beach Sand, An Analysis Using*

Flourescent Grains – Developments in Sedimentology, v. 5. Elsevier, Amsterdam, 221 pp.

IVERSEN, J.D. and WHITE, B.R., 1982, Saltation threshold on Earth, Mars and Venus. *Sedimentology,* v. 29, pp. 111-119

JACOBI, R.D. and MROZOWSKI, C.L., 1979, Sediment slides and sediment waves in the Bonin Trough, western Pacific. *Marine Geology,* v. 29, pp. M1-M9

JEFFREYS, H., 1928, The stability of a layer of fluid heated below. *Philosophical Magazine,* v. 2, pp. 833-844

JEFFREYS, H., 1965, *Cartesian Tensors.* University Press, Cambridge, 92 pp.

KELLY, R.D., 1982, A single Doppler radar study of horizontal roll convection in a lake-effect snow storm. *Journal of Atmospheric Sciences,* v. 39, n. 7, pp. 1521-1531

_____ , 1984, Horizontal roll and boundary-layer interrelationships observed over Lake Michigan. *Journal of Atmospheric Sciences,* v. 41, n. 11, pp. 1816-1826

KENNEDY, J.F., 1969, The formation of sediment ripples, dunes and anti-dunes. in: *Annual Review of Fluid Mechanics,* v.1, pp. 366-368

KINSMAN, B., 1965, *Wind Waves: Their Generation and Propagation in the Ocean Surface.* Prentice-Hall, Englewood Cliffs, N.J., 676 pp.

KOEPPL, G.W., 1982, *Putnam's Power from the Wind.* Van Nostrand Reinhold, New York, 470 pp.

KROPFLI, R.A. and KOHN, N.M., 1978, Persistent horizontal rolls in the urban mixing layer as revealed by dual-Doppler radar. *Journal of Applied Meteorology,* v. 17, pp. 669-676

KUETTNER, J., 1959, The band structure of the atmosphere. *Tellus,* v. 2, n. 3, pp. 267-294

_____ , 1965, Cloudstreets: Theory and satellite observations. *10th OSTIV Congress,* South Gerney, U.K., June 1965. Also *Aero Revue,* 1967, v. 42, pp. 52-56, 109-112

KUO, H.L., 1963, Perturbations of plane Couette flow in stratified fluid and origin of cloud streets. *Physics of Fluids,* v. 6, n. 2, pp. 195-211

LANCASTER, N., 1980, Formation of sief dunes from barchans. *Zeitschrift für Geomorphologie,* v. 24, pp. 160-167

_____, 1983, Controls of dune morphology in the Namib sand sea. in: *Eolian Sediments and Processes – Developments in Sedimentology v. 38* (M.E. Brookfield and T.S. Ahlbrandt, editors). Elsevier, Amsterdam, pp. 261-289

LANGHORNE, D.N., 1982, A study of the dynamics of a marine sandwave. *Sedimentology,* v. 29, pp. 571-594

LANGMUIR, I., 1938, Surface motion of water induced by wind. *Science,* v. 87, n. 2250, pp. 119-123

LAWRENCE, E.M., 1969, *Introduction to the mechanics of a continuous medium.* Prentice-Hall, Englewood Cliffs, N.J., 156 pp.

LEMONE, M.A., 1973, The structure and dynamics of horizontal roll vortices in the planetary boundary layer. *Journal of Atmospheric Sciences,* v. 30, pp. 1077-1091

——————— , 1976, Modulation of turbulence energy by longitudinal rolls in an unstable planetary boundary layer. *Journal of Atmospheric Sciences,* v. 33, pp. 1308-1320

LENSCHOW, D.H., 1970, Airplane measurements of planetary boundary structure. *Journal of Applied Meteorology,* v. 9, pp. 874-884

——————— , 1972, *The measurement of air velocity and temperature using the NCAR Buffalo aircraft measuring system – NCAR-TN/EDD-74,* National Center for Atmospheric Research, 39 pp.

LEOPOLD, L.B. and LANGBEIN, W.B., 1966, River meanders. *Scientific American,* v. 214, n. 6, pp. 60-70

LEOPOLD, L.B. and WOLMAN, M.G., 1957, *River Channel Patterns: Braided, Meandering and Straight – U.S. Geological Survey Professional Paper 282-B,* pp. 39-73

LEOPOLD, L.B., BAGNOLD, R.A., WOLMAN, M.G. and BRUSH, Jr., L.M., 1960, *Flow Resistance in Sinuous or Irregular Channels – U.S. Geological Survey Professional Paper 282-D,* pp. 111-134

LILLY, D.K., 1966, On the instability of Ekman boundary flow. *Journal of Atmospheric Sciences,* v. 23, pp. 481-494

LILLY, D.K. and LENSCHOW, D.H., 1974, Aircraft measurements of the atmospheric mesoscales using an inertial reference system. *Proceedings of thew First Symposium on Flow, its Measurements and Control in Science and Industry,* Instrument Society of America, Pittsburgh, Pa., pp. 369-377

LONG, J.T. and SHARP, R.P., 1964, Barchan dune movement in Imperial Valley, California. *Bulletin of the Geological Society of America,* v. 78, pp. 1039-1044

LONG, R.R., 1961, *Mechanics of Solids and Fluids.* Prentice-Hall, Englewood Cliffs, N.J., 156 pp.

NAVIER, C.L.M.H., 1823, Mémoire sure les lois du movement des fluids. *Mémior Lu à l'Académie Royale des Sciences,* Paris, v. 6, pp. 389-416

NICKLING, W.G., 1984, The stabilizing role of bonding agents on the entrainment of sediment by wind. *Sedimentology,* v. 31, pp. 111-117

NICKLING, W.G. and ECCLESTONE, M., 1980, A technique for detecting grain motion in wind tunnels and flumes. *Journal of Sedimentary Petrology,* v. 50, pp. 652-654

—————————, 1981, The effects of soluble salts on the threshold shear velocity of fine sand. *Sedimentology,* v. 28, pp. 505-510

MABBUTT, J.A. and SULLIVAN, M.E., 1968, The formation of longitudinal dunes: Evidence from the Simpson Desert. *Australian Geographer,* v. 10, n. 6, pp. 483-487

MABBUTT, J.A., WOODING, R.A. and JENNINGS, J.N., 1969, The asymmetry of Australian desert sand ridges. *Australian Journal of Science,* v. 32, n. 4, pp. 159-160

MAINGUET, M., 1978, The influence of trade winds, local air-masses and topographic obstacles on the aeolian movement of sand particles and the origin and distribution of dunes and ergs in the Sahara and Australia. *Geoforum,* v. 9, pp. 17-28

—————————, 1980, *Utilisation des images mètèosat pour prèciser les trajectoires èoliennes au sol, au Sahara et sur les Marges Sahèliennes – Bulletin No. 78-2.* Sociètè Française de Photogrammètrie et de Tèlèdètection, 13 pp.

—————————, 1982, Les dunes d'érosion: signification morphodynamique et climatique de leur existence. *Würzberger Geographische Arbeiten,* v. 56, pp. 79-92

—————————, 1984a, A classification of dunes based on aeolian dynamics and the sand budget – ch. 2 of *Deserts and arid lands* (F. El-Baz, editor). Martinus Nijhoff, The Hague, pp. 31-58

—————————, 1984b, Space observation of Saharan aeolian dynamics – ch. 3 of *Deserts and arid lands* (F. El-Baz, editor). Matinus Nijhoff, The Hague, pp. 59-77

MAINGUET, M. and CALLOT, Y., 1978, *L'Erg de Fachi-Bilma (Tchad- Niger): Contribution à la connaissance de la dynamique des ergs et des dunes des zones arides chandes – Mémoires et documents, 19.* CNRS, Paris, 185 pp.

MAINGUET, M. and CHEMIN, M.-C., 1983, Sand seas of the Sahara and Sahel; An explanation of their thickness and sand dune type by the sand budget principle. in: *Eoilan Sediments and Processes* (M.E. Brookfield and T.S. Ahlbrandt, editors). Elsevier, Amsterdam, pp. 353-363

MAINGUET, M., VIMEUX-RICHEUX, M. and CHEMIN, M.-C., 1983, Autochtonie et allochtonie des sables de la zone sahara- sahélienne au Niger. *Revue de Géologie Dynamique et de Géographie Physique,* v. 24, Fasc. 2, pp. 167-

175

MARKSON, R., 1975, Atmospheric electrical detection of organized convection. *Science,* v. 188, n. 4194, pp. 1171-1177

MATHER, K.B., 1963, Why do roads corrugate?. *Scientific American,* v. 208, n. 1, pp. 128-136

MAXWELL, J.C., 1892, *Matter and Motion.* D. Van Nostrand Co., New York, 224 pp.

McLEISH, W., 1968, On the mechanism of wind-slick generation. *Deep-sea Research,* v. 15, pp. 461-469

MITCHELL, J.H., 1898, The wave-resistance of a ship. *London, Edinburgh and Dublin Philosophical Magazine,* v. 45, pp. 106-123

MILES, J.W., 1959, On the generation of surface waves by shear flows, Part 2. *Journal of Fluid Mechanics,* v. 6, p. 4, pp. 568-598

OFF, T., 1963, Rhythmic linear sand bodies caused by tidal currents. *Bulletin of the American Association of Petroleum Geologists,* v. 47, pp. 324-341

PANOFSKY, H.A., 1974, The atmospheric boundary layer below 150 meters. *Annual Review of Fluid Mechanics,* v. 6, pp. 147-177

PANOFSKY, H.A. and DUTTON, J.A., 1984, *Atmospheric Turbulance: Models and Methods for Engineering Applications.* John Wiley & Sons, New York, 397 pp.

PELLEW, A. and SOUTHWELL, R.V., 1940, Convective motion in a fluid. *Proceedings of the Royal Society of London, Series A,* v. 176, pp. 312-343

PITTOCK, A.B., FRAKES, L.A., JENSSEN, D., PETERSON, J.A. and ZILLMAN, J.W., editors, 1978, *Climatic change and variability: A southern perspective.* University Press, Cambridge, 455 pp.

PLANCK, V.G., 1966, Wind conditions in situations of pattern-form and non-pattern-form cumulus convection. *Tellus,* v. 18, pp. 1-12

POISSON, S.D., 1833, Mémoire sur les equations generalés de l'equilibre et du movement du corps solides elastiques et des fluides. *Journal de l'Ecole Polytechnique,* Paris, v. 13, pp. 139-166

PRANDTL, L., 1952, *The Essentials of Fluid Dynamics.* Blackie & Son, London, 452 pp.

PUTNAM, P.C., 1948, *Power from the Wind.* Van Nostrand Reinhold, New York, 224 pp.

QUENEY, P., 1960, *The Airflow over Mountains – World Meteorological Organization Technical Note No. 34,* 134 pp.

RAYLEIGH, J.W.S. (Lord), 1880, On the stability or instability of certain fluids. *Scientific Papers, v. 1* (published 1899). University Press, Cambridge, pp. 474-487

_____ , 1887, On the stability or instability of certain fluid motions, II. *Scientific Papers, v. 3* (published 1902). University Press, Cambridge, pp. 17-23

_____ ,1901, The mechanical principles of flight. in: *Scientific Papers, v. 4* (published 1903). C.T. Clay and Sons, London, pp. 412-479

_____ , 1913, On the motion of a viscous fluid. *Scientific Papers, v. 6* (published 1920). University Press, Cambridge, pp. 187-204

_____ , 1916, On convection currents in a horizontal layer of fluid when the higher temperature is on the under side. *Philosophical Magazine, Series 6, v. 32, n. 192,* pp. 530-546

REBA, I., 1966, Applications of the Coanda effect. *Scientific American,* June, 1966, pp. 84-92

REID. W.H., 1958, On the stability of viscous flow in a curved channel. *Proceedings of the Royal Society of London, Series A, v. 244,* pp. 186-198

RILEY, D.S., DONELAN, M.A. and HUI, W.A., 1982, Extended Mile's theory for wave generation by wind. *Boundary-Layer Meteorology, v. 22, n. 2,* pp. 209-225

RODI, A.R. and SPYERS-DURAN, P.A., 1971, Analysis of time response of airbourne temperature sensors. *Journal of Applied Meteorology, v. 11,* pp. 554-556

ROTTNER, J., 1959, A formula for bed-load transportation. *La Houille Blanche.* n. 3, pp. 301-307

RUBIN, D.M., 1984, Factors determining desert dune type (discussion). *Nature, v. 309,* pp. 91-92

_____ , 1985, Lateral migration, internal structure, and climbing of linear dunes in the Strzelecki Desert, Australia (in press). (For Dr. Rubin's address, see list of researchers referenced.)

RUBIN, D.M. and HUNTER, R.E., 1985, Why deposits of longitudinal dunes are rarely recognized in the geologic record. *Sedimentology, v. 32, n. 1,* pp. 147-157

RUBIN, D.M. and McCULLOUGH, D.S., 1980, Single and superimposed bedforms: A synthesis of San Francisco Bay and flume observations. *Sedimentary Geology, v. 26,* pp. 207-231

SABERSKY, R.H., ACOSTA, A.J. and HAUPTMANN, E.G., 1971, *Fluid Flow: A First Course in Fluid Mechanics, 2nd Ed.* Macmillan, New York, 519 pp.

SAGAN, C. and BAGNOLD, R.A., 1975, Fluid transport on earth and eolian transport on Mars. *Icarus*, v. 26, pp. 206-218

SAINT-VENANT, B., 1843, Mémoire sur la dynamique des fluids. *Comptes Rendus de l'Academie de Sciences*, Paris, v. 17, pp. 1240-1242

SCORER, R.W., 1958, *Natural Aerodynamics*. Pergamon Press, New York, 312 pp.

SETHURAMAN, S., 1977, The observed generation and breaking of atmospheric internal gravity waves over the ocean. *Boundary-Layer Meteorology*, v. 12, pp. 331-349

SHAMES, I.H., 1982, *Mechanics of Fluids*. McGraw-Hill, New York, 692 pp.

SCHLICHTING, H., 1960, *Boundary Layer Theory*. McGraw-Hill, New York, 647 pp.

SOKOLNIKOFF, E.S. and SOKOLNIKOFF, I.S., 1941, *Higher Mathematics for Engineers and Physicists*. McGraw-Hill, New York, 587 pp.

SPRIGG, R.C., 1981, Alternating wind cycles of the Quaternary Era and their influence on aeolian sedimentation in and around the dune deserts of southeastern Australia. *INQUA – Loess Commission Workshop*, Canberra, 39 pp.

SQUIRE, H.B., 1933, On the stability of three-dimensional disturbances of viscous fluid flow between parallel walls. *Proceedings of the Royal Society of London, Series A*, v. 142, pp. 621-628

STERN, M.E., 1960, Instability of Ekman flow at large Taylor numbers. *Tellus*, v. 12, pp. 399-417

STERNBERG, R.W., 1972, Predicting initial motion and bedload transport of sediment particles in the shallow marine environment. in: *Shelf Sediment Transport Process and Pattern* (D.J.P. Swift, D.B. Duane and O.H. Pikey, editors). Dowden, Hutchinson and Ross, Stroudsburg, pp. 61-82

STOKES, G.G., 1845, On the theories of the internal friction of fluids in motion, and of the equilibrium and motion of elastic solids. *Transactions of the Cambridge Philosophical Society*, v. 8, pp. 287-305. Also *Mathematics and Physics Paper 1*. University Press, Cambridge, pp. 75-129

SUTTON, O.G., 1950, On the stability of a fluid heated from below. *Proceedings of the Royal Society of London, Series A*. v. 204, pp. 297-309

TERADA, T., 1928, Some experiments on periodic columnar formations of vortices caused by convection. *Report of the Aeronautical Research Institute, Tokyo University* v. 3, pp. 1-46

THOMSON, J., 1882, On a changing tessellated structure in certain liquids. *Proceedings of the Royal Philosophical Society of Glasgow*, v. 13, pp. 464-468

THWAITES, B., ed., 1960, *Incompressible Aerodynamics*. Clarendon Press, Oxford, 636 pp.

TOLLMEIN, W., 1935, Ein allgemeines Kriterium der Instabilität laminarer Geschwindigkeitsverteilungen. *Nachrichten Gesellshaft der Wissenshaften zu Göttingen, Mathematisch-physikalische Klasse, Fachgruppe I*, v. 1, pp. 79-114 Also *NACA TM 792* (1936)

TSOAR, H., 1978, *The Dynamics of Longitudinal Dunes*. U.S. Army, European Research Office, London, 171 pp.

TSOAR, H., GREEELEY, R. and PETERFREUND, A.R., 1979, Mars: The north polar sand sea and related wind patterns. *Journal of Geophysical Research*, v. 84, n. B14, pp. 8167-8180

TUCK, E.O. and NEWMAN, J.N., 1974, Hydrodynamic interactions between ships. *10th Symposium on Naval Hydrodynamics*, Office of Naval Research, Washington D.C., pp. 35-58

TWIDALE, C.R., 1972a, Evolution of sand dunes in the Simpson Desert, central Australia. *Transactions of the Institute of British Geographers*, v. 56, pp. 77-109

—————————, 1981, Age and origin of longitudinal dunes in the Simpson and other sand ridge deserts. *Die Erde*, v. 112, pp. 231-247

TWIDALE, C.R. and WOPFNER, M.W., 1981, Aeolian landforms of central Australia. *Zeitschrift für Geomorphologie*, v. 25, pp. 353-358

VINCIENT, C.E., YOUNG, R.A. and SWIFT, D.J.P., 1981, Bed-load transport under waves and currents. *Marine Geology*, v. 39, pp. M71-M80

VONNEGUT, B. and McCRAIG, D.A., 1960, Airplane instrument for measurement and vertical presentation of electrical potential gradient. *Journal of Geophysical Research*, v. 65, n. 7, pp. 1959-1963

VONNEGUT, B., MOORE Jr., C.B. and MALLAHAN, F.J., 1961, Adjustable potential-gradient-measuring apparatus for airplane use. *Journal of Geophysical Research*, v. 66, n. 8, pp. 2393-2397

WARREN, A., 1970, Dune trends and their implications in the central Sudan. in: *Zeitschrift für Geomorphologie, Supplementband 10*, pp. 154-179

—————————, 1972, Observations on dunes and bi-modal sands in the Ténéré Desert. *Sedimentology*, v. 19, pp. 37-44

—————————, 1976b, Dune trend and the Ekman spiral. *Nature*, v. 259, pp. 653-654

WARREN, A. and KNOTT, P., 1983, Desert dunes: A short review of needs in desert dune research and a recent study of micrometeorological dune-

initiation mechanisms. *Eolian Sediments and Processes – Developments in Sedimentology, v. 38* (M.E. Brookfield and T.S. Ahlbrandt, editors). Elsevier, Amsterdam, pp. 343-352

WEBER, E.H., 1955, Mikroskopische Beobachtungen sehr gesetzmässiger Bewegungen welche die Bildung von Niederschlagenharziger Körper aus Weingeistbegleiten. *Annalen der Physik,* Leipzig, v. 94, pp. 447-458

WILSON, I.G., 1972, Aeolian bedforms: Their development and origins. *Sedimentology,* v. 19, pp. 173-210

WIPPERMAN, F., 1969, Orientation of vortices due to instability of the Ekman-boundary layer. *Beiträger zur Physik der Atmosphäre,* 42 Band, s. 225-244

WOODCOCK, A.H., 1940, Convection and soaring over the open ocean. *Journal of Marine Research, v. 3, pp. 248-253*

————— , *1944, A theory of surface water motion deduced from the wind-induced motion of the physalia. Journal of Marine Research,* v. 5, pp. 196-205

————— , 1947, Soaring over the open sea. *The Scientific Monthly,* v. 55, pp. 226-232

WOODCOCK, A.H. and WYMAN, J., 1947, Convective motion in air over the sea. *Annals New York Academy of Sciences,* v. 48, pp. 749-776

YALIN, M.S., 1963, An expression for bed-load transportation. *Journal of the Hydraulic Division, Proceedings of the American Society of Civil Engineers,* pp. 221-250

**Location of researchers
referred to in the text**

BAGNOLD, R.A., 7 Manor Way, Blackheath, SE3 9EF, U.K.

BENNETT, J.M., Flinders Institute of Atmospheric and Marine Sciences, School of Earth sciences, Flinders University, Bedford Park, South Australia 5042, Australia

BYRON-SCOTT, R.A.D., same as BENNETT

BOWLER, J.M., Department of Biogeography and Geomorphology, The Australian National University, P.O. Box 4, Canberra, A.C.T. 2600, Australia

BURROWS, K., Bureau of Meteorology, Regional Directors Office, 25 College Road, Kent Town, South Australia 5067, Australia

HUTHNANCE, J.M., Institute of Oceanographic Sciences, Bidston Observatory, Birkenhead, Merseyside L43 7RA, U.K.

MAINGUET, M., Université De Reims, U.E.R. Lettres & Sciences Humaines, Laboratoire de Géographie Physique Zonale et D'Études des Paysages en Roches Sédimentaires, 57, rue Pierre Taittinger, 51096 REIMS CEDEX, France

RUBIN, D.M., Branch of Pacific Marine Geology, U.S. Geological Survey, Menlo Park, California 94025, U.S.

SPRIGG, R., Arkaroola Travel Centre, 50 Pirie St., Adelaide, South Australia 5000, Australia

TWIDALE, C.R., Department of Geography, University of Adelaide, Adelaide, South Australia 5000, Australia

WASSON, R.J., C.S.I.R.O., Division of Land Use Research, P.O. Box 1666, Canberra City, A.C.T. 2601, Austrialia